

SEISMIC PERFORMANCE OF MULTISIMPLE-SPAN SKEW BRIDGES
RETROFITTED WITH LINK SLABS

A THESIS SUBMITTED TO
THE GRADUATE SCHOOL OF NATURAL AND APPLIED SCIENCES
OF
MIDDLE EAST TECHNICAL UNIVERSITY

BY

GİZEM SEVGİLİ

IN PARTIAL FULFILLMENT OF THE REQUIREMENTS
FOR
THE DEGREE OF MASTER OF SCIENCE
IN
CIVIL ENGINEERING

JANUARY 2007

Approval of Graduate School of Natural and Applied Sciences

Prof. Dr. Canan Özgen
Director

I certify that this thesis satisfies all the requirements as a thesis for the degree of
Master of Science

Prof. Dr. Güney Özcebe
Head of Department

This is to certify that we have read this thesis and that in our opinion it is fully
adequate, in scope and quality, as a thesis for the degree of Master of Science

Asst. Prof. Dr. Alp Caner
Supervisor

Examining Committee Members

Dr. Erhan Karaesmen (METU, CE) _____

Asst. Prof. Dr. Alp Caner (METU, CE) _____

Assoc. Prof. Dr. Cem Topkaya (METU, CE) _____

Asst. Prof. Dr. Murat Altuğ Erberik (METU, CE) _____

Özgür Madenli, M.S. (TENDA Engineering) _____

I hereby declare that all information in this document has been obtained and presented in accordance with academic rules and ethical conduct. I also declare that, as required by these rules and conduct, I have fully cited and referenced all material and results that are not original to this work.

Name, Last name: Gizem SEVGİLİ

Signature:

ABSTRACT

SEISMIC PERFORMANCE OF MULTISIMPLE-SPAN SKEW BRIDGES RETROFITTED WITH LINK SLABS

SEVGİLİ, Gizem

M.Sc., Department of Civil Engineering

Supervisor: Asst. Prof. Dr. Alp CANER

January 2007, 161 pages

Investigation of more than seventy highway bridges revealed that multisimple-span skew bridges with expansion joints were very common in Turkish practice. The expansion joints, used to provide deck expansion against shrinkage, creep and thermal effects, create costly maintenance problems due to leaked water, impact loads and accumulated debris in the joints. Therefore, elimination of expansion joints decreases the maintenance cost for the bridges. Reinforced concrete link slabs provide continuity at the deck level with the elimination of expansion joints. This thesis focuses on evaluating the seismic behavior of the skew multisimple-span bridges in Turkey and also discusses the use of reinforced concrete link slabs as a seismic retrofit option. The effects of addition of link slab and varying skew angle on the performance of the bridges were investigated. The use of link slabs can provide a better seismic displacement control, can decrease the member forces and can prevent or reduce deterioration of the top of the piers and ends of the girders from the water and chemical leakage by abandoning or minimizing number of expansion joints.

Keywords: Bridge, Skew, Expansion joint, Seismic, Retrofit

ÖZ

BAĞLANTI DÖŞEMELERİYLE GÜÇLENDİRİLMİŞ ÇOK AÇIKLIKLIL BASİT MESNETLİ VEREV KÖPRÜLERİN DEPREM PERFORMANSI

SEVGİLİ, Gizem

Yüksek Lisans, İnşaat Mühendisliği Bölümü

Tez Yöneticisi: Yrd. Doç. Dr. Alp CANER

Ocak 2007, 161 sayfa

Yetmişten fazla otoyol köprüsüyle yapılan araştırma sonucunda, Türk mühendislik pratiğinde çok açıklıklı basit mesnetli vev köprülerin çok yaygın olduğu ortaya konulmuştur. Büzülmeye, sünmeye ve ısı etkilere karşı döşemenin genleşmesini sağlayabilmek için kullanılan derzler akan sulardan, darbe yüklerinden ve biriken kirlere dolaylı maliyeti yüksek bakım masrafları yaratırlar. Bu nedenle, derzlerin kaldırılması köprülerdeki bakım masraflarını azaltmaktadır. Betonarme bağlantı döşemeleri sayesinde derzler çıkartılarak döşeme seviyesinde devamlılık sağlanır. Bu tez, Türkiye'deki çok açıklıklı basit mesnetli vev köprülerin sismik davranışlarını incelemektedir. Ayrıca, betonarme bağlantı döşemelerinin sismik güçlendirme metodu olarak kullanılmaları da irdelenmiştir. Bağlantı döşemelerinin ve farklı vev açıklıklarının köprü performansı üzerindeki etkileri incelenmiştir. Bağlantı döşemesi kullanımı, deprem esnasında oluşabilecek deplasman ve eleman kuvvetlerini ve ayrıca su ya da kimyevi maddelerin derzlerden sızarak kolon ve kirişlerde meydana getirdiği bozunmaları azaltabilmektedir.

Anahtar Kelimeler: Köprü, Vev, Derz, Sismik, Güçlendirme

To my family

ACKNOWLEDGEMENTS

The author would like to thank to;

Assist. Prof. Dr. Alp Caner, for his continuous guidance, endless patience, valuable knowledge and background which he never hesitated to share throughout this research.

Dr. Erhan Karaesmen, for providing precious motivation, criticism and constant faith in me since the day I met him. I also appreciate him for introducing me to Assist. Prof. Dr. Alp Caner to complete this thesis.

Mega Mühendislik and Mr. Arman Domaniç who provided valuable data during this study.

Mr. Can Seyhun for his constant supports, endless patience and love.

TABLE OF CONTENTS

PLAGIARISM	iii
ABSTRACT	iv
ÖZ	v
DEDICATION	vi
ACKNOWLEDGEMENTS	vii
TABLE OF CONTENTS	viii
LIST OF TABLES	xi
LIST OF FIGURES	xiii
LIST OF SYMBOLS AND ABBREVIATIONS	xxi

CHAPTER

1. INTRODUCTION	1
1.1 Statement of the Problem	1
1.2 The Objectives and Scope of the Study	3
2. LITERATURE REVIEW	6
2.1 Deck Continuous Bridges	6
2.1.1 Years 1956 – 1996	6
2.1.2 Years 1997 to Present	9
2.2 Skew Bridges	10
3. IDENTIFICATION OF THE MOST COMMON TYPES OF HIGHWAY BRIDGES IN TURKEY	13
3.1 Bridge Survey	13
3.2 Generated Bridge Models	16

4. ANALYSIS PROCEDURE	20
4.1 Computer Modeling	20
4.1.1 Introduction	20
4.1.2 Modeling of Superstructure	21
4.1.3 Modeling of Substructure	25
4.1.4 Supports	26
4.2 Analytical Methods	30
4.2.1 Response Spectra Analysis (RSA)	30
4.2.2 Linear Time History Analysis (LTHA)	34
4.2.3 Non-linear Time History Analysis (NLTHA)	49
4.2.4 Service Load Analyses	54
5. ANALYSIS RESULTS	57
5.1 Introduction	57
5.2 Eigenvalue Analysis Results	61
5.3 Response Spectra Analysis (RSA) Results	65
5.4 Service Load Analysis Results	103
5.4.1 Live Load Girder Stresses	103
5.4.2 Link Slab Cracking Control	107
5.5 Linear Time History Analysis (LTHA) Results.....	111
5.6 Non-Linear Time History Analysis (NLTHA) Results.....	114
6. DISCUSSION ON RESULTS	120
6.1 Discussion on Eigenvalue Analysis Results	120
6.2 Discussion on Response Spectra Analysis (RSA) Results.....	121
6.3 Discussion on Service Load Analysis Results	128
6.4 Discussion on Linear Time History Analysis (LTHA) Results.	129
6.5 Discussion on Non-Linear Time History Analysis (NLTHA) Results.....	131

7. SUMMARY AND CONCLUSIONS.....	132
REFERENCES	134
APPENDICES	
A. BRIDGE SURVEY RESULTS.....	139
B. BRIDGE MODELS.....	143
C. MACRO CODE FOR BRIDGE MODEL GENERATION.....	147

LIST OF TABLES

TABLES

Table 3.1: Bridge parameters	17
Table 3.2: Column Cross Sections	17
Table 3.3: Column Heights	18
Table 4.1: Material properties of the bridge components	21
Table 4.2: Shear key properties	28
Table 4.3: Properties of elastomeric bearings	30
Table 4.4: Earthquake records used for the THA	37
Table 4.5: Peak ground accelerations.....	49
Table 5.1: Fundamental Periods of Group A Bridges	61
Table 5.2: Fundamental Periods of Group B Bridges	63
Table 5.3: Fundamental Periods of Group C Bridges.....	64
Table 5.4: Fundamental Periods of Group D Bridges.....	65
Table 5.5: Girder Live Load Stresses of Group A Bridges	103
Table 5.6: Girder Live Load Stresses of Group B Bridges	105
Table 5.7: Girder Live Load Stresses of Group C Bridges.....	106
Table 5.8: Girder Live Load Stresses of Group D Bridges.....	107
Table 5.9: Properties of bridges used in LTHA.....	111
Table 5.10: Displacements calculated from LTHA and RSA.....	112
Table 5.11: Member forces and moments calculated from LTHA and RSA.....	113
Table 5.12: Link Slab Forces calculated from LTHA and RSA.....	114
Table 5.13: NLTHA and LTHA Results.....	119
Table A.1: Properties of the surveyed bridges.....	139
Table B.1: Group A Bridges: $L/H = 1.0$ and $I_{capbeam}/I_{column} = 0.1$	143
Table B.2: Group B Bridges: $L/H = 1.5$ and $I_{capbeam}/I_{column} = 0.1$	144
Table B.3: Group C Bridges: $L/H = 1.0$ and $I_{capbeam}/I_{column} = 1.5$	145

Table B.4: Group D Bridges: $L/H = 1.0$ and $I_{cb}/I_{col} = 0.1$ with fully continuous deck.....	146
---	-----

LIST OF FIGURES

FIGURES

Figure 1.1: Deterioration of girder ends and cap beam at expansion joint location due to leaked water.....	2
Figure 1.2: Damage in expansion joints caused by impact.....	2
Figure 1.3: New bridge with link slab.....	4
Figure 2.1: Link slab details for above interior piers and abutments.....	9
Figure 3.1: Typical bridge components.....	14
Figure 3.2: Skew angle.....	15
Figure 3.3: Maximum span length.....	15
Figure 3.4: Number of spans.....	15
Figure 3.5: Ratio of beam to column inertia.....	16
Figure 3.6: Bent characteristics.....	16
Figure 3.7: Deck plan of Group A, B and C bridges with link slab.....	19
Figure 3.8: Deck plan of Group D bridges.....	19
Figure 4.1: Bridge components.....	21
Figure 4.2: Plate geometry of deck elements.....	22
Figure 4.3: Girder cross-section 1; for SL=18 m.....	23
Figure 4.4: Girder cross-section 2; for SL=25 m.....	23
Figure 4.5: Longitudinal close view of a bridge model with link slab.....	24
Figure 4.6: Bridge bents for different L/H.....	25
Figure 4.7: Column cross sections.....	25
Figure 4.8: Elastomeric bearing, AASHTO, 1996.....	26
Figure 4.9: Bearing dimensions.....	27
Figure 4.10: AASHTO normalized elastic response spectrum for 5% damping.....	33
Figure 4.11: Acceleration time histories of Yarımca record.....	39

Figure 4.12: Normalized pseudo acceleration response spectra of Yarımca record together with AASHTO, 1996 response spectrum.....	40
Figure 4.13: Acceleration time histories of İzmit record.....	41
Figure 4.14: Normalized pseudo acceleration response spectra of İzmit record together with AASHTO, 1996 response spectrum.....	42
Figure 4.15: Acceleration time histories of Gebze record.....	43
Figure 4.16: Normalized pseudo acceleration response spectra of Gebze record together with AASHTO, 1996 response spectrum.....	44
Figure 4.17: Acceleration time histories of Düzce record.....	45
Figure 4.18: Normalized pseudo acceleration response spectra of Düzce record together with AASHTO, 1996 response spectrum.....	46
Figure 4.19: Acceleration time histories of Bolu record.....	47
Figure 4.20: Normalized pseudo acceleration response spectra of Bolu record together with AASHTO, 1996 response spectrum.....	48
Figure 4.21: ATC-32 model for seat type abutment.....	50
Figure 4.22: Force-displacement graph of springs between adjacent spans.	51
Figure 4.23: Typical abutment dimensions.....	52
Figure 4.24: Force-displacement graph of springs between spans and abutments.....	53
Figure 4.25: Truck loads on 25 m. long span.....	55
Figure 5.1: Longitudinal, transverse and vertical directions of the bridge..	58
Figure 5.2: Longitudinal and transverse deck displacements of 2 spanned and 4 spanned bridges.....	58
Figure 5.3: Direction of the cap beam local moment.....	59
Figure 5.4: Direction of the column local longitudinal and transverse moments.....	59
Figure 5.5: Stress points at girder cross-sections.....	60
Figure 5.6: Change in longitudinal deck displacement with skew angle for 2 span bridges in Group A.....	67

Figure 5.7: Change in longitudinal deck displacement with skew angle for 4 span bridges in Group A.....	67
Figure 5.8: Change in longitudinal deck displacement with skew angle for 2 span bridges in Group B.....	68
Figure 5.9: Change in longitudinal deck displacement with skew angle for 4 span bridges in Group B.....	68
Figure 5.10: Change in longitudinal deck displacement with skew angle for 2 span bridges in Group C	69
Figure 5.11: Change in longitudinal deck displacement with skew angle for 2 span bridges in Group C	69
Figure 5.12: Change in longitudinal deck displacement with skew angle for 2 span bridges in Group D.....	70
Figure 5.13: Change in longitudinal deck displacement with skew angle for 4 span bridges in Group D	70
Figure 5.14: Change in transverse deck displacement with skew angle for 2 span bridges in Group A	71
Figure 5.15: Change in transverse deck displacement with skew angle for 4 span bridges in Group A.....	71
Figure 5.16: Change in transverse deck displacement with skew angle for 2 span bridges in Group B	72
Figure 5.17: Change in transverse deck displacement with skew angle for 4 span bridges in Group B	72
Figure 5.18: Change in transverse deck displacement with skew angle for 2 span bridges in Group C.....	73
Figure 5.19: Change in transverse deck displacement with skew angle for 4 span bridges in Group C	73
Figure 5.20: Change in transverse deck displacement with skew angle for 2 span bridges in Group D	74
Figure 5.21: Change in transverse deck displacement with skew angle for 4 span bridges in Group D	74

Figure 5.22: Change in longitudinal bearing displacement with skew angle for 2 span bridges in Group A.....	75
Figure 5.23: Change in longitudinal bearing displacement with skew angle for 4 span bridges in Group A	75
Figure 5.24: Change in longitudinal bearing displacement with skew angle for 2 span bridges in Group B	76
Figure 5.25: Change in longitudinal bearing displacement with skew angle for 4 span bridges in Group B.....	76
Figure 5.26: Change in longitudinal bearing displacement with skew angle for 2 span bridges in Group C.....	77
Figure 5.27: Change in longitudinal bearing displacement with skew angle for 4 span bridges in Group	77
Figure 5.28: Change in longitudinal bearing displacement with skew angle for 2 span bridges in Group D.....	78
Figure 5.29: Change in longitudinal bearing displacement with skew angle for 4 span bridges in Group D.....	78
Figure 5.30: Change in local cap beam moment with skew angle for 2 span bridges in Group A.....	79
Figure 5.31: Change in local cap beam moment with skew angle for 4 span bridges in Group A.....	79
Figure 5.32: Change in local cap beam moment with skew angle for 2 span bridges in Group B.....	80
Figure 5.33: Change in local cap beam moment with skew angle for 4 span bridges in Group B.....	80
Figure 5.34: Change in local cap beam moment with skew angle for 2 span bridges in Group C.....	81
Figure 5.35: Change in local cap beam moment with skew angle for 4 span bridges in Group C.....	81

Figure 5.36: Change in local cap beam moment with skew angle for 2 span bridges in Group D.....	82
Figure 5.37: Change in local cap beam moment with skew angle for 4 span bridges in Group D.....	82
Figure 5.38: Change in local diaphragm shear with skew angle for 2 span bridges in Group A.....	83
Figure 5.39: Change in local diaphragm shear with skew angle for 4 span bridges in Group A.....	83
Figure 5.40: Change in local diaphragm shear with skew angle for 2 span bridges in Group B.....	84
Figure 5.41: Change in local diaphragm shear with skew angle for 4 span bridges in Group B.....	84
Figure 5.42: Change in local diaphragm shear with skew angle for 2 span bridges in Group C.....	85
Figure 5.43: Change in local diaphragm shear with skew angle for 4 span bridges in Group C.....	85
Figure 5.44: Change in local diaphragm shear with skew angle for 2 span bridges in Group D.....	86
Figure 5.45: Change in local diaphragm shear with skew angle for 4 span bridges in Group D.....	86
Figure 5.46: Change in local column transverse moment with skew angle for 2 span bridges in Group A.....	87
Figure 5.47: Change in local column transverse moment with skew angle for 4 span bridges in Group A.....	87
Figure 5.48: Change in local column transverse moment with skew angle for 2 span bridges in Group B.....	88
Figure 5.49: Change in local column transverse moment with skew angle for 4 span bridges in Group B.....	88
Figure 5.50: Change in local column transverse moment with skew angle for 2 span bridges in Group C.....	89

Figure 5.51: Change in local column transverse moment with skew angle for 4 span bridges in Group C.....	89
Figure 5.52: Change in local column transverse moment with skew angle for 2 span bridges in Group D.....	90
Figure 5.53: Change in local column transverse moment with skew angle for 4 span bridges in Group D.....	90
Figure 5.54: Change in local column longitudinal moment with skew angle for 2 span bridges in Group A.....	91
Figure 5.55: Change in local column longitudinal moment with skew angle for 4 span bridges in Group A.....	91
Figure 5.56: Change in local column longitudinal moment with skew angle for 2 span bridges in Group	92
Figure 5.57: Change in local column longitudinal moment with skew angle for 4 span bridges in Group B.....	92
Figure 5.58: Change in local column longitudinal moment with skew angle for 2 span bridges in Group C.....	93
Figure 5.59: Change in local column longitudinal moment with skew angle for 4 span bridges in Group C.....	93
Figure 5.60: Change in local column longitudinal moment with skew angle for 2 span bridges in Group D.....	94
Figure 5.61: Change in local column longitudinal moment with skew angle for 4 span bridges in Group D.....	94
Figure 5.62: Change in link slab axial force with skew angle for 2 span bridges in Group A.....	95
Figure 5.63: Change in link slab axial force with skew angle for 4 span bridges in Group A.....	95
Figure 5.64: Change in link slab axial force with skew angle for 2 span bridges in Group B	96
Figure 5.65: Change in link slab axial force with skew angle for 4 span bridges in Group B	96

Figure 5.66: Change in link slab axial force with skew angle for 2 span bridges in Group C.....	97
Figure 5.67: Change in link slab axial force with skew angle for 4 span bridges in Group C	97
Figure 5.68: Change in link slab axial force with skew angle for 2 span bridges in Group D.....	98
Figure 5.69: Change in link slab axial force with skew angle for 4 span bridges in Group D.....	98
Figure 5.70: Change in link slab moment with skew angle for 2 span bridges in Group A.....	99
Figure 5.71: Change in link slab moment with skew angle for 4 span bridges in Group A.....	99
Figure 5.72: Change in link slab moment with skew angle for 2 span bridges in Group B.....	100
Figure 5.73: Change in link slab moment with skew angle for 4 span bridges in Group B	100
Figure 5.74: Change in link slab moment with skew angle for 2 span bridges in Group C	101
Figure 5.75: Change in link slab moment with skew angle for 4 span bridges in Group C	101
Figure 5.76: Change in link slab moment with skew angle for 2 span bridges in Group D	102
Figure 5.77: Change in link slab moment with skew angle for 4 span bridges in Group D.....	102
Figure 5.78: Link slab cracking control for Group A bridges under live loads.....	109
Figure 5.79: Link slab cracking control for Group B bridges under live loads.....	109
Figure 5.80: Link slab cracking control for Group C bridges under live loads.....	110

Figure 5.81: Link slab cracking control for Group D bridges under live loads.....	110
Figure 5.82: Link slab cracking control for Group D bridges under thermal loads.....	111
Figure 5.83: Longitudinal and transverse deck displacements of the bridge without link slab.....	115
Figure 5.84: Local longitudinal and transverse column moments of the bridge without link slab.....	115
Figure 5.85: Pounding force at the center pier of the bridge without link slab.....	116
Figure 5.86: Abutment pounding force of the bridge without link slab....	116
Figure 5.87: Longitudinal and transverse deck displacements of the bridge with link slab.....	117
Figure 5.88: Local longitudinal and transverse column moments of the bridge with link slab.....	117
Figure 5.89: Abutment pounding force of the bridge with link slab.....	118
Figure 5.90: Link slab axial force at edge and center.....	118
Figure 6.1: Span separation problem of the multisimple-span bridge with expansion joints.	123
Figure 6.2: Pounding of the spans in the multisimple-span bridge with expansion joints.	123
Figure 6.3: The deformed shape of the multisimple-span bridge retrofitted with link slabs.	123
Figure 6.4: A sample link slab details practiced in Turkey.....	127
Figure 6.5: A sample link slab axial force distribution due to earthquake loading along the bridge width.....	127
Figure 6.6: Live load distribution for straight and skew bridges	129

LIST OF SYMBOLS AND ABBREVIATIONS

A:	the acceleration coefficient
A_{bearing} :	plan area of elastomeric element or bearing
a_0 :	mass-proportional rayleigh damping constant
a_1 :	stiffness-proportional rayleigh damping constant
c:	rayleigh damping
c_{cover} :	total concrete clean cover
C_s :	elastic seismic coefficient
E_{conc} :	modulus of elasticity of concrete
E_c :	effective modulus of elastomeric bearing in compression
F:	force in the longitudinal direction of the elastomeric bearing
F_c :	axial load strength
f_c :	compressive strength of concrete at 28 days
G:	shear modulus of the elastomer
H:	height of the column
H_{cb} :	height of cap beam
H_m :	maximum horizontal load for elastomeric bearing
h_{rt} :	total elastomer thickness
I:	impact fraction for live load
I_{bearing} :	moment of inertia of plan shape of bearing
I_c :	column moment of inertia
I_{cb} :	cap beam moment of inertia
$I_{\text{eff}(\text{shear key})}$:	effective moment of inertia of shear key
k_{abut} :	stiffness of the abutment
k_{deck} :	stiffness of the deck
K_{long} :	horizontal longitudinal stiffness of elastomeric bearings
K_{trans} :	horizontal transverse stiffness of elastomeric bearings
K_{vertical} :	vertical stiffness of elastomeric bearing

$K_{\theta l}$:	Longitudinal rotational stiffness elastomeric bearing
$K_{\theta t}$:	Transverse rotational stiffness elastomeric bearing
L :	column spacing in a bent
L_{cb} :	length of cap beam
LS :	link slab
m :	mass of the system
M_m :	maximum bending moment for elastomeric bearing
p_{ga} :	peak ground acceleration
S :	coefficient for the soil profile characteristics of the site
$S_{bearing}$:	shape factor of one layer of an elastomeric bearing
SL :	span length
T :	the period of the bridge
V :	shear at critical section of back wall during flexural failure
W_{cb} :	width of cap beam
Δd :	displacement of the bearing in the longitudinal direction
Δ_s :	maximum shear deformation of the elastomer
θ_m :	maximum design rotation
ξ :	damping ratio
Φ :	strength reduction factor for axial load capacity
ω_i :	natural frequency for the i^{th} mode
ω_j :	natural frequency for the j^{th} mode

CHAPTER 1

INTRODUCTION

1.1 Statement of the Problem

Multisimple-span skew bridges are the majority of the crossings used in the Turkish highway system. A typical span has a reinforced concrete deck over precast prestressed I-girders and span lengths range from 15 to 35 meters. Expansion joint devices are accommodated between two adjacent spans to allow deck movements induced by temperature, creep and shrinkage. However, having expansion joints between adjacent spans develops costly maintenance problems. The main issues that generate the need for maintenance are:

- Water leakage through expansion joints,
- Accumulation of debris in the joints,
- Loss of function due to impact induced by heavy truck loads.

Water leakage through the expansion joints can cause deterioration at bearings, decks, girder ends and at cap beams as shown in Figure 1.1 [1], [2].



Figure 1.1: Deterioration of girder ends and cap beam at expansion joint location due to leaked water (By courtesy of Caner)

Accumulated debris at the joints can restrain deck expansion and can cause undesirable damages to the structure. Impact induced by dynamic effects of heavy truck loads can delaminate the expansion joint concrete as shown in Figure 1.2.



Figure 1.2: Damage in expansion joints caused by impact (By courtesy of Caner)

Another disadvantage of the expansion joints is the noise emission. Residents next to highway and bridges suffer from the noise caused by flow of traffic. Expansion joints placed against traffic direction can be subjected to constant intolerable impact between wheels of vehicles and steel parts of the joints that creates noise [3]. Removal of expansion joints between adjacent spans eliminates the noise emission and also more significantly can reduce the cost for construction and maintenance of the bridges [4].

Skewness of a bridge is typically defined as an angle between deck end line and the hypothetical line normal to the longitudinal direction of the bridge. Highly skewed bridges are typically considered as irregular bridges by the design specifications. Skew bridges not only expand or contract in longitudinal direction but can also move in transverse direction of the bridge [5]. During a seismic event, it is very important to minimize the deck displacement to prevent unseating, especially for skew bridges. In this study, problems associated with skewness of the multi-simple span bridges and expansion joints will be investigated.

1.2 The Objectives and Scope of the Study

Current design philosophy in Turkey promotes to eliminate expansion joints by continuous decks between adjacent simple-spans as shown in Figure 1.3 [2]. In the 1999 Kocaeli Earthquake, it was observed that bridges with continuous decks performed very well, even if they were very close to the fault line [5].



Figure 1.3: New bridge with link slab (By courtesy of Caner)

Caner and Zia [1] investigated the behavior of bridges having continuous deck for live load. Deck of a bridge can be made continuous by removing the expansion joints. The part of the deck connecting two adjacent simple-span girders is called “link slab” [6]. The researchers performed live load tests for bridges with link slabs (LS) and developed a design guideline for the link slab based on both service and strength level.

Seismic performance of bridges retrofitted with link slabs was studied for straight bridges, only [5]. It was found out that, for straight bridges the usage of link slabs could overcome span separation problem and could prevent the potential damage due to unseating.

Skew bridges have several disadvantages due to the unsymmetrical geometry along their longitudinal direction. Per American Association of State Highway and Transportation Officials (AASHTO) (1996) [7], skew bridges can have large displacements at supports under earthquake loads. Those large displacements are caused by the rotation of the superstructure about a vertical

axis through the center of stiffness of the substructure. Therefore, skewed spans have a higher tendency to get damage due to unseating caused by imposed earthquake loads than the straight bridges.

Per American Railway Engineering and Maintenance of Way Association (AREMA) Manual for Railway Engineering (2006) [8], it is recommended that skew concrete bridges should be avoided when possible. When skewed bridges are unavoidable, some guidelines about type and design of the structure are proposed. It is also recommended that, all other concrete bridges which are different from those guidelines should be evaluated on a case by case basis.

Several bridge design specifications, like the ones indicated above, have some restrictions in design and construction. In summary, according to those specifications, skew bridges are not preferable, and case studies are recommended when skewness is not avoidable due to alignment restrictions. In this study a closer look is taken on the seismic behavior of multisimple-span skewed bridges, and retrofit and rehabilitation methods using link slabs are discussed.

To conclude, the purpose of this study is to identify the differences in response of skew bridges under service and earthquake loads and investigate response variations due to addition of link slabs under the same set of loads.

CHAPTER 2

LITERATURE REVIEW

2.1 Bridges Having Continuous Decks

2.1.1 Years 1956 - 1996

Studies on continuous bridges between 1956 and 1996 were summarized by Caner [4] and by Caner and Zia (1998) [1].

Wasserman [9] and Loveall [10] who have designed several jointless bridge decks with continuous girders have also expressed their experiences in construction and rehabilitation of these bridges in 1956.

Burke [11] investigated the behavior and limitations of integral bridges which have continuous spans. These bridges are designed as single or multi simple-span with jointless decks and they have capped pile-stub type abutments.

Another study on jointless bridge decks with continuous girders was made by Osterle et. al. [12]. Continuity of girders was provided by using continuity steel and end diaphragms at bridge piers. Their design approach has been used by many state highway departments of the United States. However, the recommended design method requires excessive reinforcement for the deck. In actual practice, most designers use less amount of steel for the deck based on their past experience.

Freyermuth [13] developed a design procedure for continuous bridges with precast, prestressed girders connected to each other by diaphragms at the piers and a jointless deck above the girders. In his design, he also considered the effects of creep and shrinkage.

In 1981 Zuk [14], investigated continuous jointless bridge decks supported by simply supported girders. When the girders are kept simply supported, the cost for end diaphragms, used to provide continuity of the girders, is eliminated and the construction detail is greatly simplified. Zuk investigated the effects of expansion and contraction of continuous deck, and the interactive forces occurred between the continuous deck and the girders.

Gastal and Zia [15] developed a finite element method of analysis for jointless bridge decks supported with simple-span girders in the late 1980's. The analysis method considered the effects of non-linearity of material properties, cracking of concrete, thermal changes, creep, shrinkage and different load conditions. The results of computer analysis were compared with the results of different tests of simply-supported beams (without a continuous deck), because of the lack of experimental data.

Later El-Safty [6] improved the finite element program of Gastal and Zia by partial debonding of the deck from the supporting beams. He also assumed a constant strain through the depth of the link slab while Gastal and Zia used a linearly varying strain through the depth of the link slab.

Richardson [16] also developed a design guideline for jointless bridge decks. He generated computer programs to predict the crack width and spacing in the deck and to calculate the vertical deflection of the structure.

Above mentioned analytical studies about analysis and design of jointless bridge decks had no experimental validation. At mid 90's, Caner and Zia [1] performed a test program to investigate the behavior of jointless bridge deck, and they developed a simple design guideline for link slabs. During their research program live load tests for bridges with link slabs were conducted and the static response of link slabs was investigated. Their study also included time-dependent effects and thermal loads. The design method proposed by Caner and Zia can be summarized as follows:

- 1) Design each span of the bridge as simply supported without considering the effect of link slab since flexural stiffness of the link slab is much smaller than that of composite girders.
- 2) Debond the deck from girder by 5% at each girder end to provide a further increase in the flexibility of the link slab. According to the studies of El Safty [6], debonding up to 5% of the span length does not affect the load deflection behavior of the jointless bridge decks supported by simple span girders.
- 3) Determine the maximum end rotations of simply supported girders subjected to service loads. Impose those end rotations on the link slab and determine moments caused by those rotations by using the gross section property of the link slab. Design the link slab's reinforcement by using the calculated moments to a limiting allowable working stress such as 40% of the yield strength of the reinforcing bar.
- 4) Check the crack width at the surface of the link slab against AASHTO, 1996 Specifications.

2.1.2 Years 1997 to Present

Later in 2002, the seismic performance of bridges retrofitted with link slabs was studied under longitudinal earthquake only, by Caner et. al. [5]. It was found out that continuity provided by the link slabs can eliminate the span separation problem and the probable damage caused by unseating. The researchers recommended a constant reinforcement ratio in the link slab through the width of the bridge. The link slab details used in the study are shown in Figure 2.1.

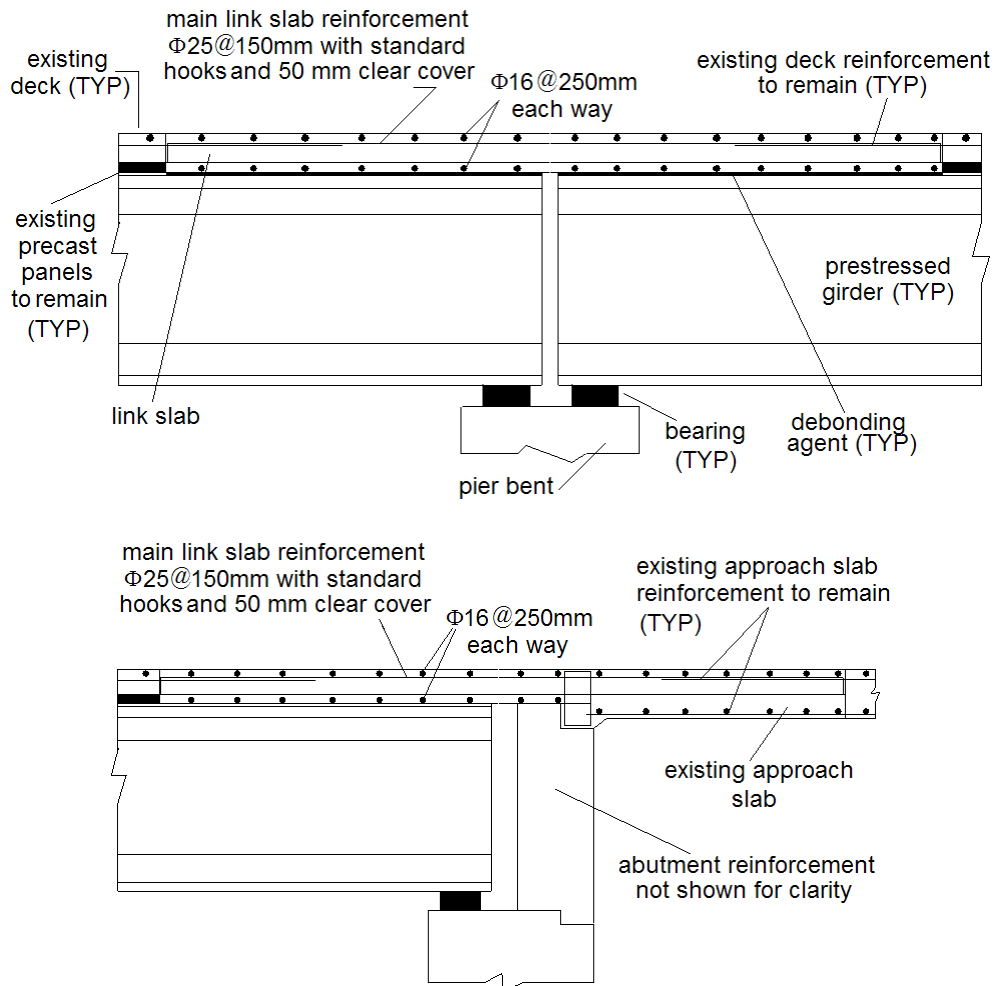


Figure 2.1: Details for link slabs above interior piers and abutments [5]

Wing et. al. [17] presented the results of a research project on the first bridge with link slab in the state of North Carolina in the United States. The bridge rehabilitation was designed according to the guideline proposed by Caner and Zia (1998). The researchers performed a full-scale live load test and long term monitoring to account for the seasonal loading conditions to investigate the performance of the bridge. The aim of the study was to confirm the design assumptions and to recommend changes to the design procedure if it is necessary. At the end of the research program researchers found out that the rotations induced within the link slab were much lower than the assumed ones calculated by the procedure proposed by Caner and Zia (1998). As a result, they concluded that the assumption of simply supported spans is feasible although it is conservative. They also recommend that the crack control criteria should be revised when saw cuts are employed to control the crack location. Moreover, they proposed a limit state method for the design of the reinforcement of the link slab depending on rotational demand.

2.2 Skew Bridges

At a multiple girder superstructure, live loads will be distributed over girders based on their spacing and girder type. Live load distribution factors are generally employed by many bridge codes to simplify the design process. In order to obtain the design live load moment for longitudinal girders, the single girder moment induced by a truck or lane load is multiplied with live load distribution factor. The factors proposed by the AASHTO Standard Specifications for Highway Bridges (1996) are developed without considering the effect of skew angle. The factors recommended by AASHTO, 1996 are applicable for bridges having a skew angle of at most 45° . For the bridges having a skew angle exceeding 45° , more precise methods for the determination of the load distribution factors are recommended.

Ebedio et al [18] found out that as the skew angle increases, span and support girder moments decrease significantly. Effect of skewness on girder moments becomes more apparent when the skew angle is greater than 30°. Therefore it can be stated that, skew angle has an important influence on design of girders. AASHTO Standard Specifications (1996) gives very conservative results for live load distribution of girders since it does not consider the effect of skew angle.

Skew angle is entered as a parameter for the live load distribution factors in AASHTO LRFD Bridge Design Specifications (1998) [19]. Barr et al [20] studied the effect of several factors on distribution factors. They discovered that for an angle of 20°, skew had a little effect on distribution factors. For wider skew angles, the factors decreased with increasing skew angle. For all bridge models analyzed, AASHTO LRFD Bridge Design Specifications (1998) gave conservative results. They observed that the decrease in distribution factors with increasing skew angle was reasonably approximated by AASHTO LRFD (1998).

Since existing design codes give conservative results for live load distribution for girders of skew bridges, live load analyses were made for all bridge models to check for girder stresses due to live loads.

Detailed modeling of bridges is considered as a time-consuming and complicated process. Instead of detailed models, simplified stick models are widely used in preliminary dynamic analysis of bridges when approximate results are satisfactory [21]. In a typical stick model, the superstructure of a bridge is represented by a single beam element and substructure is represented by torsional and translational springs. Although single beam stick models are easy to use and give approximate results, they are not always convenient for

capturing certain vibration modes. As the skew angle of the deck increases, errors become more apparent [21]. Due to the inefficiency of single beam stick models in skew bridges, Meng and Lui [21] developed a dual-beam stick model representation for the bridge deck to include the effect of skewness. The proposed method gives reasonably accurate results for preliminary dynamic analysis when compared with the single beam stick models.

In this study, analyzing the response of the superstructure is in a great importance, since the main scope is to identify the effect of link slab and skewness. Stick models may not be convenient to be used in modeling of the bridges with link slabs. In this research, detailed refined models were used for static and dynamic analyses. Details about modeling process will be given later in Chapter 4.

CHAPTER 3

IDENTIFICATION OF THE MOST COMMON TYPES OF HIGHWAY BRIDGES IN TURKEY

3.1 Bridge Survey

Types of highway bridges in Turkey were tried to be identified after conducting a survey on seventy six bridges to be used in this research. The data for 55 bridges built between 2000 and 2005 were collected from a bridge design company, MEGA Mühendislik. The rest of the data was taken from a case study done by Caner et. al. [22] on service life assessment of the existing bridges on a hundred and seventy kilometer long highway route between Çanakkale and Bursa. Detailed information of the bridge models are illustrated in Appendix A. Bridges were identified according to their skew angle, maximum span length, number of spans, ratio of cap beam inertia to column inertia (I_{cb}/I_c) and ratio of column spacing to height of the column (L/H). These factors are illustrated in Figure 3.1. Figures 3.2 through 3.6 show the characteristics of standard highway bridges in Turkey.

Skew angles of surveyed bridges range between 0° and 60° with a median frequency of 15%. The frequencies of all skew angles are close to each other. Span lengths range from 10 to 40 meters, most of them populated between 15 and 30 meters. Number of spans ranges for 1 to 9. The majority of them have 2 to 4 spans. More than 50% of the bridges have capbeam to column inertia ratio of 0.1. L/H of bridge bents generally has values between 1 and 2.

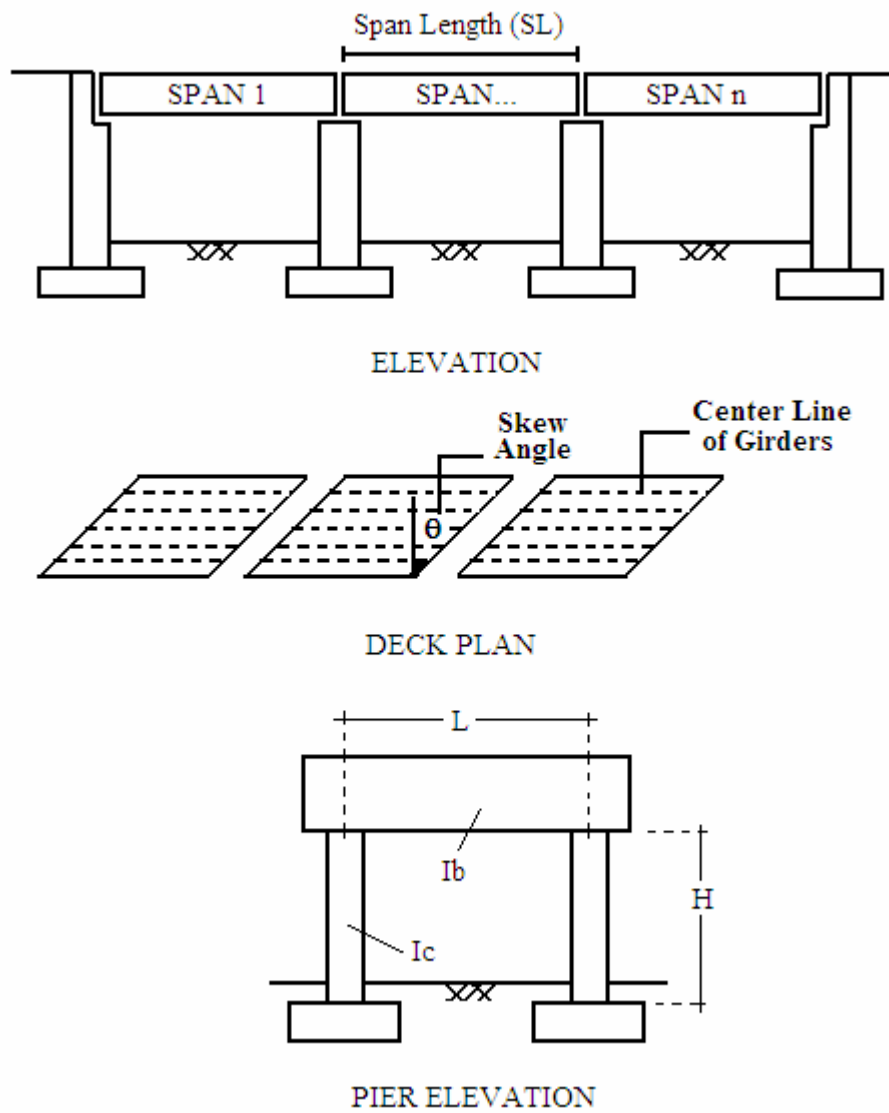


Figure 3.1: Typical bridge components

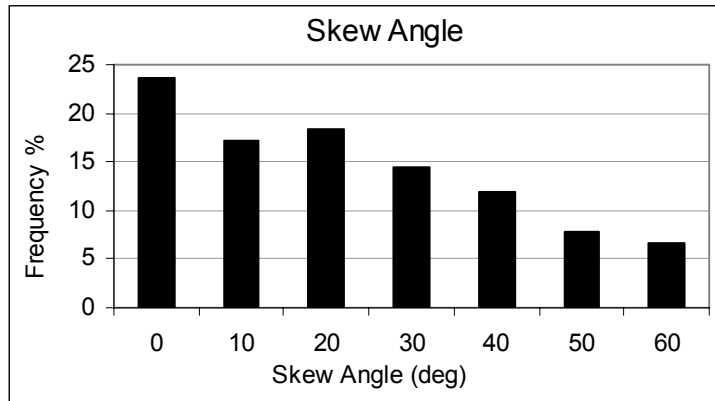


Figure 3.2: Skew angle

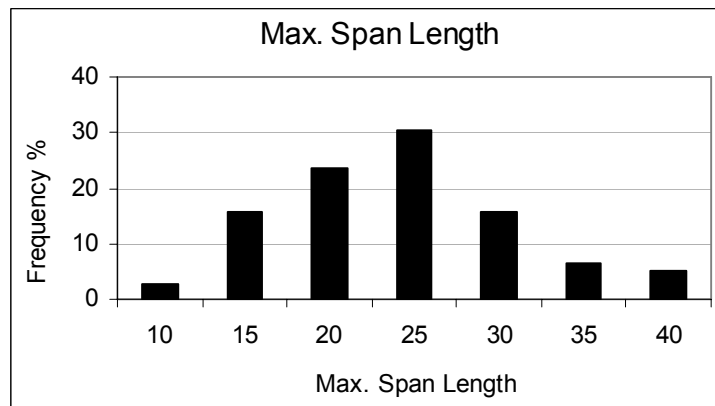


Figure 3.3: Maximum span length

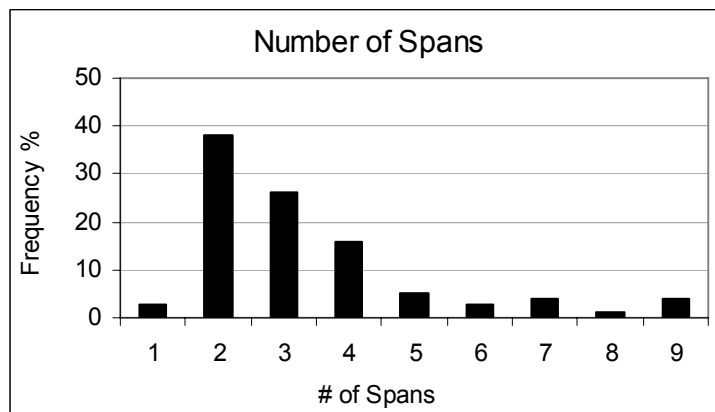


Figure 3.4: Number of spans

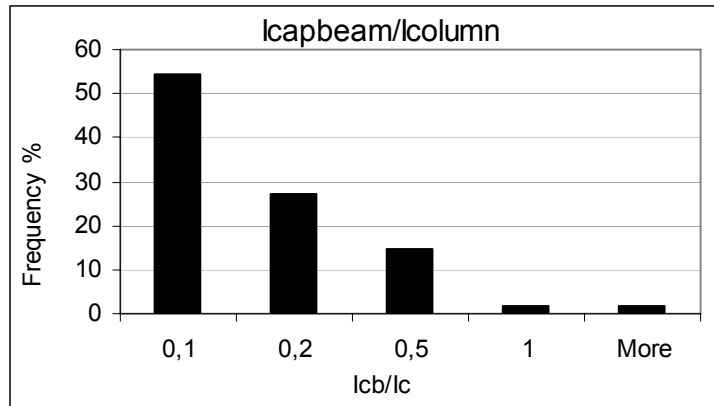


Figure 3.5: Ratio of beam to column inertia

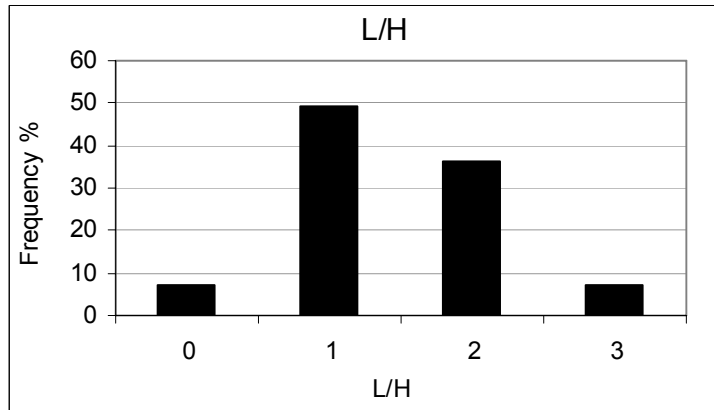


Figure 3.6: Bent characteristics

3.2 Generated Bridge Models

112 different computer models were generated to investigate the effect of the skew angle and the link slab. Those 112 different bridge models were developed to represent standard bridges with different combinations of properties namely: skew angle, number of spans, span length, L/H, I_{cb}/I_c and presence of the link slab. Different values taken for these parameters illustrate representative characteristics of surveyed bridges and are schemed in Table 3.1.

Table 3.1: Bridge parameters

Property	Values
1) Skew Angle	0°, 20°, 40°, 60°
2) Number of Spans	2, 4
3) Span Length (SL)	18 m., 25 m.
4) I_{cb}/I_c	0.1, 1.5
5) L/H	1.0, 1.5
6) Link Slab	No, yes

Two ratios of cap beam inertia to column inertia were selected to be 0.1 and 1.5. I_{cb}/I_c ratio of 0.1 was chosen depending on the results of surveyed data, in order to reflect typical Turkish design practice. The I_{cb}/I_c ratio of 1.5 was used with reference to Applied Technology Council (ATC) 32-1: Improved Seismic Design Criteria for California Bridges [23], in order to use the representative ratio based on analysis of typical bents in the USA. In the USA, it is typically desired to have weak columns rather than weak cap beams in earthquake regions. This is due to the fact that cap beam damage may cause the disturbance of the whole superstructure leading to hard and uneconomical maintenance problems. But on the contrary, in Turkey the general trend is to have stronger columns. Cap beam cross section does not change between different models and was taken as a rectangle having a depth of 1.1 m. and a width of 1.2 m. (1.1m *1.2m). Corresponding column cross sections for the two cases is given in Table 3.2.

Table 3.2: Column Cross Sections

	I_{cb}/I_c	Cap Beam Cross Section	Column Cross Section
1)	0.1	Rectangle (1.1m * 1.2m).	Rectangle (2.5m * 1m)
2)	1.5	Rectangle (1.1m * 1.2m).	Circle (D = 1.2m)

As it is shown in Figure 3.1, L is the centerline to centerline distance between two columns of the bridge bent and H is the height of the column. Two different L/H ratios of 1.0 and 1.5 were used in the study since the majority of the surveyed bridges have L/H between 1.0 and 2.0 (Figure 3.6). Column to column distance (L) is taken as 7 m. for all of the investigated bridge models where the height of the columns (H) for the two cases is shown in Table 3.3.

Table 3.3: Column Heights

	L/H	L	H
1)	1.0	7 m.	7 m.
2)	1.5	7 m.	4.6 m.

As indicated previously, 112 bridge models were created by combining six different bridge properties shown in Table 3.1. These 112 bridge models are composed of four main groups namely A, B, C and D.

Group A is the control set for the investigated bridges. Other three groups are originated from Group A bridges by changing only one property at a time. With this systematic procedure, effects of variation in properties were investigated by comparing the bridge's behavior in new groups with the behavior of the ones in Group A.

Group A has 32 bridge models all having $L/H = 1.0$ and $I_{cb}/I_c = 0.1$. All columns have a height of 7.0 m with a rectangular cross section of 2.5m by 1m. 16 of those 32 bridge models have continuous decks. For these bridges only interior deck joints are eliminated by using link slabs. Figure 3.7 shows deck plan of Group A, B and C bridges with link slabs. All the bridge models are numbered. Bridges having an even ID are the link slab versions and the bridges having an odd ID are without link slab. On the other hand, all bridge models in Group D (with even or odd ID) have link slabs.

Group B bridges are obtained from Group A bridges by changing only L/H to 1.5, in other words by decreasing the height of the columns down to 4.6 m.

Group C bridges are also created from Group A bridges, by changing this time I_{cb}/I_c to 1.5. I_{cb}/I_c of 1.5 is obtained by using circular cross sections of diameter 1.2 m for the columns.

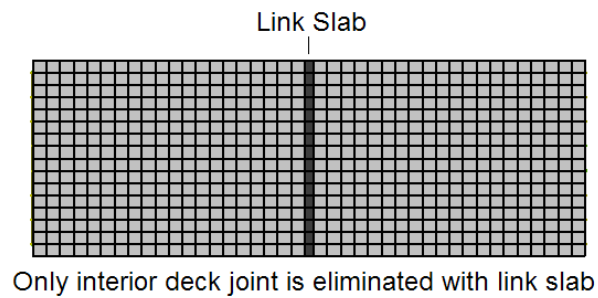


Figure 3.7: Deck plan of Group A, B and C bridges with link slab

Group D have only 16 continuous decked bridges. The bridges of Group D are created by eliminating the exterior deck joints of Group A bridges with link slab. In other words, all bridges in Group D have continuous deck between abutments. Figure 3.8 shows the deck plan of the Group D bridges with link slab.

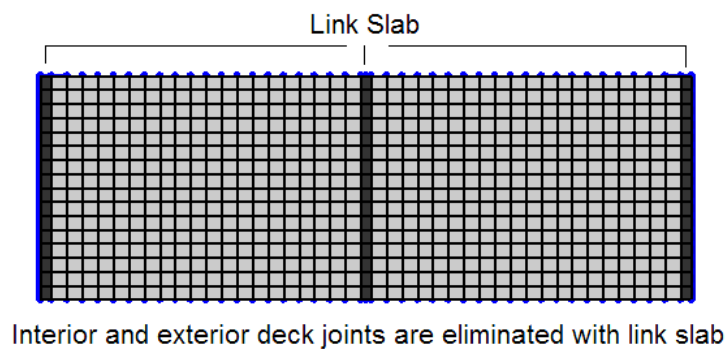


Figure 3.8: Deck plan of Group D bridges

The properties of all bridges are given in a detailed way in Appendix B.

CHAPTER 4

ANALYSIS PROCEDURE

4.1 Computer Modeling

4.1.1 Introduction

Bridges were modeled using LARSA 4D Structural and Earthquake Engineering Integrated Analysis and Design Software. Properties, and coordinates of all elements can be created by using spreadsheets in LARSA 4D. In order to model parts of the bridges (joints, deck, girders, bearings, cap beams), a macro code was developed using Microsoft Excel that can be copied to LARSA 4D. Macro code can be found in Appendix C. This advantageous feature of LARSA 4D enabled the modeling process of the bridges to be completed in a rather shorter time. Remaining components of the models were created by using drawing commands of the program.

Models have three main groups namely, superstructure, substructure and supports. Decks, link slabs, girders and cross beams constitute superstructure. Substructure has components of columns, cap beams and foundation elements. Bearings and shear keys are categorized as supporting elements. In Figure 4.1, components of a 3D bridge model are shown. In the following divisions of this subchapter modeling procedure will be described for these three main groups.

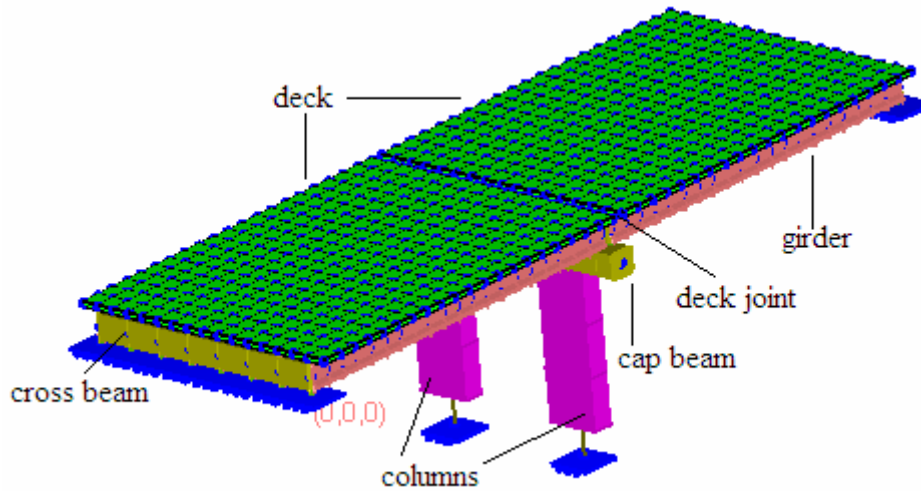


Figure 4.1: Bridge components

In Table 4.1, the material properties of components can be found. The weights of bordures, wearing surface, barriers, sidewalk, etc. are included in the unit weight of the deck.

Table 4.1: Material properties of the bridge components

Name	Modulus of Elasticity (kN/m ²)	Poisson Ratio	Shear Modulus (kN/m ²)	Unit Weight (kN/m ³)	Thermal Expansion (1/°C * 10 ⁻⁶)
Girder	$3.04 * 10^7$	0.17	$1.30 * 10^7$	23.55	9.90
Rigid	$3.04 * 10^9$	0.16	$1.30 * 10^9$	0.00	0.00
Deck	$2.48 * 10^7$	0.17	$1.06 * 10^7$	35.32	9.90
Cap Beam	$2.48 * 10^7$	0.17	$1.06 * 10^7$	23.55	9.90
Column	$2.48 * 10^7$	0.17	$1.06 * 10^7$	23.55	9.90
Crossbeam	$2.48 * 10^7$	0.17	$1.06 * 10^7$	23.55	9.90

4.1.2 Modeling of Superstructure

Bridge deck, modeled with four node plate elements, had a thickness of 220 mm. Link slabs were modeled to have an effective moment of inertia equal to

the 35% of the gross moment of inertia of the deck, to account for cracking. An effective equivalent thickness of 160 mm. was used for the link slabs. A gap of 0.05 meters was provided at expansion joints. The shell elements of regular bridges were rectangle in geometry while the ones of skewed bridges have parallelogram shapes as shown in Figure 4.2. This fact does not appear to be a problem since LARSA 4D condenses four triangles to form the quadrilateral element [24].

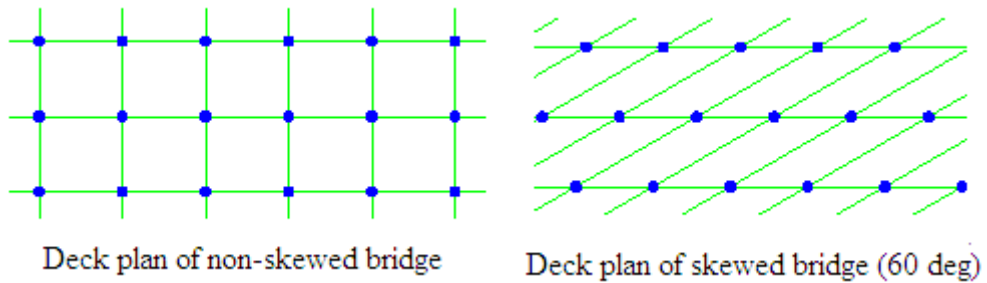


Figure 4.2: Plate geometry of deck elements

I-girders are the most commonly used bridge sections for short span bridges (span length = 15 to 30 meters). For the bridges having span length of 24 to 35 meters, prestressing against own weight; and post-tensioning against the additional weight of the slab can be utilized [25]. All modeled bridges have a width of 13 meters having eight (8) equally spaced simply supported prestressed I-girders. The prestressed I-girders were modeled by beam elements at their neutral axis. Each I-girder of a span is divided into 20 pieces to provide a fine mesh for superstructure. Two different I cross sections used in Turkish practice were chosen depending on maximum span length of the bridge. For the bridges having maximum span length of 18 meters and 25 meters, I-girder cross section of 1 and 2 were used, respectively. Girder cross sections are sketched in Figure 4.3 and 4.4.

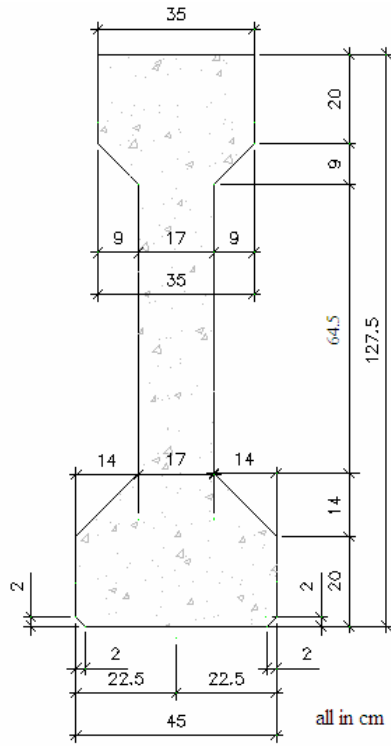


Figure 4.3: Girder cross-section 1; for SL=18 m.

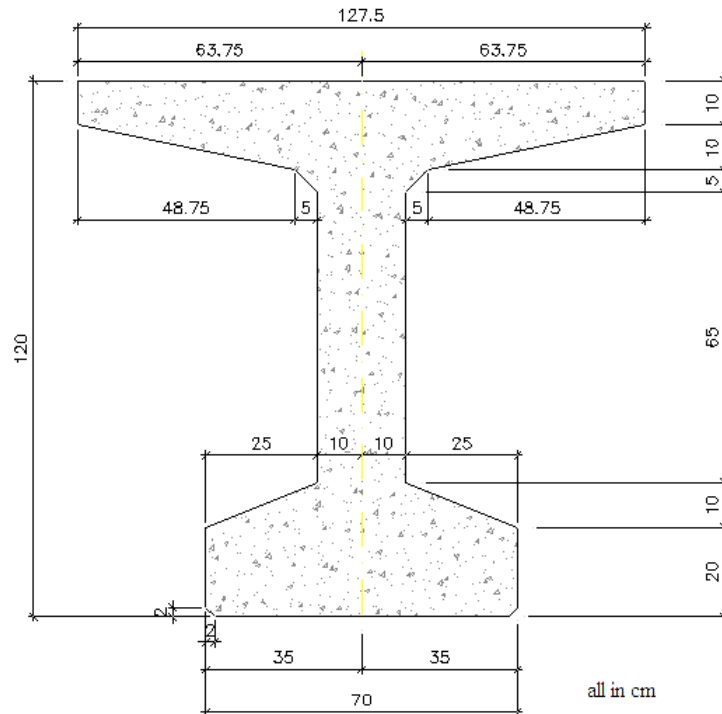


Figure 4.4: Girder cross-section 2; for SL=25 m.

Deck and the girders were made composite by means of rigid links. The link slab was debonded at girder ends by 5% of the span length as proposed by Caner ad Zia [1]. Debonding was obtained by eliminating the rigid links between the deck and the girder at debonding zones. Longitudinal close view of a bridge model with link slab is shown in Figure 4.5.

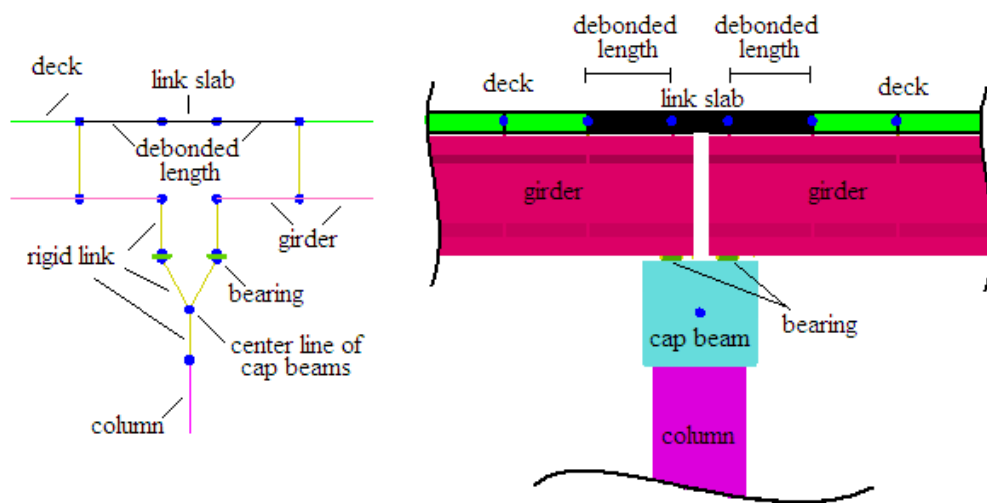


Figure 4.5: Longitudinal close view of a bridge model with link slab

Diaphragms are usually placed at the supports and along the span to provide an equal live load distribution between the girders. Possible lateral distortions of girders can be minimized by diaphragms during transverse earthquake loads [26]. The external diaphragms at end spans transfer the load from webs through the pier system. Internal diaphragms may have disadvantageous effects due to the additional structural dead load and limited slab shrinkage in transverse direction which causes deck cracking [25]. Therefore, besides the two external diaphragms at supports only one internal diaphragm existing at the middle of each span was used in the models to provide load sharing between the girders. In skewed models, they were placed parallel to the skew line. Rectangular diaphragms having a height of 1.2 meters and a width of 0.25 meters were used in models.

4.1.3 Modeling of Substructure

A typical bridge bent has two columns. Two column cross-sections used in Turkish practice were employed for the models. The first one is a 2 meter long rectangular shape whose edges are curved with half circles having a diameter of 1 meter. An equivalent rectangular cross section of 1 m * 2.5 m is used in the models. The second one has a circular cross-section having a diameter of 1.2 meters as shown in Figure 4.7. Columns were modeled by three stick elements of equal length at their neutral axis for a better mass distribution.

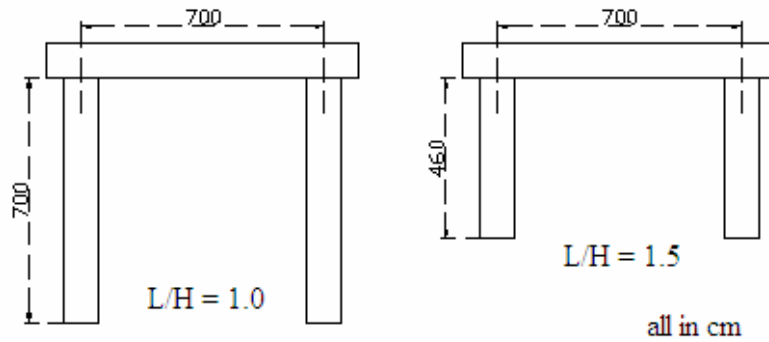


Figure 4.6: Bridge bents for different L/H

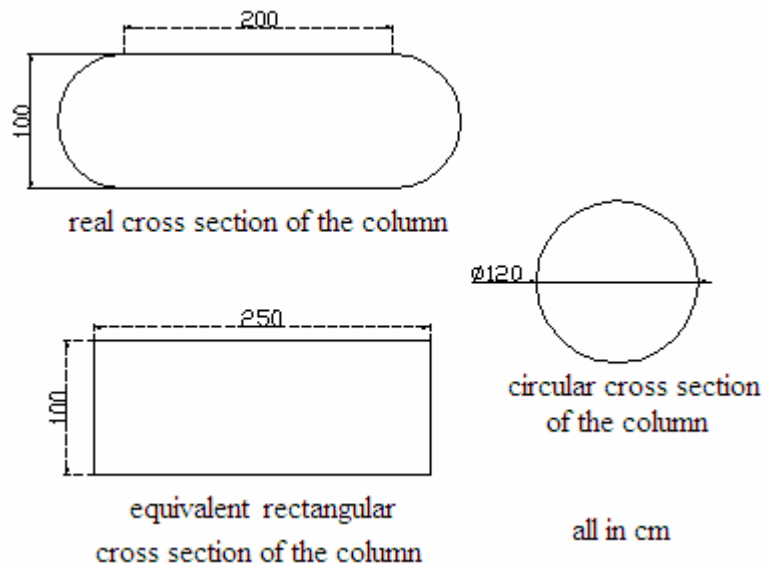


Figure 4.7: Column cross sections

Cap beams were modeled with beam elements connected to nodes at the column face with rigid link elements. They were also connected into the bearings at top by means of two rigid link elements. In skew bridges, they were placed along skew line. For cap beam elements a rectangular cross section having a height of 1.1 m. and a width of 1.2 m. was used.

At foundation level, bents were assumed not to translate or rotate representing a fixed foundation anchored into rock. This research does not include soft soil – structure interaction. Column elements were extended to the fixity point of footings with rigid link elements having a length of 1.5 m.

4.1.4 Supports

Movement joints at superstructure are provided to allow longitudinal displacement induced by temperature, shrinkage and creep effects. If the displacement capacity of movement joints is exceeded during a seismic event, span unseating can be observed. Expansion bearings, a type of movement supports placed between superstructure and substructure can provide longitudinal and transverse translation, and rotation. Elastomeric bearings recommended in AASHTO, 1996 [7] are expansion type of bearings that provide a resisting force proportional to deck displacement (Figure 4.8). Stiffness of a bearing can be adjusted depending on its dimensions and rubber thickness [25].

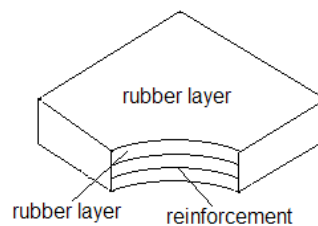


Figure 4.8: Elastomeric bearing, AASHTO, 1996 [7]

Six reinforcement sheets having a thickness of 2 mm were used for each bearing. The dimensions of the bearings are shown in Figure 4.9.

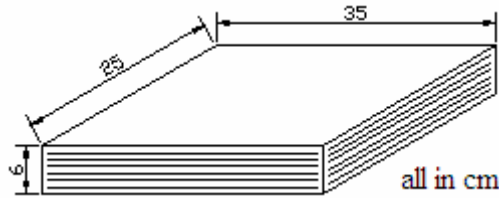


Figure 4.9: Bearing dimensions

Shear modulus of the elastomer was obtained according to its hardness per AASHTO, 1996. Shear modulus was taken as 1103 kN/m^2 for a nominal hardness of 60 on the Shore A scale.

Investigated bridges do not have any fixed supports in longitudinal direction which is very common in Turkish engineering practice. Maximum horizontal load of elastomeric bearings was calculated by the following formula per AASHTO, 1996.

$$H_m = G(A_{\text{bearing}})\Delta_s/h_{rt} \quad (4.1)$$

where:

G = shear modulus of the elastomer (kN/m)

A_{bearing} = plan area of elastomeric element or bearing (m^2)

Δ_s = maximum shear deformation of the elastomer (m)

h_{rt} = total elastomer thickness (m)

and

$$K_{\text{long}} = H_m / \Delta_s \quad (4.2)$$

where:

K_{long} is the horizontal longitudinal stiffness of the bearing (kN/m).

During an earthquake, adjacent superstructure elements can move out of phase in transverse direction, relative to each other. Shear keys were employed between the girders to restrain transverse bearing displacements and to control the unseating of the girders during a seismic activity. Shear keys typically are sacrificial seismic elements of the bridges. Sectional and material properties of the shear key are listed in Table 4.2.

Table 4.2: Shear key properties

Width =	1.125 m
Length =	1.200 m
Height =	0.400 m
f_c' =	$2.50 * 10^7$ kN/m ²
E_{conc} =	$2.40 * 10^7$ kN/m ²
$I_{eff}(shear\ key)$ =	0.071 m ⁴
$K_{transverse}$ =	$7.90 * 10^7$ kN/m

where:

f_c' = compressive strength of concrete at 28 days (in MPa)

E_{conc} = modulus of elasticity of concrete in MPa calculated from the following formula;

$$E_{conc} = 4800 (f_c')^{0.5} \quad (4.3)$$

$I_{eff}(shear\ key)$ = effective moment of inertia (= $0.5 * I_{gross}$)

K_{trans} = stiffness of the shear key calculated from the following approximation;

$$K_{trans} = 3E_{conc}I_{eff}/L^3 \quad (4.4)$$

Vertical stiffness of a bearing can be calculated by using following formula taken from AASHTO, 1996:

$$K_{vertical} = E_c A/L \quad (4.5)$$

$$E_c = 6G(S_{(bearing)})^2 \quad (4.6)$$

where:

G = shear modulus of elastomer (kN/m^2)

E_c = effective modulus of elastomeric bearing in compression (kN/m)

$S_{(\text{bearing})}$ = shape factor of one layer of an elastomeric bearing calculated from the following formula;

= Plan Area / Area of Perimeter Free to Bulge

= $LW/(2h_{\text{max}}(L+W))$ for rectangular bearings without holes (4.7)

Rotational stiffness of a bearing can be calculated by using following formula per AASHTO, 1996:

$$k_{\theta} = M_m / \theta_m \quad (4.8)$$

$$M_m = (0.5E_c I_{\text{bearing}}) \theta_m / h_{rt} \quad (4.9)$$

where:

M_m = maximum bending moment for elastomeric bearing

I_{bearing} = moment of inertia of plan shape of bearing (m^4)

θ_m = maximum design rotation (rad)

E_c = effective modulus of elastomeric bearing in compression (kN/m)

h_{rt} = total elastomer thickness (m)

Properties of an elastomeric bearing are listed in Table 4.3.

Table 4.3: Properties of elastomeric bearings

Steel thickness =	0.002 m
Number of steel layer =	6
Width (transverse) =	0.35 m
Length (longitudinal) =	0.25 m
Height =	0.06 m
Total elastomer thickness =	0.048 m
Bearing area =	0.0875 m ²
Shape factor (S) =	9.114583
Shear Modulus (G)	1.10 * 10 ³ kN/m ²
Elastic modulus =	5.50 * 10 ⁵ kN/m ²
Longitudinal translational stiffness (K _{long})=	2.01 * 10 ³ kN/m
Transverse translational stiffness (K _{trans}) =	7.90 * 10 ⁷ kN/m
Vertical translational stiffness (K _{vertical}) =	8.02 * 10 ⁵ kN/m
Longitudinal rotational stiffness (K _{θl}) =	2.61 * 10 ³ kNm/rad
Transverse rotational stiffness (K _{θt}) =	5.12 * 10 ³ kNm/rad

4.2 Analytical Methods

4.2.1 Response Spectra Analysis (RSA)

Response spectrum concept is an extensively used tool in earthquake engineering to express characteristics of ground motions and their effects on structures. Response spectrum represents the maximum response of a single-degree-of-freedom (SDOF) system, as a function of its natural frequency and damping ratio, to an earthquake motion [27]. Response spectrum curves are plots of maximum responses (acceleration, velocity, displacement) of a SDOF system to a particular excitation at different natural frequencies (or periods) for a specified damping ratio. Response Spectra Analysis (RSA) provides computation of peak responses of a multi-degree-of-freedom (MDOF) system by using these response spectra curves. In RSA, structural responses (member forces, displacements, etc.) are computed under a spectrum of earthquake records for each mode of vibration combined by some statistical procedures to

give possible maximum response of the structure. The main modal combination rules are absolute sum (ABSSUM), complete quadratic combination (CQC) and square-root-of-sum-of-squares (SRSS) [28].

Response spectra analysis was performed for all investigated bridge models using bridge analysis program LARSA 4D. It should be underlined that, for each model, 60 modes of vibration were analyzed. LARSA 4D uses CQC modal combination formulation proposed by A. Der Kiureghian (1981) [24].

RSA is a static elastic analysis method which uses the natural frequencies, mode shapes and modal damping ratios of the structure and the dynamic properties of the excitation in computation. Consequently, it is a well established procedure for dynamic analysis [24].

RSA is a commonly utilized method in structural design compared to time history analysis. It provides a rational and time efficient method for dynamic analysis of structures. Time history analysis, which is an exact dynamic analysis method, is not implemented for regular design practice since it requires a huge amount of time and effort. Using linear time history analysis for design is uneconomical and time inefficient. Using non-linear time history analysis for design is almost impossible. Designer has to know sizes and reinforcement beforehand to make a non-linear analysis. Run time for non-linear time history analysis can be beyond tolerable limits. If an engineer selects non-linear time history analysis as a design tool, and if the engineer makes a wrong selection in sizing the structure that will require iterative runs, it may be very costly for the client. In industry practice, based on personal communication with Caner, the computer runs were limited for a maximum of 15 minutes of run-time so that if there is an error in design, the designer can give a quick decision by a simple iteration to correct it. Therefore; the

designers typically select time-efficient response spectra analysis for the design that requires time efficient iterations.

The design spectra used for design of new structures and for assessment of existing buildings are utilized in RSA to expected earthquakes with a return period of 475 years. A response spectrum obtained from a particular ground motion happened in a past earthquake can not be directly used unless engineer approves. Response spectra curves obtained from past earthquakes have highly irregular response based on the soil conditions, frequency content and closeness to fault line. Design response spectra specified in codes typically cover all of the possible earthquakes at a site rather than a particular one [28]. A design spectrum is achieved by smoothing, averaging or enveloping the response spectra of ground motions developed during past earthquakes at a site. If there exists no recorded excitations for the site, ground motions recorded at different sites under similar conditions should be used to generate the design spectrum [27].

RSA of the investigated bridges were based on the design response spectrum recommended in AASHTO, 1996. A seismic response coefficient characterizes the earthquake load to be used in the elastic analysis for seismicity. The elastic seismic coefficient is given in AASHTO, 1996 by the dimensionless formula:

$$C_s = 1.2AS/T^{(2/3)} \quad (4.10)$$

where:

A = the acceleration coefficient

S = coefficient for the soil profile characteristics of the site

T = the period of the bridge (sec)

Most of the bridges in surveyed data happened to be at high risk seismic zones. Therefore, the acceleration coefficient (A) was taken to be 0.4g, which is the maximum value per Turkish Specification for Structures to be Built in Disaster Areas, 1997 for a return period of 475 years [29].

As it was previously mentioned, for simplicity, all bridges were assumed to be located on rock sites since the focus of the study is not related with soil – structure interaction. Soil profile type I of ASSHTO, 1996 is used for any type of rock sites. Therefore, the coefficient for the soil profile (S) was taken equal to 1.0, accordingly.

It is also indicated in AASHTO, 1996 that C_s need not exceed 2.5A. The corresponding response spectrum used for RSA of the bridges is sketched in Figure 4.10.

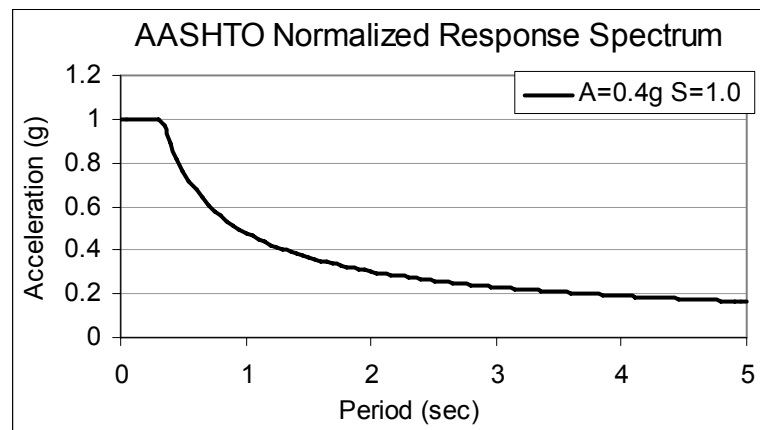


Figure 4.10: AASHTO normalized elastic response spectrum for 5% damping

The load combinations used in the analyses for earthquake loadings are;

$$DL + EQ_L + 0.3EQ_T + 0.3EQ_V$$

$$DL + 0.3EQ_L + EQ_T + 0.3EQ_V$$

$$DL + 0.3EQ_L + 0.3EQ_T + EQ_V$$

Typically, EQ_v component is not included in the analysis except for the case when the engineer sees using the vertical component as essential. In this study, EQ_v RSA is assumed to be equal to the EQ_L & EQ_T RSA. In practice, sometimes 2/3 of EQ_L or EQ_T is used in analysis based on common engineering judgment [23].

4.2.2 Linear Time History Analysis (LTHA)

Time history analysis is a dynamic analysis method, which gives the response of a structure in a time domain. Time-dependent loads are either in the form of excitation records, or curves [24]. Time history analysis gives an exact dynamic analysis procedure by using a number of earthquake records. It is a more reliable and rational method used for dynamic analysis. The analysis should be repeated for a number earthquake motion in order to obtain accurate results.

Using LTHA in this study serves two purposes:

- 1) Compare RSA results with LTHA results. RSA was applied for all of the models. However, LTHA, a time inefficient analysis tool, was applied only for selected models.
- 2) Compare responses of Turkish time history records with American response spectra to observe the safety of the AASHTO requirements. In Turkey AASHTO specifications are used for bridge design.

Four bridges namely, A7, A8, A31 and A32 were investigated with LTHA. 4 spanned bridges having a span length of 25 meters were chosen for LTHA, since they are the longest bridges models. Properties of the selected bridges can be found in Appendix B. To evaluate bridge skew angle factor, straight bridges (A7 and A8) and bridges having a skew angle of 60° (A31 and A32) were analyzed. Link slab versions (A8 and A32) of the bridges (A7 and A31) were also evaluated.

Time history excitation records were assigned to mass joints excluding the supports. Throughout the integration processes, constant time step sizes were used. The ending time for the integration process was chosen to be 25 seconds.

In a time history analysis, Rayleigh damping is utilized. Rayleigh damping is [28]:

$$c = a_0m + a_1k \quad (4.11)$$

where;

c = Rayleigh damping

m = mass of the system

k = stiffness of the system

a_0 = mass-proportional Rayleigh damping constant

a_1 = stiffness-proportional Rayleigh damping constant

If both i^{th} and j^{th} modes are assumed to have the same damping ratio ξ , then mass-proportional and stiffness-proportional Rayleigh damping constants can be calculated by using the following formulas:

$$a_0 = (2\xi\omega_i \omega_j) / (\omega_i + \omega_j) \quad (4.12)$$

and

$$a_1 = 2\xi / (\omega_i + \omega_j) \quad (4.13)$$

where;

ω_i and ω_j = natural frequencies in rad/sec for the i^{th} and j^{th} modes, respectively.

In a time history analysis natural periods T_i and T_j are selected as 0.05 seconds and 1.5 seconds, respectively to cover the range of bridges. For the natural periods between $T_i = 0.05$ sec. and $T_j = 1.5$ sec., the Rayleigh damping will be smaller than the constant damping ratio of $\xi = 0.05$. Therefore, it was guaranteed that, corresponding modal responses will not be eliminated because of high damping. Corresponding natural frequencies ω_i and ω_j are appeared to be 125.66 and 4.19 hertz depending on the formula:

$$\omega = 2\pi / T \quad (4.14)$$

where:

T = natural period of the system (second)

For the selected natural periods 0.05 and 1.5 seconds and a constant damping ratio of $\xi = 0.05$, the Rayleigh damping constants were calculated as $a_0 = 0.405$ and $a_1 = 0.0008$.

Previously, it was mentioned that a set of five earthquake records was used, depending on AASHTO, 1996 requirement, for LTHA of the four models (A7, A8, A31 and A32). The earthquake records were taken from the study of Akkar [30], [31].

The earthquake records taken from the study of Akkar used for THA are near-fault records of 1999 Marmara earthquakes. Unlike Uniform Building Code [32] or Caltrans Seismic Design Criteria [33], AASHTO, 1996 does not have amplification factors for spectral acceleration for the structures in the close

proximity to an active fault. Therefore different from RSA, the results of THA will also include near-fault effects on seismic behavior of generated models.

The vertical components of earthquake records are in great importance for structural design of bridges, unlike most other kinds of structures. The vertical components of excitations can lead to deck unseating when they are combined with the horizontal components. They may also create significant bending moments in long prestressed bridge spans [25]. Because of the above mentioned importance of vertical earthquake component on bridge behavior, the records having three components (two horizontal and one vertical) were chosen for THA.

Since all the bridge models were assumed to be placed on rock sites, the records which were taken on rock were tried to be employed for the THA. Three of the selected excitations were recorded on rock sites and the other two of them were on soil. The details of earthquake records used in the analyses are shown in Table 4.4.

Even if the AASHTO RSA has a 475 years return period, the selected time history records has about 250 years return period based on personal communication with Dr. Semih Yücemem.

Table 4.4: Earthquake records used for the THA

Earthquake	Magnitude (Mw)	Recorded place	Distance to fault (km)	Site classification
1999 İzmit	7.4	Yarımca	3.28	rock
1999 İzmit	7.4	İzmit	4.26	rock
1999 İzmit	7.4	Gebze	7.74	rock
1999 İzmit	7.4	Düzce	17.06	soil
1999 Düzce	7.2	Bolu	20.41	soil

In the following Figures 4.11 through 4.20 acceleration time histories of the records and also pseudo acceleration spectra of the records together with AASHTO, 1996 response spectrum for rock sites are plotted even if some records taken from a soil site.

The results of first three records reported to be taken from rock site were compared to the RSA rock site responses. The results of last two records were compared to the first three records to evaluate the importance of soil site.

e-w, n-s and v abbreviations used in the following figures stand for east-west, north-south and vertical directions, respectively. In all of the THA, e-w components of the records were applied in transverse direction of the bridges. Similarly, n-s components of the earthquake records were applied in longitudinal direction, and v components of the records were applied in the vertical direction of the bridges at the same time domain.

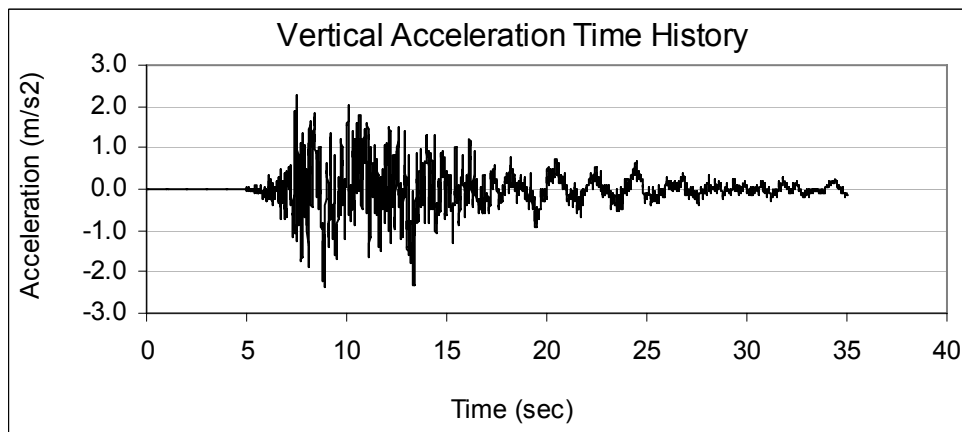
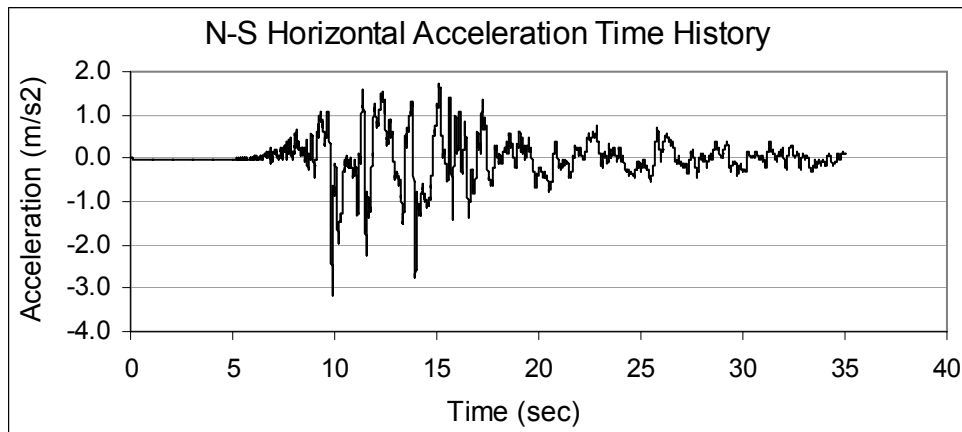
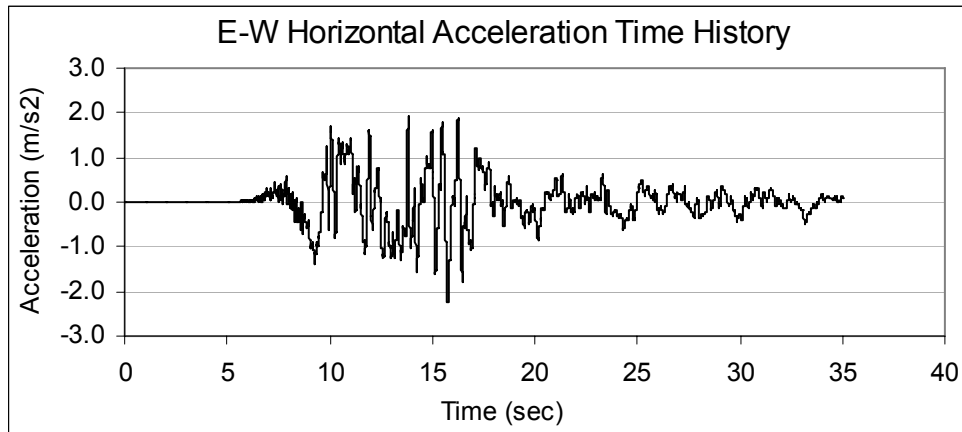


Figure 4.11: Acceleration time histories of Yarımcı record

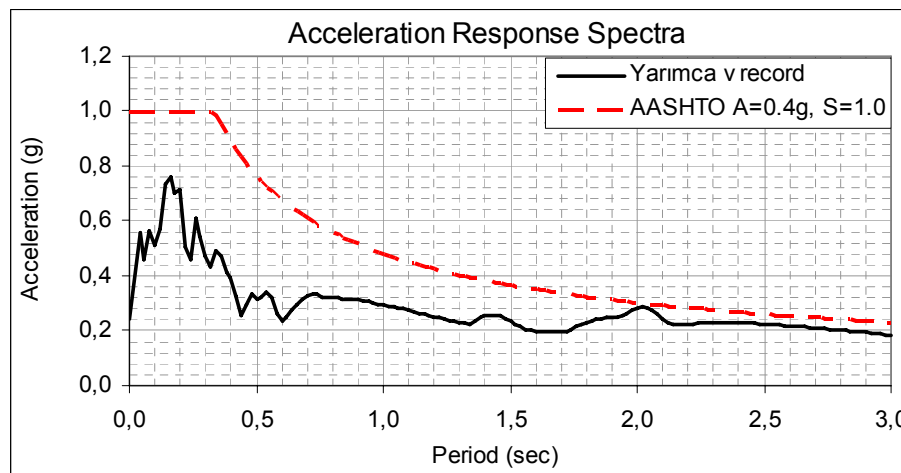
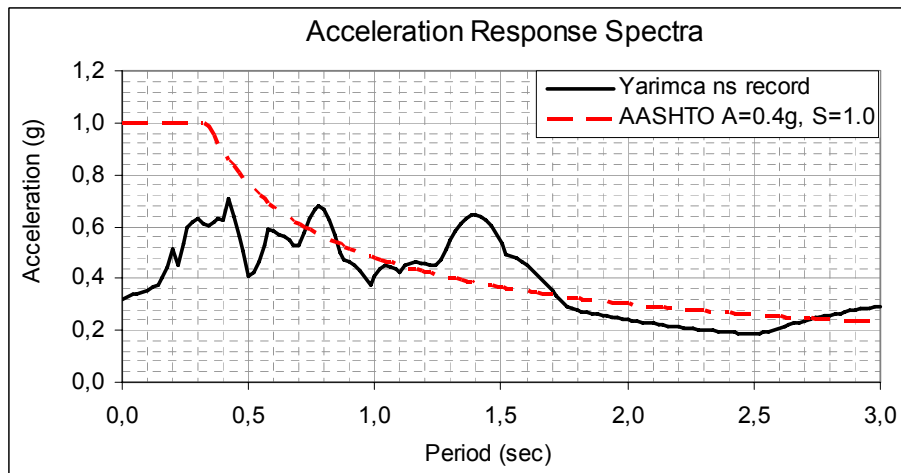
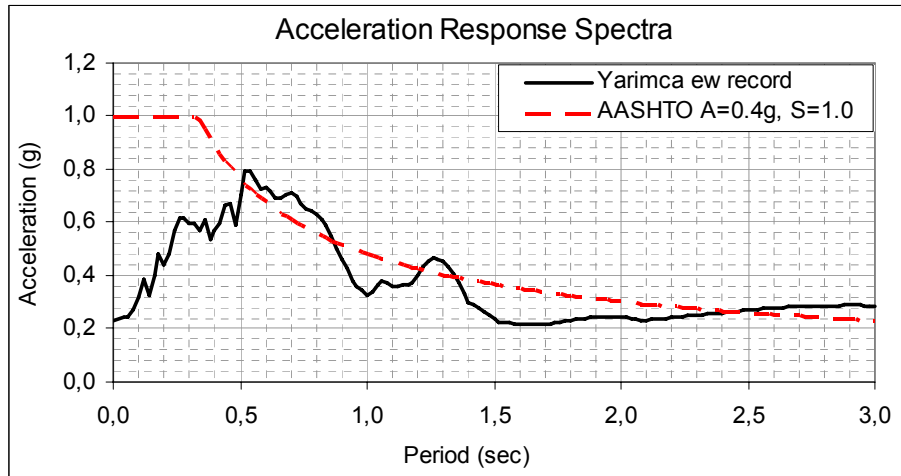


Figure 4.12: Normalized pseudo acceleration response spectra of Yarimca record together with AASHTO, 1996 response spectrum

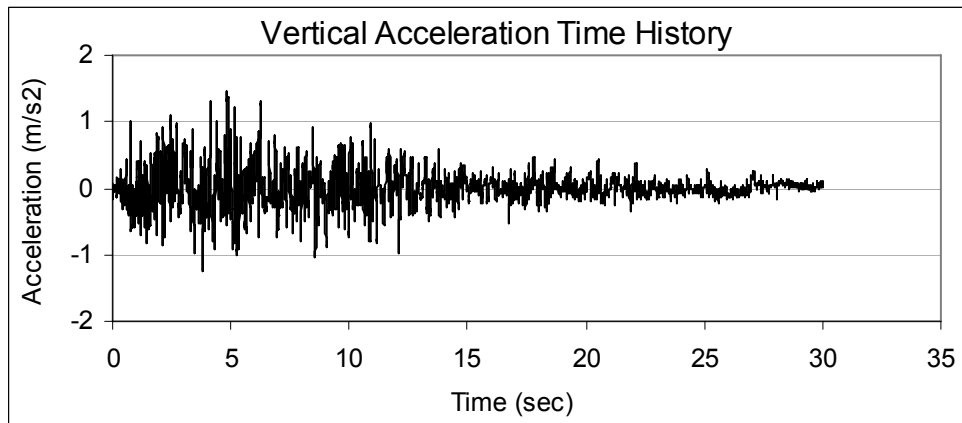
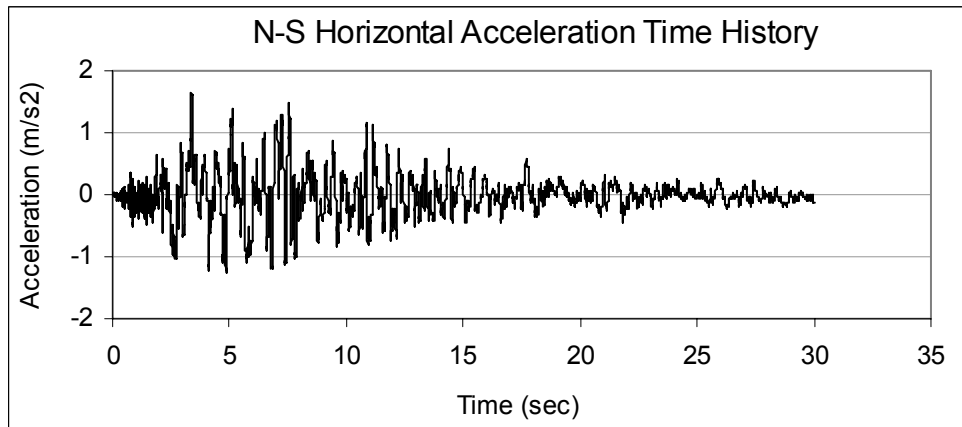
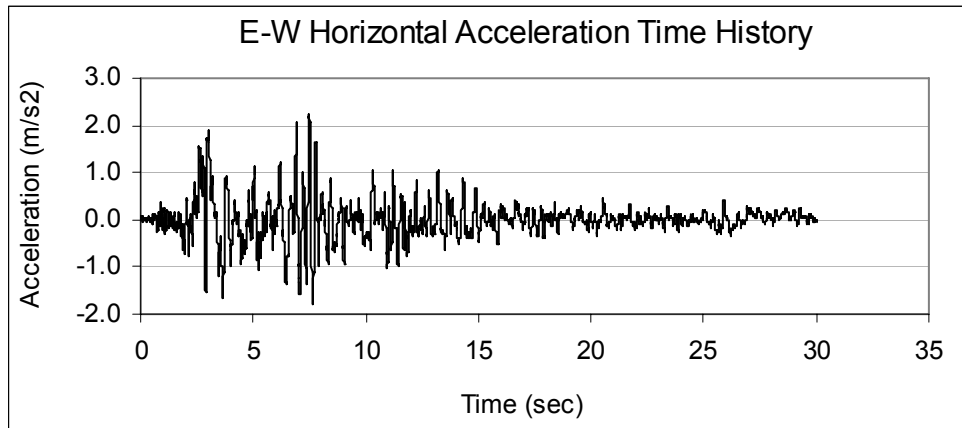


Figure 4.13: Acceleration time histories of İzmit record

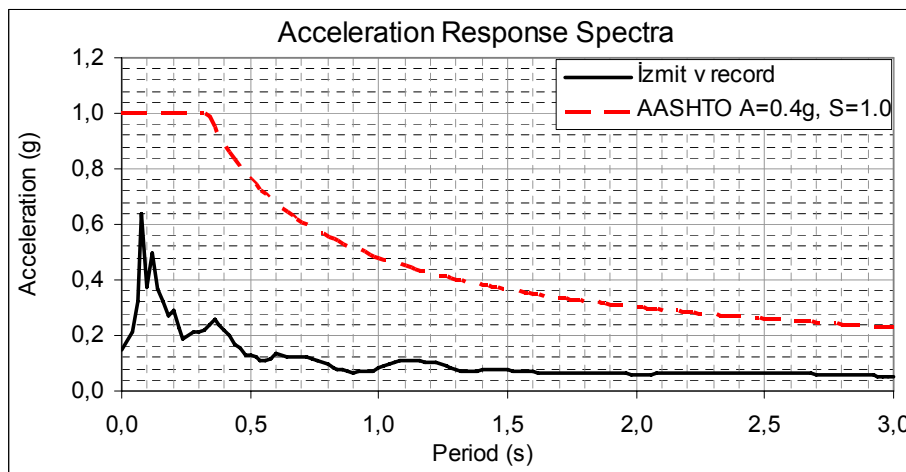
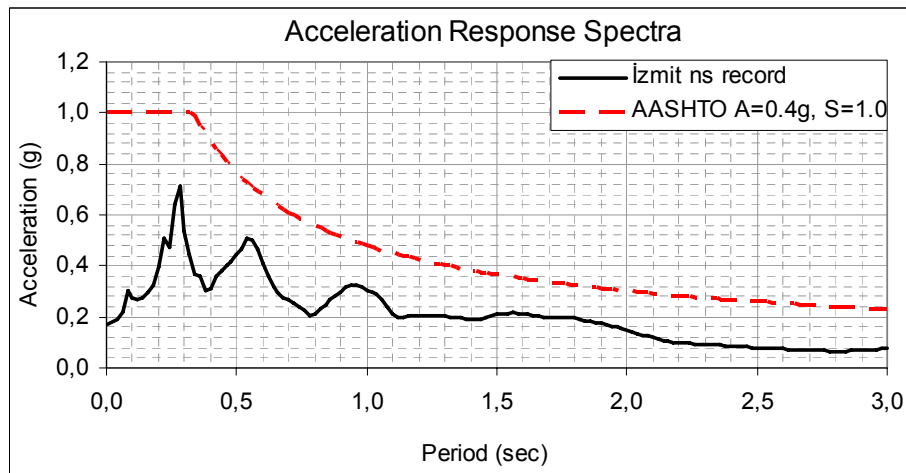
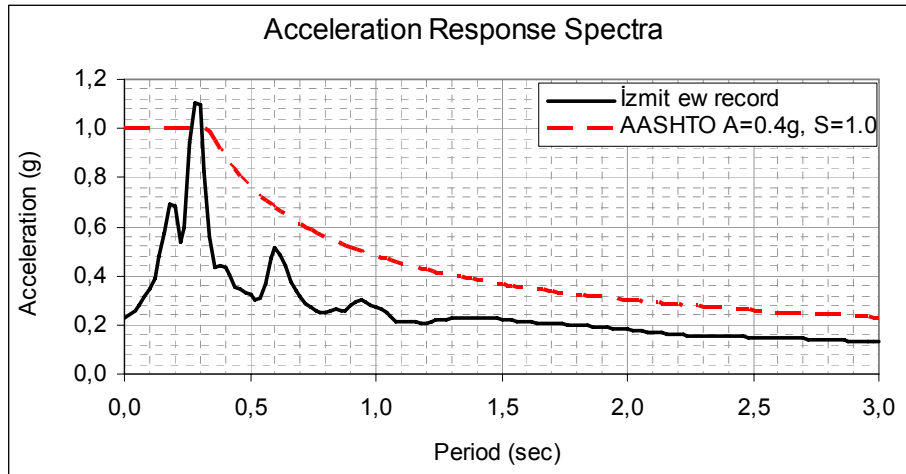


Figure 4.14: Normalized pseudo acceleration response spectra of İzmit record together with AASHTO, 1996 response spectrum

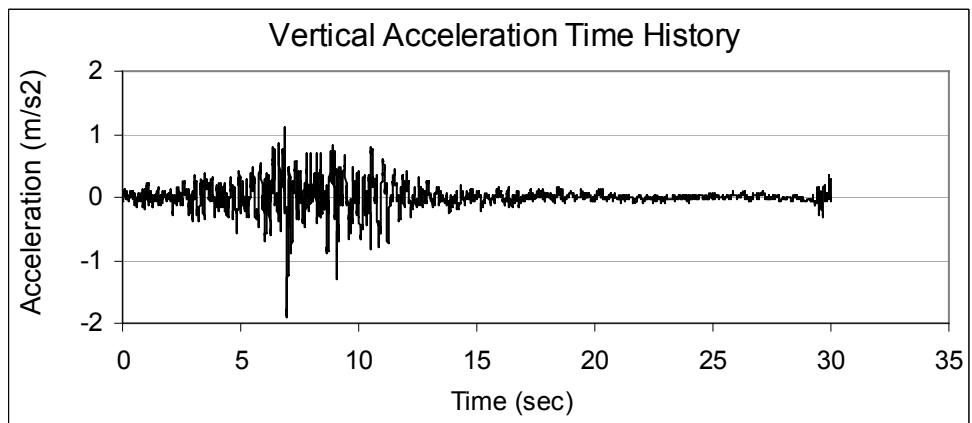
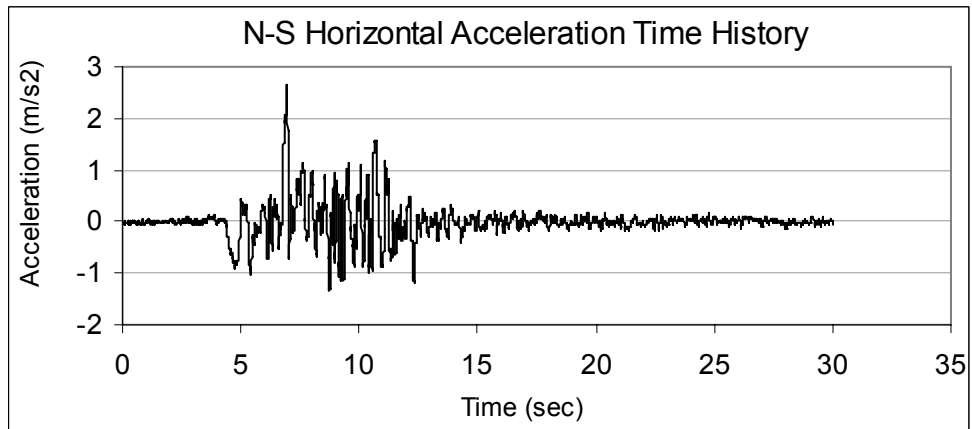
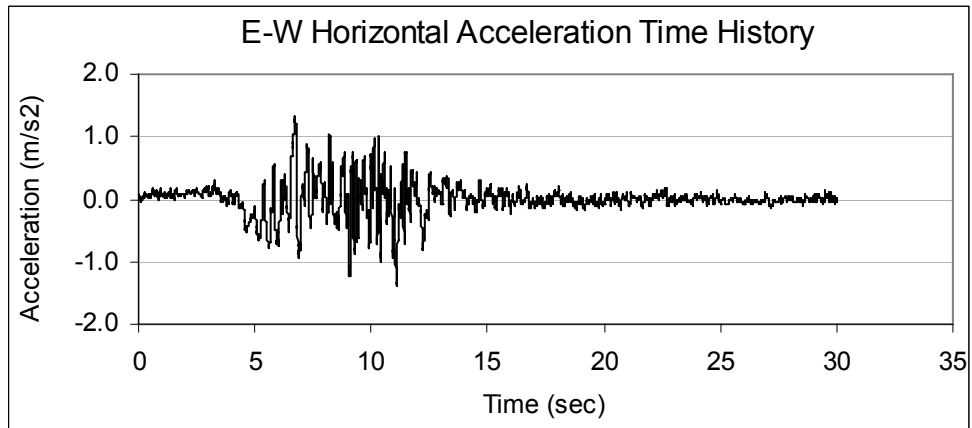


Figure 4.15: Acceleration time histories of Gebze record

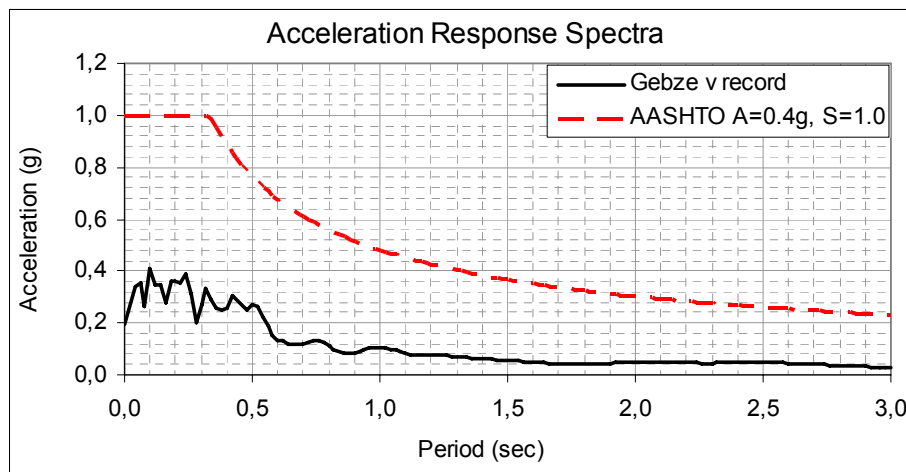
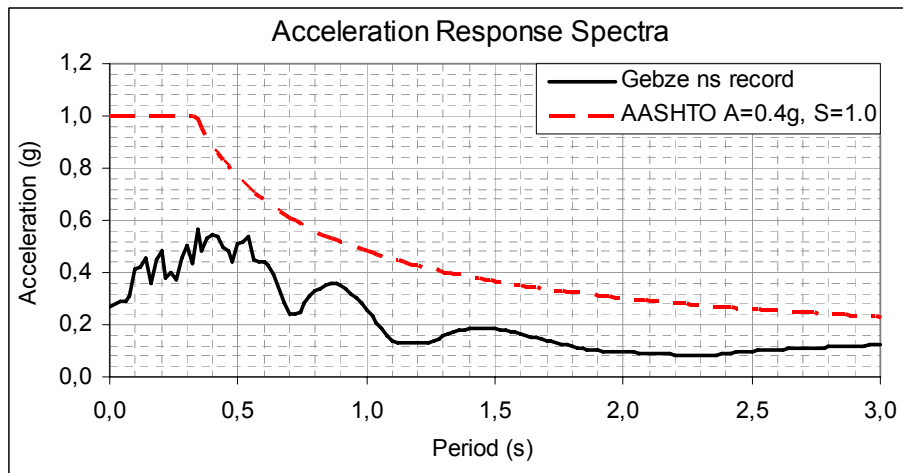
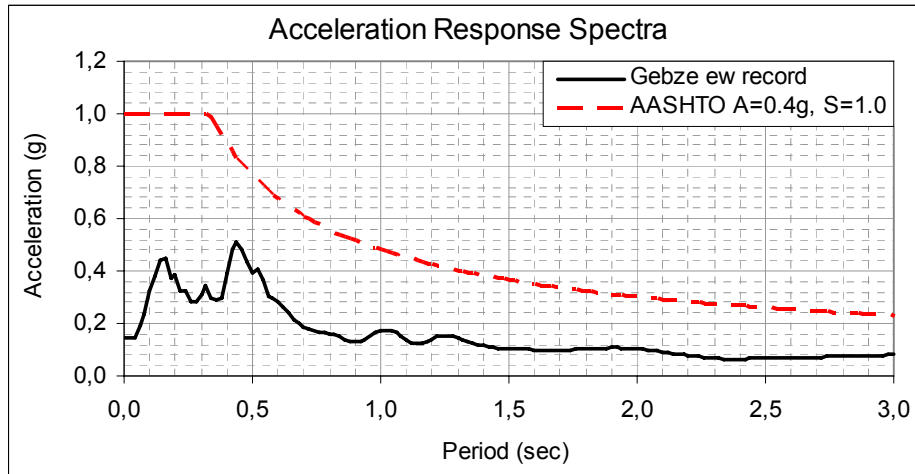


Figure 4.16: Normalized pseudo acceleration response spectra of Gebze record together with AASHTO, 1996 response spectrum

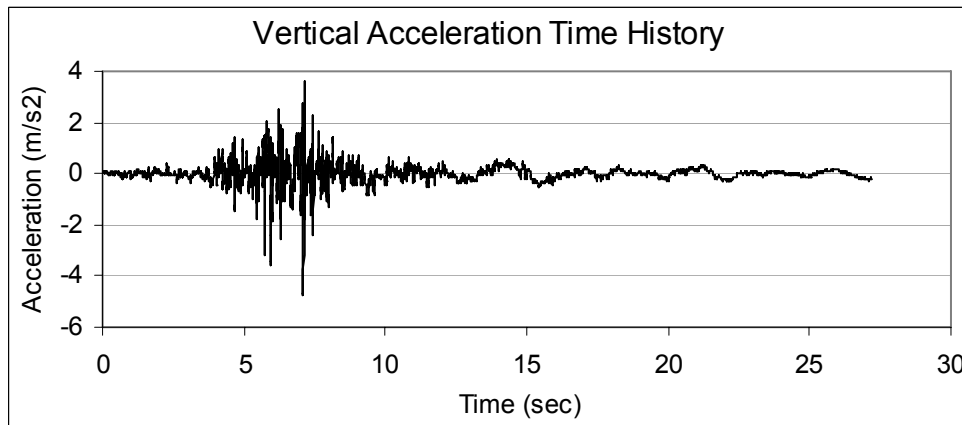
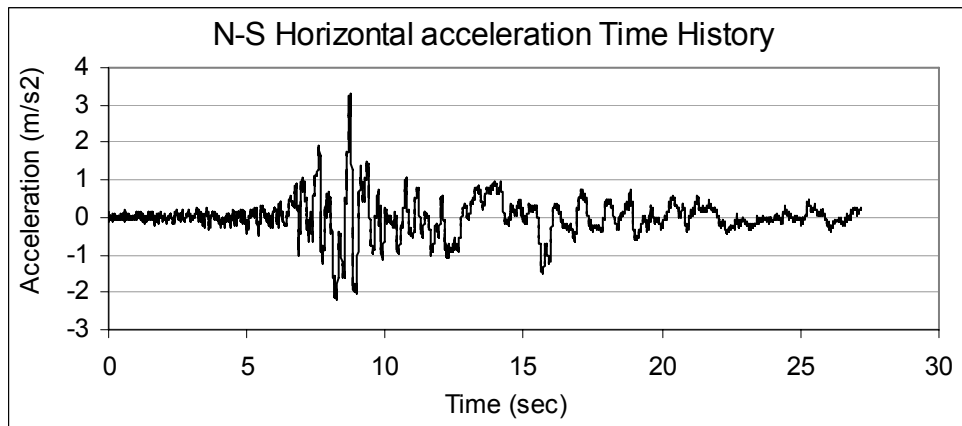
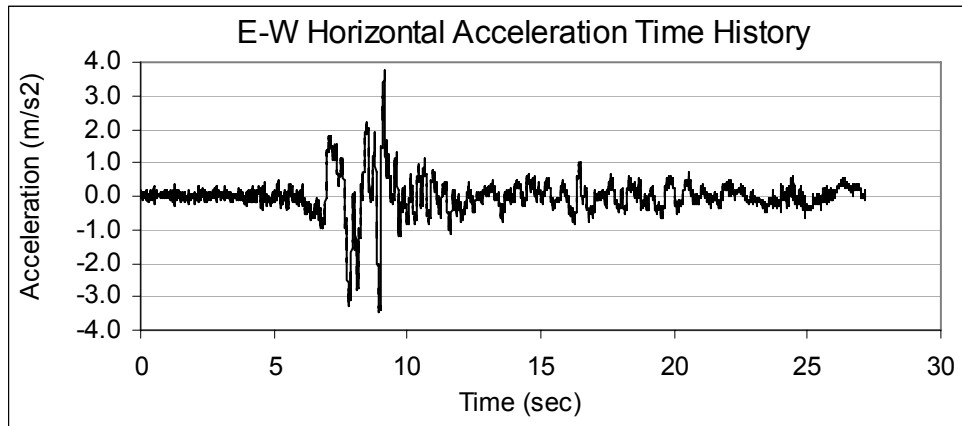


Figure 4.17: Acceleration time histories of Düzce record

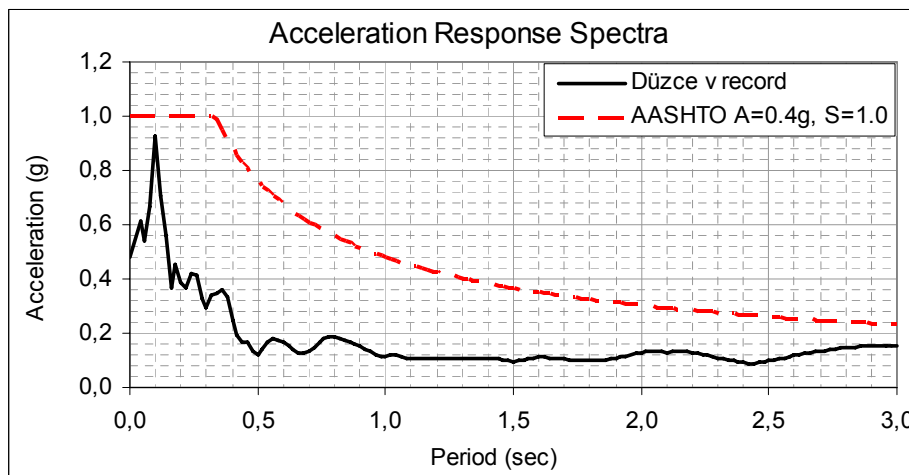
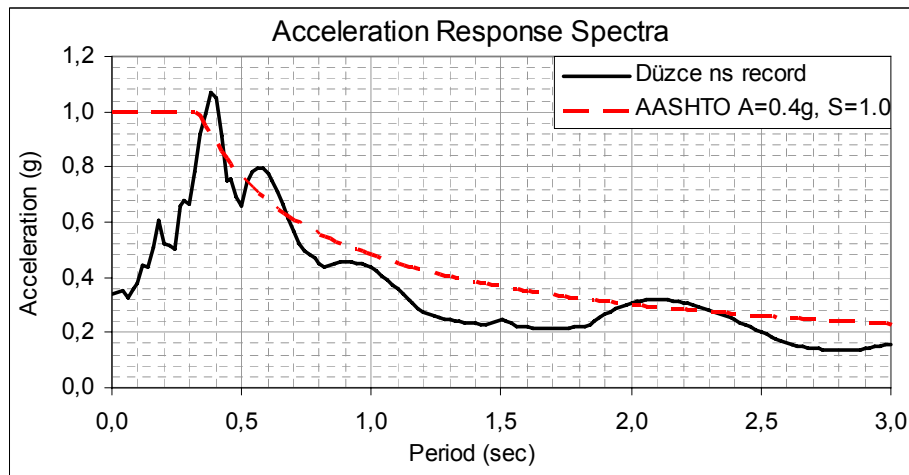
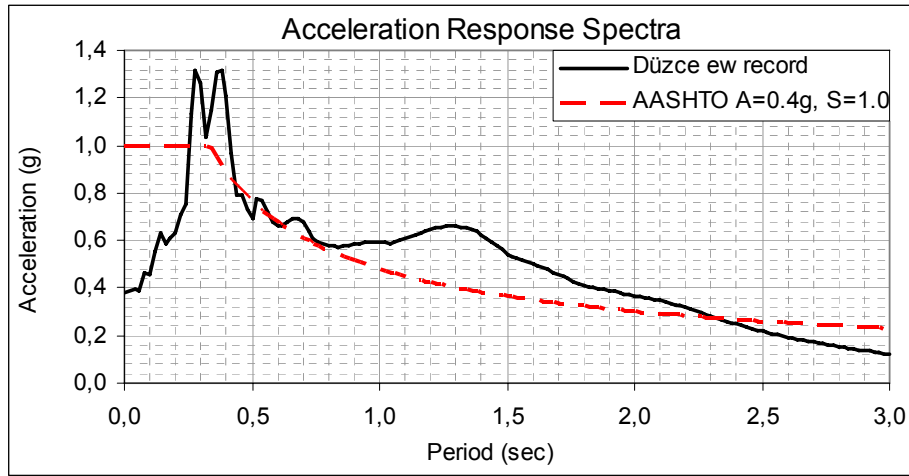


Figure 4.18: Normalized pseudo acceleration response spectra of Düzce record together with AASHTO, 1996 response spectrum

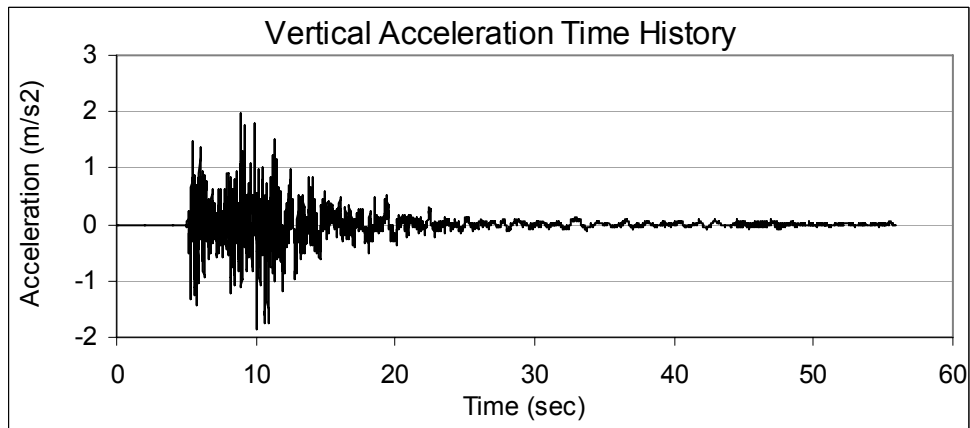
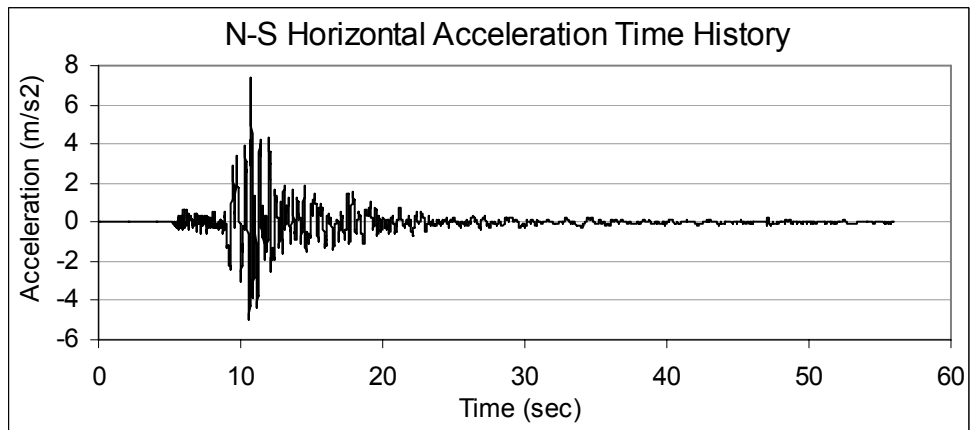
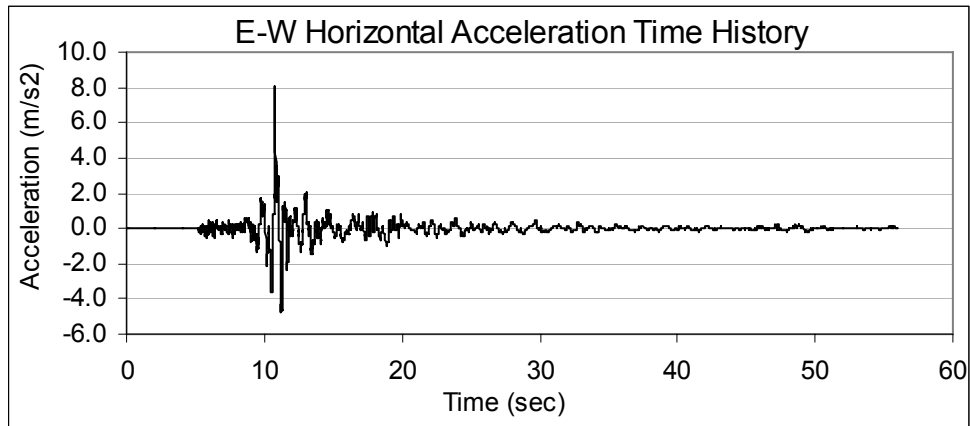


Figure 4.19: Acceleration time histories of Bolu record

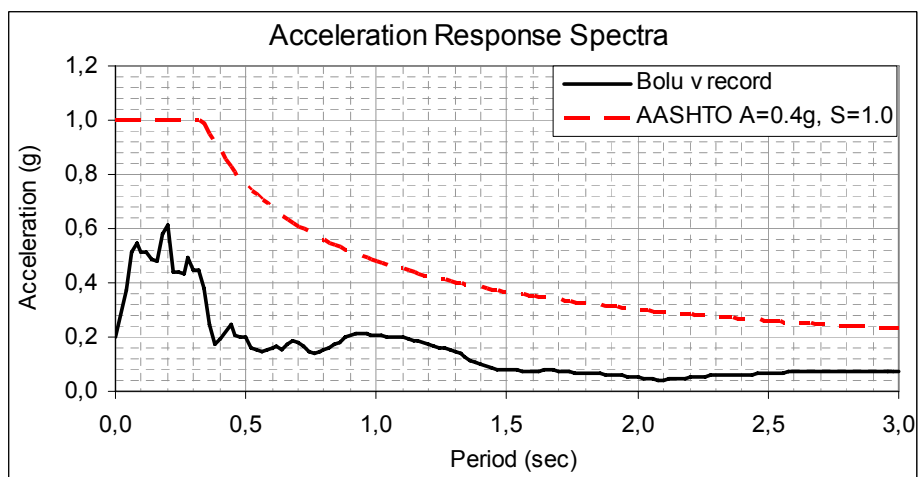
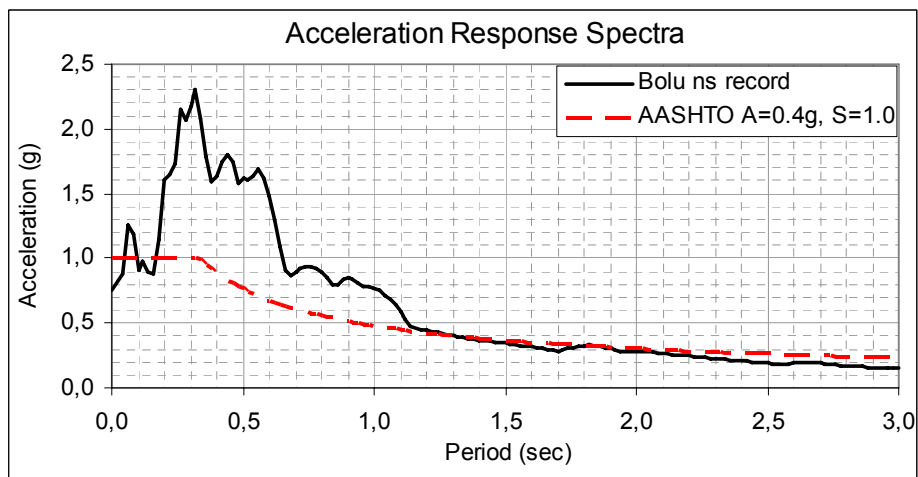
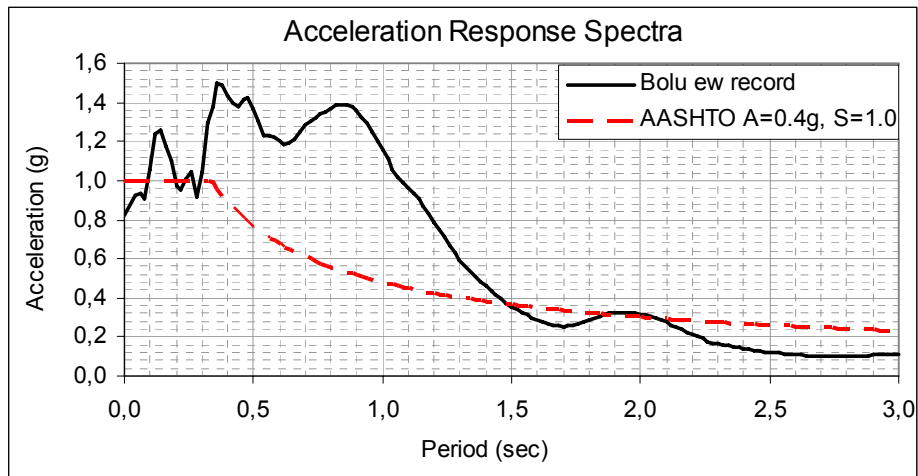


Figure 4.20: Normalized pseudo acceleration response spectra of Bolu record together with AASHTO, 1996 response spectrum

In Table 4.5 peak ground accelerations in terms of gravitational acceleration ($g=9.81 \text{ m/s}^2$) of the excitations in three orthogonal directions are tabulated.

Table 4.5: Peak ground accelerations

Record	E-W PGA (g)	N-S PGA (g)	Vert. PGA(g)
Yarımca	0.230	0.322	0.291
İzmit	0.227	0.167	0.149
Gebze	0.143	0.269	0.195
Düzce	0.383	0.337	0.480
Bolu	0.821	0.754	0.200

4.2.3 Non-linear Time History Analysis (NLTHA)

Non-linear time history analysis is an advanced version of LTHA. In NLTHA, non-linear material properties and geometric non-linearity of elements can be taken into consideration. It is an advanced and time consuming procedure for dynamic analysis of structures [24].

In elastic analysis methods, due to the nature of analysis system, the pounding between adjacent spans and between span and abutment back wall is ignored. Ignoring pounding effects is conservative for design of substructure. The purpose of making NLTHA in this study is to investigate the effect of pounding on structure response. In current Turkish bridge design practice, column and foundation designs are done very conservatively. Therefore, no hysteretic moment – curvature elements were defined for substructure elements. It is evaluated that the structure remains essentially elastic.

In order to model the abutment for NLTHA, the model for seat-type abutment recommended in ATC-32 was used. The model can be seen in the following Figure 4.21.

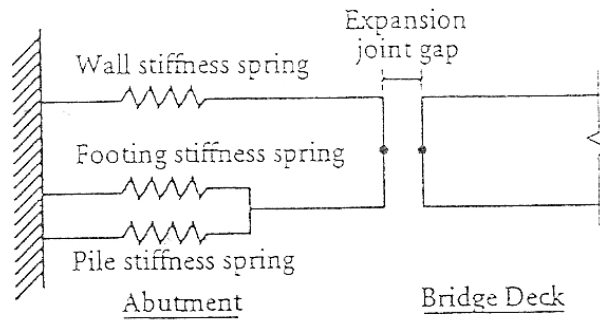


Figure 4.21: ATC-32 model for seat type abutment

For NLTHA, only Yarimca record out of three rock site records that gives maximum deck displacement was used since it takes a significant time to run and process an analysis. The bridge models A31 and A32 were analyzed since they are the longest bridges with 60° of skew angle.

All analysis properties carried out for LTHA were also applied for NLTHA except that springs having non-linear properties were placed between adjacent spans and between spans and abutments. In order to include non-linear properties, displacement-force diagrams were assigned for each spring.

The non-linear properties of springs placed between adjacent spans were calculated based on crushing of concrete cover during pounding by the following formulas:

$$k_{\text{deck}} = F_c / c_{\text{cover}} \quad (4.15)$$

in which:

F_c = axial load strength per meter (kN/m)

$$F_c = 0.85f_c' A \Phi \quad (4.16)$$

f_c' = compressive strength of concrete at 28 days (= 25 Mpa)

A = area of the deck per 1 meter (= 0.22 m²)

Φ = strength reduction factor for axial load capacity (=0.55)

c_{cover} = total concrete clean cover (= 2 * 0.05 = 0.1 m)

therefore; $k_{\text{deck}} = 25700 \text{ kN/m}$

The evaluation of pounding between adjacent spans is very difficult to assess since the expansion gap between adjacent spans can be (+) or (-) of the magnitude of the gap shown on as-built drawings. Damping or hysteretic behavior is neglected and Rayleigh damping of the global model is used. Ignoring hysteretic behavior of pounding may result in conservative results. Therefore, it should be kept in mind that, the procedure proposed hereby to evaluate pounding effect is essentially an appropriate method.

The non-linear spring property between adjacent spans is shown in Figure 4.22.

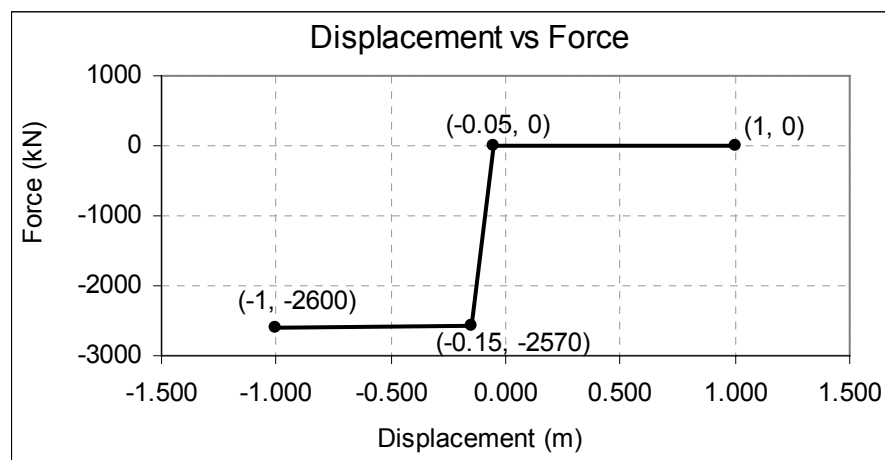


Figure 4.22: Force-displacement graph of springs between adjacent spans

The non-linear properties of springs placed between spans and abutments were calculated in a similar way accounting for concrete cover crushing or spalling. Footing and pile for the abutment were not modeled and hence the stiffness of these elements was not considered while calculating the spring properties. The

dimensions of the abutment shown in Figure 4.23 were used to calculate the spring properties. In determining the abutment dimensions, the researchers have been inspired by the as-built design projects prepared by one of the Turkish companies activating on bridge design.

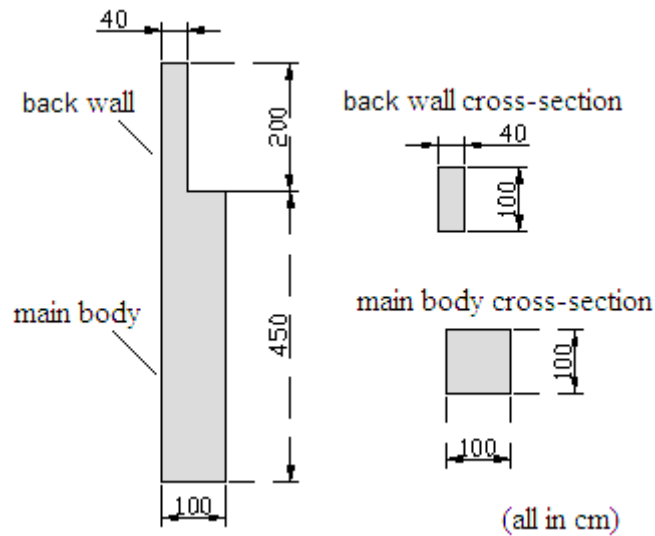


Figure 4.23: Typical abutment dimensions

The elastic parts of abutment nonlinear springs are computed from

$$k_{\text{abut}} = V / c_{\text{conc}} \quad (4.17)$$

where:

V = shear at critical section of back wall during flexural failure (kN)

c_{cover} = total concrete clean cover (= 0.1 m)

Shear force resulting from plastic hinging (V) was calculated to be 245 kN for back wall reinforcement of 8 Φ 18. Force – displacement graph of non-linear springs between spans and abutments is sketched in Figure 4.24.

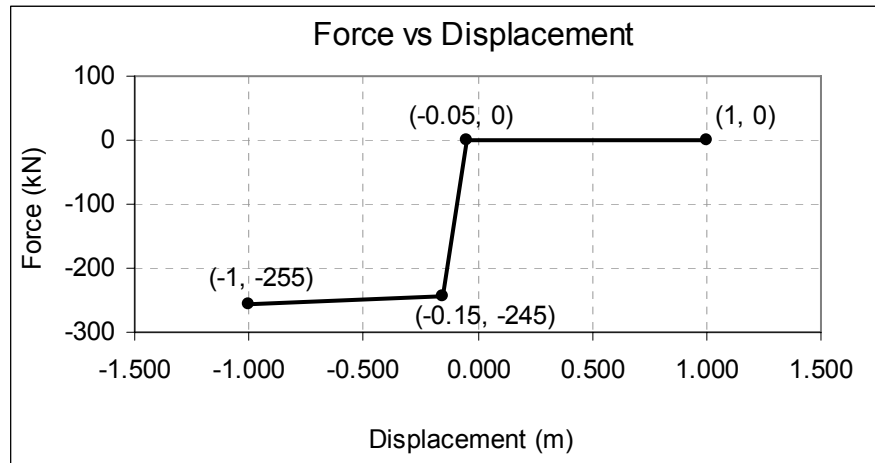


Figure 4.24: Force-displacement graph of springs between spans and abutments

Indeed, evaluation and investigation of the earthquake forces affecting the structures have started recently to be effectuated with reference to “planar spectrum” concept. Most violently hazardous earthquakes in Turkey and in other parts of the world during the last fifteen years have been investigated by a group of experts focusing on the topic [34, 35, 36].

Earthquake excitations surge in multiple directions during the main shock of the seismic action. Then, for a given constant period T , a group of response quantities should be evaluated for each angle specifying the direction of the oscillator motion. Therefore, a group of spectral graphs could be defined for a lap of a strong motion. The envelope of this set of linear spectra is referred as planar spectrum [34]. This approach is well recognized by the scientific communities and institutions specialized in the area of earthquake investigations. But, it is not referred yet in national and international codes and standards. It is why the numerical operations pertinent to estimation of earthquake forces and displacements were not realized considering this advanced new approach.

4.2.4 Service Load Analyses

Service load analysis consists, as its name indicates, the analysis of the structure for the loads, under service conditions. In this study, the service loads that were taken into consideration are dead load (DL), live load (LL) and temperature load (TL).

Live loads were computed according to the AASHTO, 1996 Specifications. Turkish bridges were designed to accommodate a H30-S24 truck which is similar to HS20-44 but about 50% heavier. AASHTO HS20-44 truck has three axles. The spacing between the axles were taken as 14 feet (= 4.3 m). The width of the trucks were taken as 6 feet (= 1.8 m) and a 4 feet (= 1.2 m) of clearance were placed between trucks.

The amount of impact increment is calculated as a part of live load stress in ASSHTO, 1996 and is determined by using the following formula:

$$I = 50/(L+125) \quad (4.18)$$

in which,

I = impact fraction for live load (maximum 30%)

L = the span length in feet

For the bridge models having span lengths of 18 m and 25 m, the impact fractions were calculated as 0.27 and 0.24, respectively. With these fractions, total live loads including impact effect were calculated as follows. For the 18 m spanned bridges, for the first axle 68 kN, for the second and the third axles 272 kN load were computed. Likely, for the 25 m spanned bridges, the load of the first axle was calculated as 66 kN, and the ones for the second and the third axles were calculated as 264 kN. The axle loads were applied as two equal

wheel loads. Two trucks were placed for each span side by side with a clearance of 1.2 meters.

For simple span bridges without link slabs, only one span was loaded by two trucks in order to achieve maximum span moment. For the ones having link slabs, additional to the first loading case, two adjacent spans were loaded by two trucks in order to maintain the maximum moments on the link slabs between them. For analysis purposes, the trucks were located on the bridge in such a way that the centroid of the point loads exerted by trucks coincides with the centerline of the bridge span. This configuration is used in the analysis since it is a common method used in engineering practice. In Figure 4.25 sample live loads applied on 25 m. long span are shown.

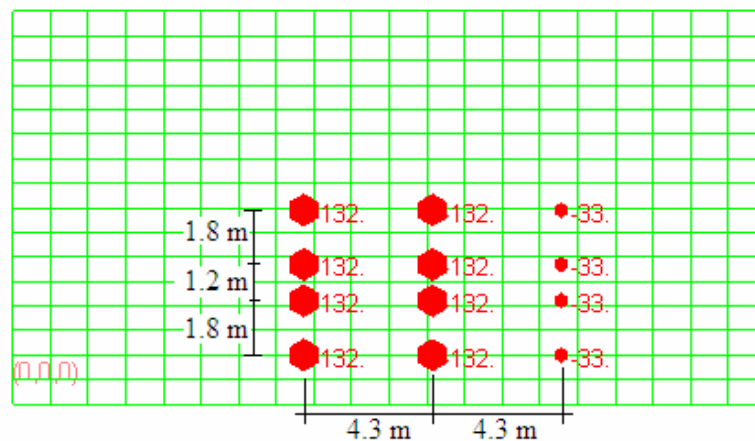


Figure 4.25: Truck loads on 25 m. long span

When expansion deck joints are eliminated and jointless continuous decks are used, fine cracks can occur at link slabs. These cracks can occur either as a result of girder end rotations caused by live loads or due to loads induced by variations in temperature [1]. In order to check for the cracks occur at link slabs in models having continuous decks (Group D bridges); in addition to the

live load analyses, thermal analyses were also made. Thermal analyses were made according to AASHTO, 1996 Specifications. The seasonal temperature change in Turkey is not mild. Therefore, the range of temperature was chosen for the cold climate conditions. 45° F (= 25°C) of temperature fall was used for thermal analyses of the bridges having continuous decks.

CHAPTER 5

ANALYSIS RESULTS

5.1 Introduction

In this chapter, the results of RSA, LTHA, NLTHA, eigenvalue, live load and thermal analysis were presented. Addition of link slab and variation in skew angle were investigated on several parameters such as deck and bearing displacements, member forces, member stresses and fundamental periods of the bridges.

Fundamental periods of bridges calculated by the eigenvalue analysis, in longitudinal, transverse and vertical directions were taken as the first modal period of the bridge in corresponding direction, which gives a mass participation of 10% or higher. Global (bridge's) longitudinal, transverse and vertical directions are shown in the following Figure 5.1.

Deck displacements of bridges were taken as the displacement of the last joint of the deck of the first span in 2 spanned bridges and of the second span in 4 spanned bridges, as illustrated in the following Figure 5.2.

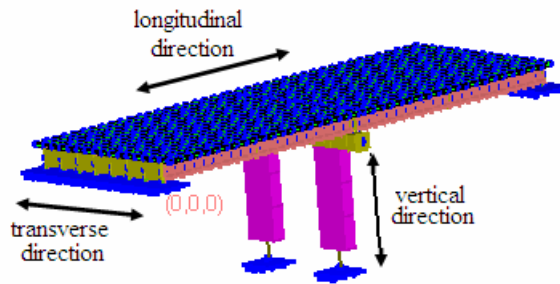


Figure 5.1: Longitudinal, transverse and vertical directions of the bridge

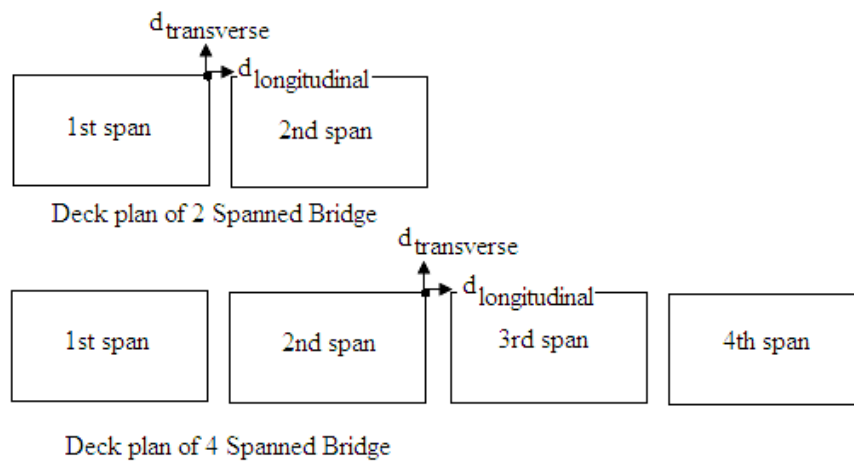


Figure 5.2: Longitudinal and transverse deck displacements of 2 spanned and 4 spanned bridges

Longitudinal displacements of elastomeric bearings are calculated by the following formula:

$$\Delta d = F / K_{long} \quad (5.1)$$

in which;

Δd = displacement in the longitudinal direction (m)

F = force in the longitudinal direction of the elastomeric bearing (kN)

K_{long} = longitudinal translational stiffness of the elastomeric bearing
 = 2011 kN/m

In transverse direction, bearing displacement was restricted by the shear keys placed between the girders.

Member forces, namely cap beam moment, diaphragm shear and column moments were studied for each of the models. The direction of the local cap beam moment and the directions of the local column longitudinal and transverse moments for straight and skewed bridges are sketched in Figure 5.3 and Figure 5.4 below.

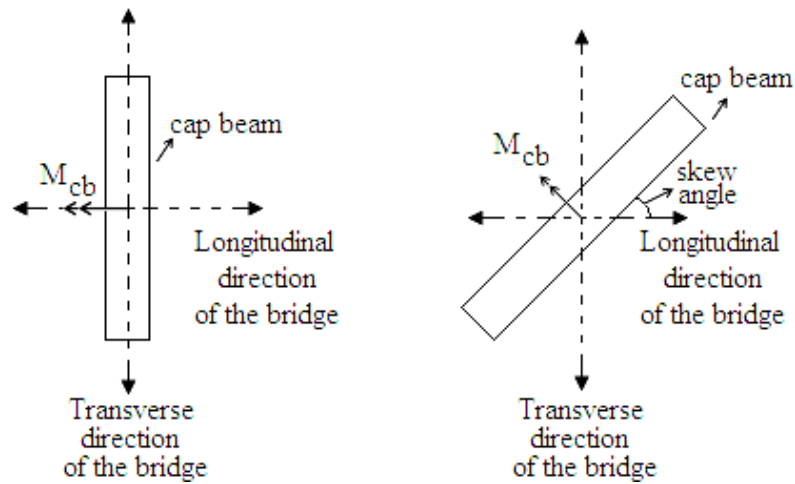


Figure 5.3: Direction of the cap beam local moment

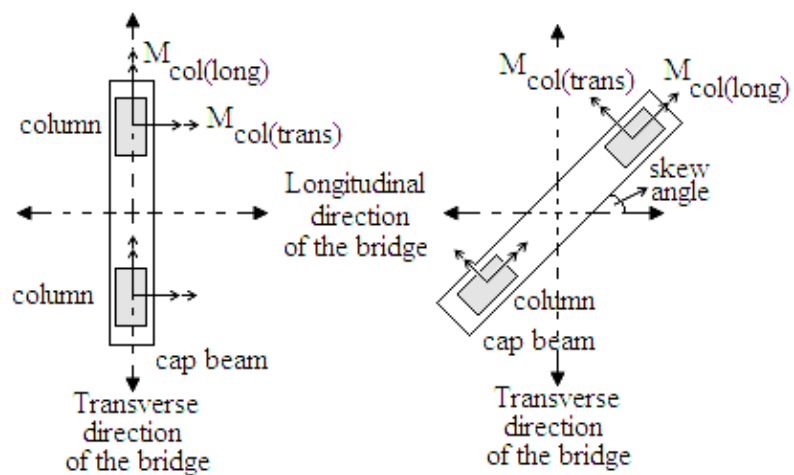


Figure 5.4: Direction of the column local longitudinal and transverse moments

Changes in the live load stress of the girders due to change in skew angle and link slab were also investigated in the study. Only the girders of the spans having truck loads were examined for live load stresses since the spans are simply supported. The stress points at the girder sections are shown in Figure 5.5. The live load stresses only at points S-2 and S-3 were analyzed since tension stresses occur at the bottom of the section.

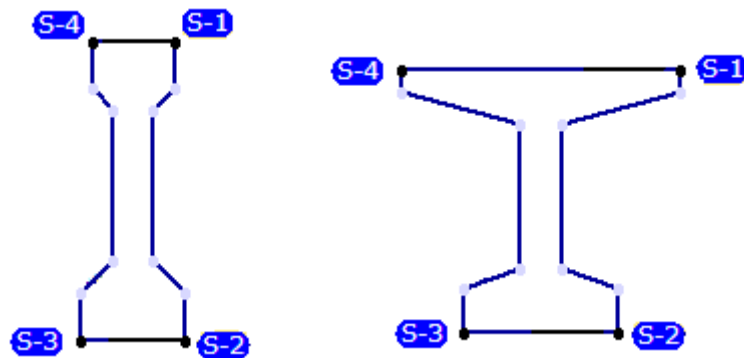


Figure 5.5: Stress points at girder cross-sections

Live load forces on center of the link slab plates were checked for the AASHTO crack control criterion. Two different load cases were analyzed to give the maximum live load forces in link slabs. In the first loading condition, only one span was loaded by two trucks, and in the second one two adjacent spans were loaded by two trucks to get the maximum response of the link slab lying between them. Only tension forces occurred in the link slab were saved since the purpose is to check for the surface cracks.

In the following figures and tables the results of eigenvalue analysis, RSA, live load and thermal analysis, LTHA and NLTHA are represented.

5.2 Eigenvalue Analysis Results

Fundamental periods for all studied bridge structures have been evaluated with help of the eigenvalue analysis program of the LARSA software system. The results are given in tabulated forms separately for all four groups (Group A, B, C and D).

Table 5.1: Fundamental Periods of Group A Bridges

Model #	# of spans	skew angle (deg)	SL (m)	LS	L/H	I_{cb}/I_c	Long. period (sec)	Trans. Period (sec)	Vert. Period (sec)
A1	2	0	18	no	1	0.1	0.73	0.19	0.14
A2	2	0	18	yes	1	0.1	0.71	0.15	0.14
A3	2	0	25	no	1	0.1	0.95	0.24	0.25
A4	2	0	25	yes	1	0.1	0.92	0.24	0.25
A5	4	0	18	no	1	0.1	0.84	0.20	0.14
A6	4	0	18	yes	1	0.1	0.77	0.20	0.14
A7	4	0	25	no	1	0.1	1.09	0.26	0.25
A8	4	0	25	yes	1	0.1	1.00	0.27	0.25
A9	2	20	18	no	1	0.1	0.72	0.23	0.14
A10	2	20	18	yes	1	0.1	0.69	0.16	0.14
A11	2	20	25	no	1	0.1	0.94	0.30	0.25
A12	2	20	25	yes	1	0.1	0.90	0.25	0.24
A13	4	20	18	no	1	0.1	0.83	0.28	0.14
A14	4	20	18	yes	1	0.1	0.75	0.25	0.14
A15	4	20	25	no	1	0.1	1.08	0.34	0.25
A16	4	20	25	yes	1	0.1	0.98	0.33	0.24
A17	2	40	18	no	1	0.1	0.68	0.23	0.14
A18	2	40	18	yes	1	0.1	0.67	0.17	0.14
A19	2	40	25	no	1	0.1	0.89	0.32	0.25
A20	2	40	25	yes	1	0.1	0.87	0.27	0.23
A21	4	40	18	no	1	0.1	0.77	0.36	0.15
A22	4	40	18	yes	1	0.1	0.71	0.29	0.14
A23	4	40	25	no	1	0.1	1.02	0.46	0.25
A24	4	40	25	yes	1	0.1	0.94	0.41	0.23
A25	2	60	18	no	1	0.1	0.67	0.23	0.15
A26	2	60	18	yes	1	0.1	0.67	0.20	0.14

Table 5.1 Cont'd

Model #	# of spans	skew angle (deg)	SL (m)	LS	L/H	I_{cb}/I_c	Long. period (sec)	Trans. Period (sec)	Vert. Period (sec)
A27	2	60	25	no	1	0.1	0.87	0.33	0.24
A28	2	60	25	yes	1	0.1	0.86	0.29	0.21
A29	4	60	18	no	1	0.1	0.72	0.43	0.17
A30	4	60	18	yes	1	0.1	0.69	0.34	0.12
A31	4	60	25	no	1	0.1	0.94	0.58	0.26
A32	4	60	25	yes	1	0.1	0.89	0.48	0.19

Table 5.2: Fundamental Periods of Group B Bridges

Model #	# of spans	skew angle (deg)	SL (m)	LS	L/H	I_{cb}/I_c	Long. period (sec)	Trans. Period (sec)	Vert. Period (sec)
B1	2	0	18	no	1.5	0.1	0.67	0.12	0.14
B2	2	0	18	yes	1.5	0.1	0.67	0.14	0.14
B3	2	0	25	no	1.5	0.1	0.88	0.15	0.25
B4	2	0	25	yes	1.5	0.1	0.87	0.23	0.25
B5	4	0	18	no	1.5	0.1	0.72	0.13	0.14
B6	4	0	18	yes	1.5	0.1	0.70	0.17	0.15
B7	4	0	25	no	1.5	0.1	0.84	0.27	0.25
B8	4	0	25	yes	1.5	0.1	0.90	0.21	0.25
B9	2	20	18	no	1.5	0.1	0.67	0.17	0.14
B10	2	20	18	yes	1.5	0.1	0.66	0.14	0.14
B11	2	20	25	no	1.5	0.1	0.87	0.24	0.25
B12	2	20	25	yes	1.5	0.1	0.86	0.23	0.24
B13	4	20	18	no	1.5	0.1	0.71	0.19	0.14
B14	4	20	18	yes	1.5	0.1	0.69	0.18	0.14
B15	4	20	25	no	1.5	0.1	0.92	0.25	0.25
B16	4	20	25	yes	1.5	0.1	0.89	0.25	0.24
B17	2	40	18	no	1.5	0.1	0.66	0.19	0.14
B18	2	40	18	yes	1.5	0.1	0.65	0.15	0.14
B19	2	40	25	no	1.5	0.1	0.85	0.26	0.25
B20	2	40	25	yes	1.5	0.1	0.84	0.24	0.23
B21	4	40	18	no	1.5	0.1	0.69	0.26	0.15
B22	4	40	18	yes	1.5	0.1	0.67	0.23	0.13
B23	4	40	25	no	1.5	0.1	0.90	0.33	0.25
B24	4	40	25	yes	1.5	0.1	0.87	0.31	0.24
B25	2	60	18	no	1.5	0.1	0.66	0.21	0.15
B26	2	60	18	yes	1.5	0.1	0.66	0.18	0.14
B27	2	60	25	no	1.5	0.1	0.85	0.29	0.24
B28	2	60	25	yes	1.5	0.1	0.84	0.27	0.21
B29	4	60	18	no	1.5	0.1	0.68	0.33	0.16
B30	4	60	18	yes	1.5	0.1	0.67	0.27	0.12
B31	4	60	25	no	1.5	0.1	0.87	0.43	0.25
B32	4	60	25	yes	1.5	0.1	0.86	0.38	0.19

Table 5.3: Fundamental Periods of Group C Bridges

Model #	# of spans	skew angle (deg)	SL (m)	LS	L/H	I_{cb}/I_c	Long. period (sec)	Trans. Period (sec)	Vert. Period (sec)
C1	2	0	18	no	1	1.5	0.77	0.41	0.14
C2	2	0	18	yes	1	1.5	0.74	0.16	0.14
C3	2	0	25	no	1	1.5	1.00	0.50	0.25
C4	2	0	25	yes	1	1.5	0.96	0.28	0.25
C5	4	0	18	no	1	1.5	0.96	0.35	0.15
C6	4	0	18	yes	1	1.5	0.83	0.34	0.15
C7	4	0	25	no	1	1.5	1.24	0.57	0.25
C8	4	0	25	yes	1	1.5	1.07	0.50	0.25
C9	2	20	18	no	1	1.5	0.76	0.31	0.14
C10	2	20	18	yes	1	1.5	0.74	0.16	0.14
C11	2	20	25	no	1	1.5	0.99	0.44	0.25
C12	2	20	25	yes	1	1.5	0.95	0.27	0.24
C13	4	20	18	no	1	1.5	0.95	0.45	0.15
C14	4	20	18	yes	1	1.5	0.82	0.34	0.14
C15	4	20	25	no	1	1.5	1.23	0.59	0.25
C16	4	20	25	yes	1	1.5	1.06	0.51	0.25
C17	2	40	18	no	1	1.5	0.74	0.24	0.15
C18	2	40	18	yes	1	1.5	0.72	0.18	0.14
C19	2	40	25	no	1	1.5	0.95	0.36	0.25
C20	2	40	25	yes	1	1.5	0.93	0.28	0.23
C21	4	40	18	no	1	1.5	0.88	0.46	0.15
C22	4	40	18	yes	1	1.5	0.79	0.34	0.14
C23	4	40	25	no	1	1.5	1.16	0.63	0.25
C24	4	40	25	yes	1	1.5	1.02	0.52	0.23
C25	2	60	18	no	1	1.5	0.73	0.24	0.15
C26	2	60	18	yes	1	1.5	0.72	0.21	0.14
C27	2	60	25	no	1	1.5	0.93	0.35	0.25
C28	2	60	25	yes	1	1.5	0.92	0.30	0.22
C29	4	60	18	no	1	1.5	0.83	0.50	0.16
C30	4	60	18	yes	1	1.5	0.78	0.36	0.13
C31	4	60	25	no	1	1.5	1.07	0.70	0.26
C32	4	60	25	yes	1	1.5	0.99	0.54	0.21

Table 5.4: Fundamental Periods of Group D Bridges

Model #	# of spans	skew angle (deg)	SL (m)	LS	L/H	I_{cb}/I_c	Long. period (sec)	Trans. Period (sec)	Vert. Period (sec)
D1	2	0	18	yes	1	0.1	0.17	0.14	0.14
D2	2	0	25	yes	1	0.1	0.19	0.24	0.24
D3	4	0	18	yes	1	0.1	0.21	0.20	0.14
D4	4	0	25	yes	1	0.1	0.28	0.27	0.24
D5	2	20	18	yes	1	0.1	0.16	0.13	0.13
D6	2	20	25	yes	1	0.1	0.18	0.23	0.23
D7	4	20	18	yes	1	0.1	0.24	0.24	0.14
D8	4	20	25	yes	1	0.1	0.27	0.33	0.23
D9	2	40	18	yes	1	0.1	0.15	0.14	0.13
D10	2	40	25	yes	1	0.1	0.18	0.20	0.21
D11	4	40	18	yes	1	0.1	0.20	0.25	0.13
D12	4	40	25	yes	1	0.1	0.27	0.37	0.21
D13	2	60	18	yes	1	0.1	0.15	0.06	0.11
D14	2	60	25	yes	1	0.1	0.19	0.09	0.18
D15	4	60	18	yes	1	0.1	0.21	0.20	0.12
D16	4	60	25	yes	1	0.1	0.26	0.35	0.18

5.3 Response Spectra Analysis (RSA) Results

RSA investigation was made for all types of bridges studied in this thesis work. Resulting outputs are provided in the form of graphics taking place in the Figures 5.6 to 5.77. In these graphics for Group A, B and C, there exist four series for each skew angle. The first series is for the bridge models with expansion joints and having span lengths of 18m and is shown by the white blocks. The second series is represented by black blocks and composed of the bridge models having 18m of span length and link slab. The third series is for the models having expansion joints and 25 m of span length. They are represented by the columns having downward diagonal lines. Finally, the fourth series is represented by blocks having black dots and composed of models having span lengths of 25m and also link slabs. Moreover, the results

of the two spanned and four spanned bridges are separately shown on different figures.

As for the figures belonging to Group D, there are only two series for each of the graphic since all the bridge models in Group D have link slabs. In these figures the first series represented by black blocks are for the models having 18m of span length and the second series are for the models having span lengths of 25m and represented by blocks having black dots. The analysis results of two spanned and four spanned bridges are also presented separately for Group D bridges.

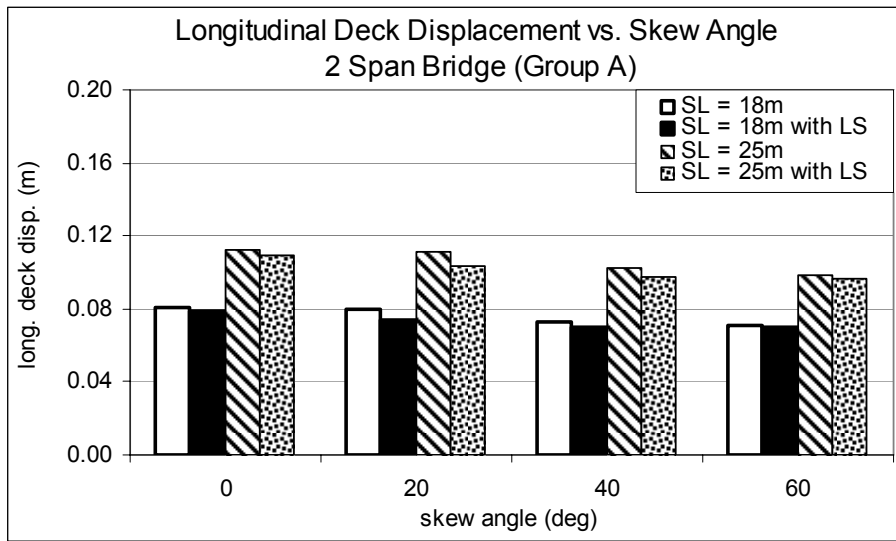


Figure 5.6: Change in longitudinal deck displacement with skew angle for 2 span bridges in Group A

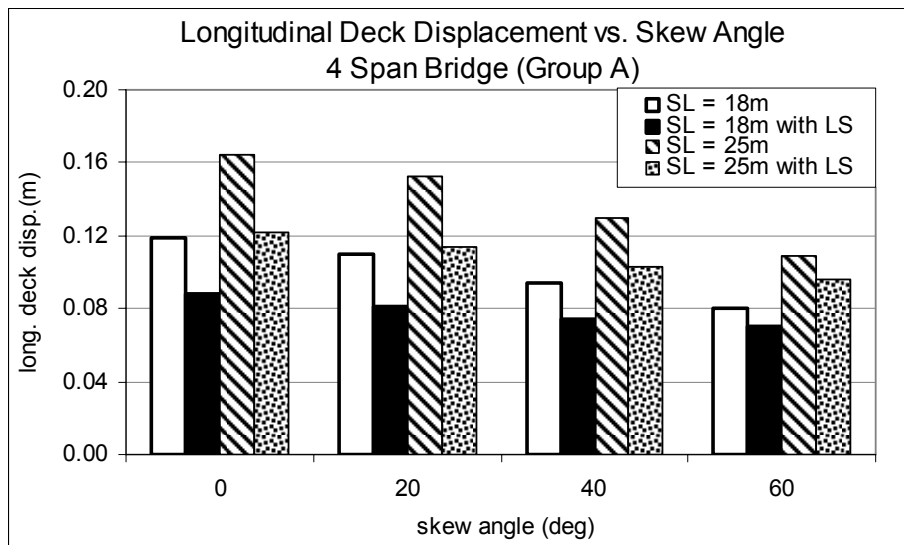


Figure 5.7: Change in longitudinal deck displacement with skew angle for 4 span bridges in Group A

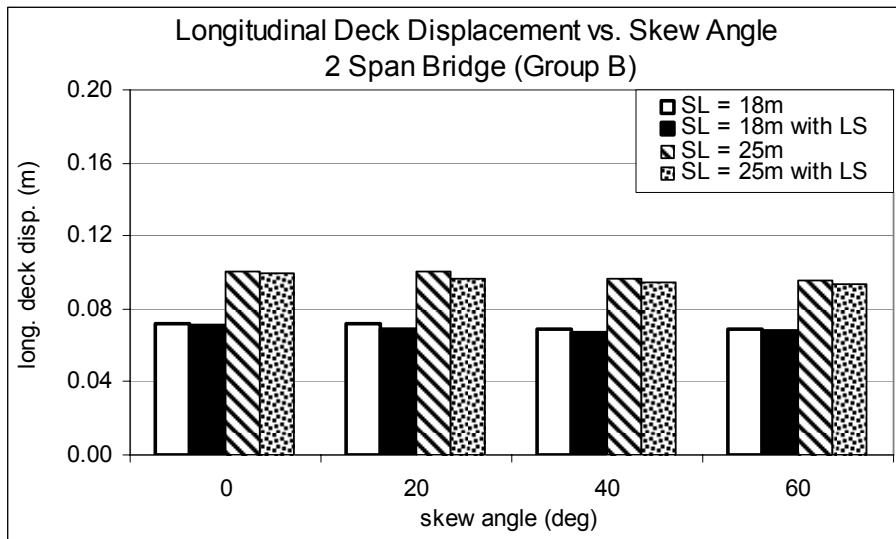


Figure 5.8: Change in longitudinal deck displacement with skew angle for 2 span bridges in Group B

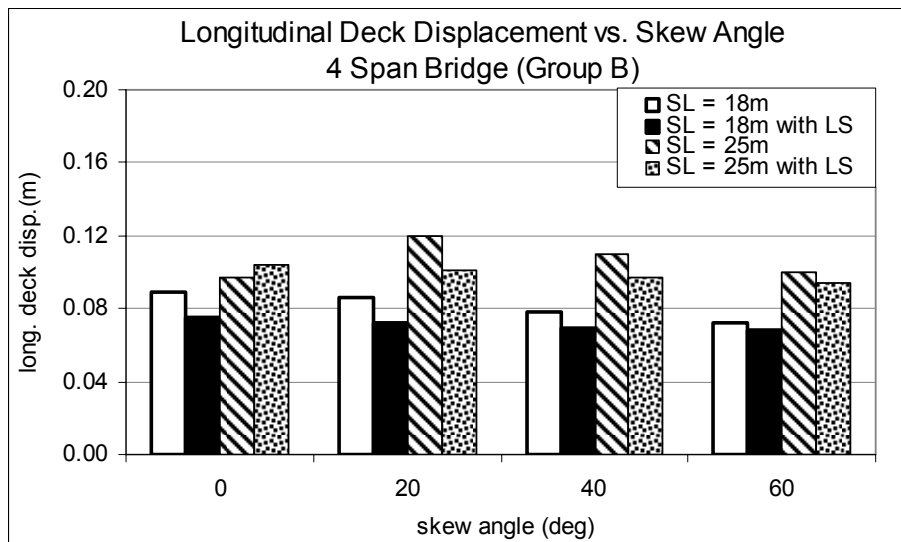


Figure 5.9: Change in longitudinal deck displacement with skew angle for 4 span bridges in Group B

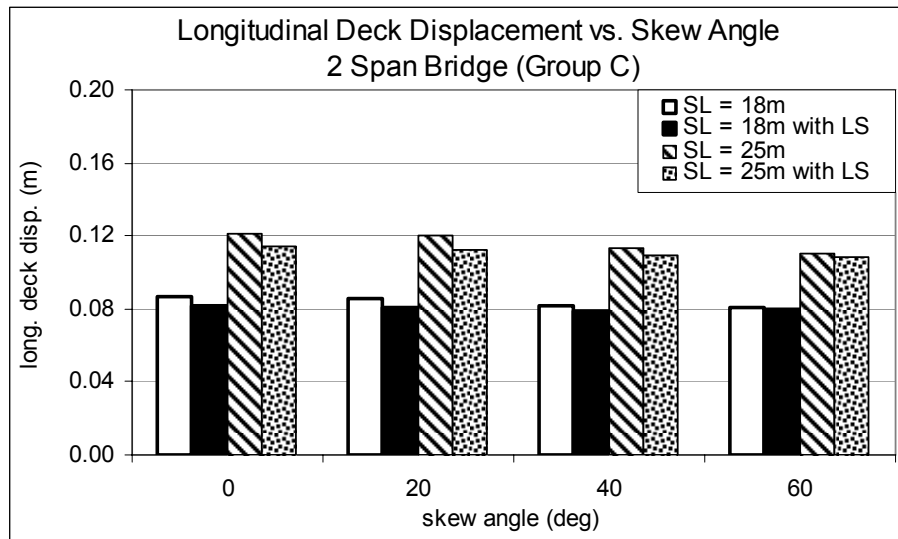


Figure 5.10: Change in longitudinal deck displacement with skew angle for 2 span bridges in Group C

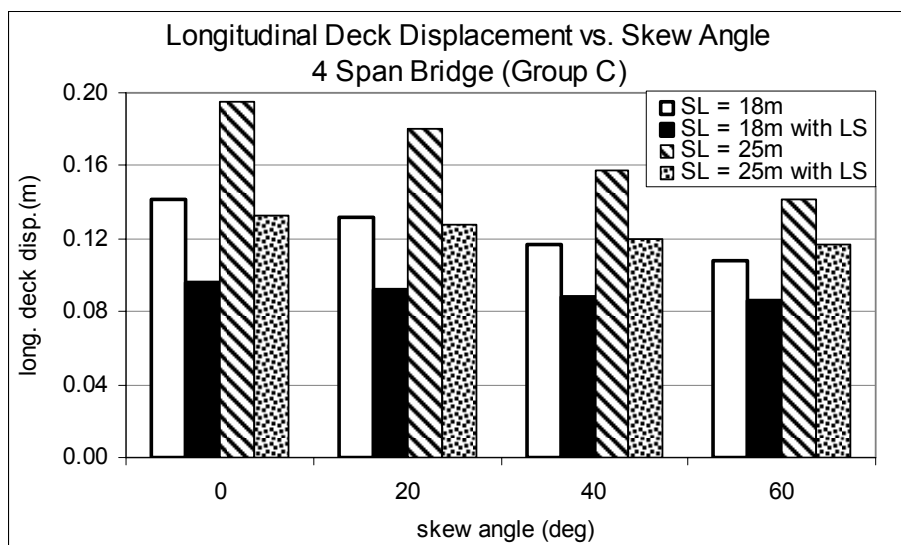


Figure 5.11: Change in longitudinal deck displacement with skew angle for 4 span bridges in Group C

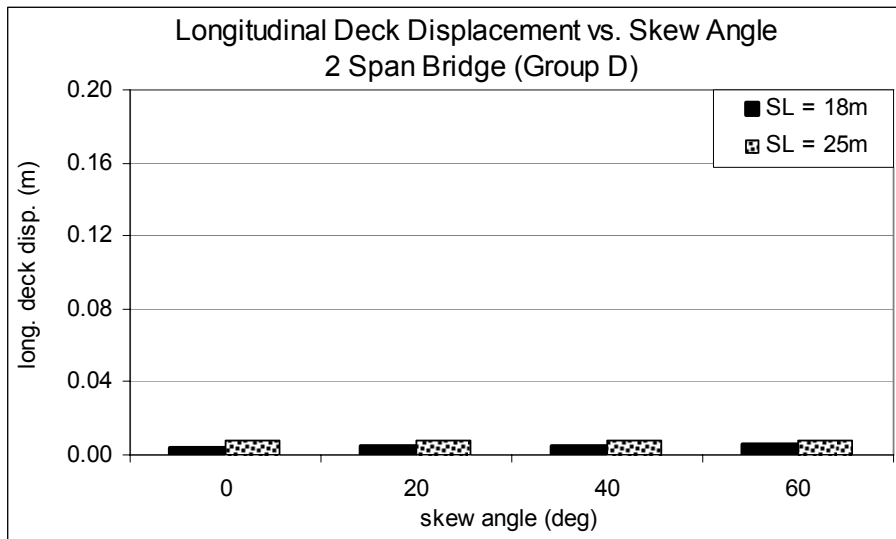


Figure 5.12: Change in longitudinal deck displacement with skew angle for 2 span bridges in Group D

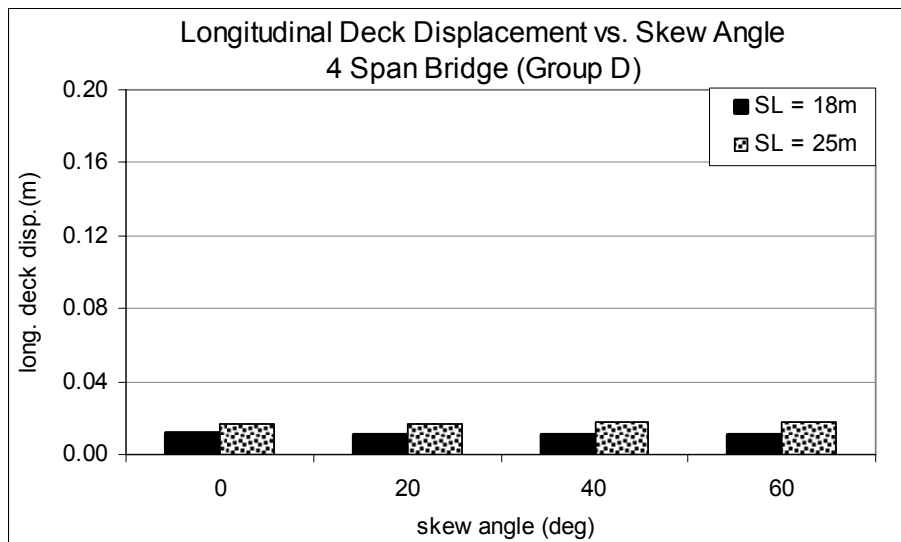


Figure 5.13: Change in longitudinal deck displacement with skew angle for 4 span bridges in Group D

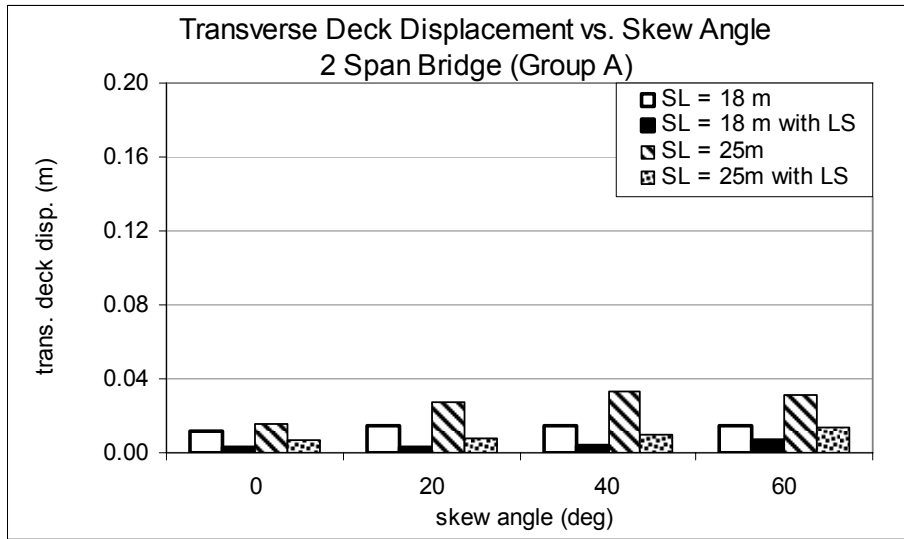


Figure 5.14: Change in transverse deck displacement with skew angle for 2 span bridges in Group A

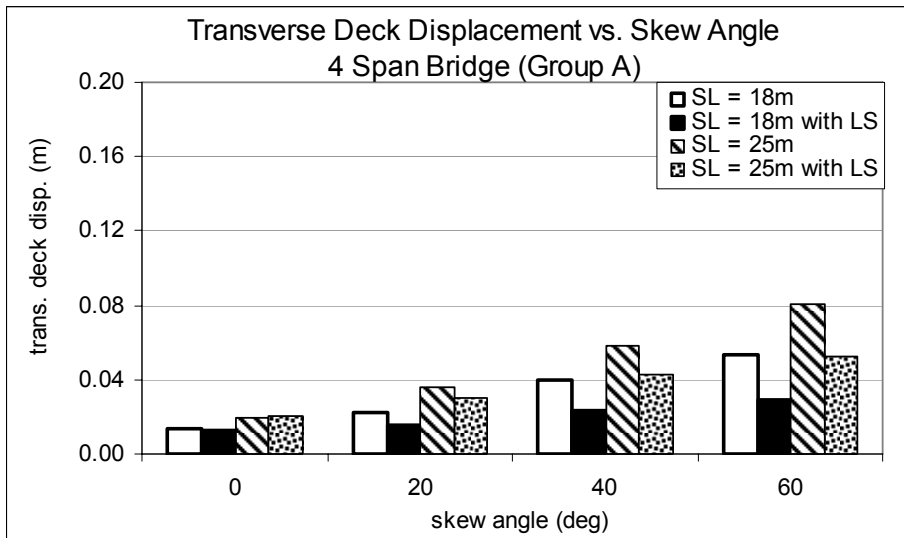


Figure 5.15: Change in transverse deck displacement with skew angle for 4 span bridges in Group A

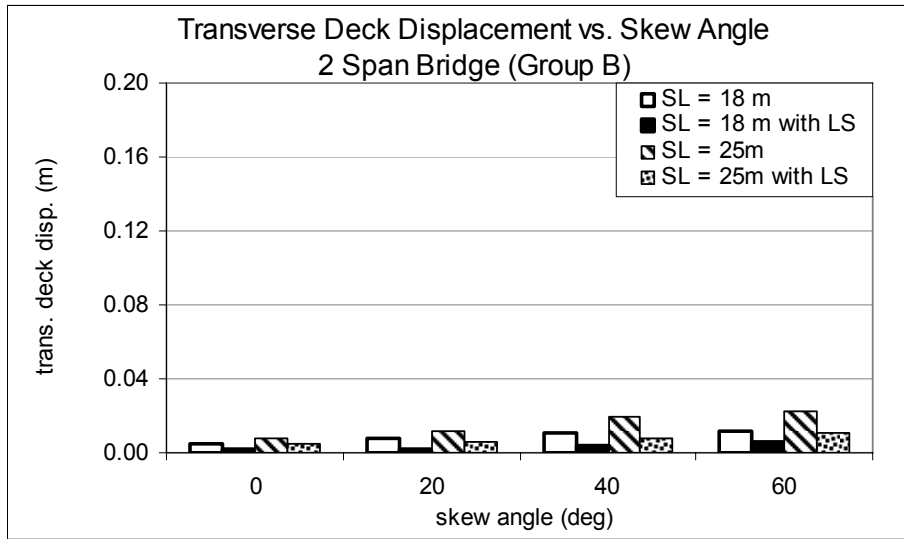


Figure 5.16: Change in transverse deck displacement with skew angle for 2 span bridges in Group B

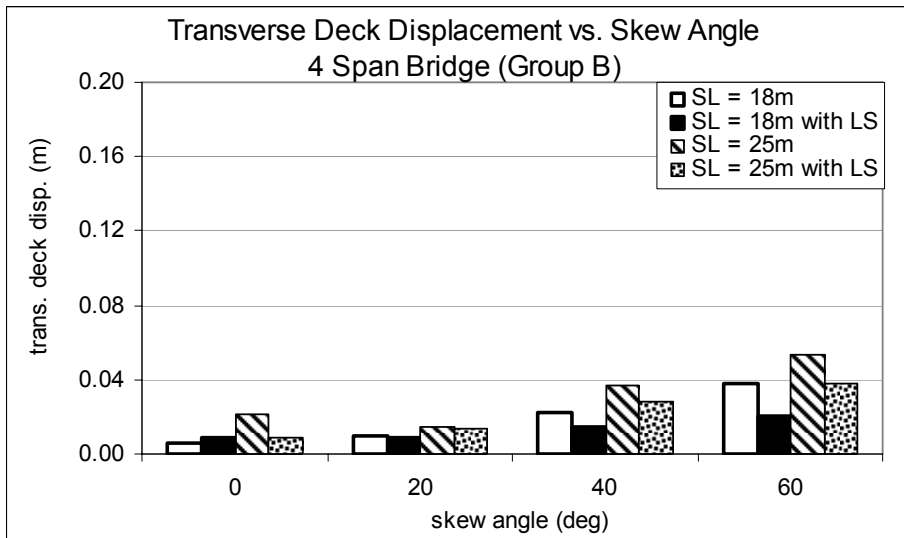


Figure 5.17: Change in transverse deck displacement with skew angle for 4 span bridges in Group B

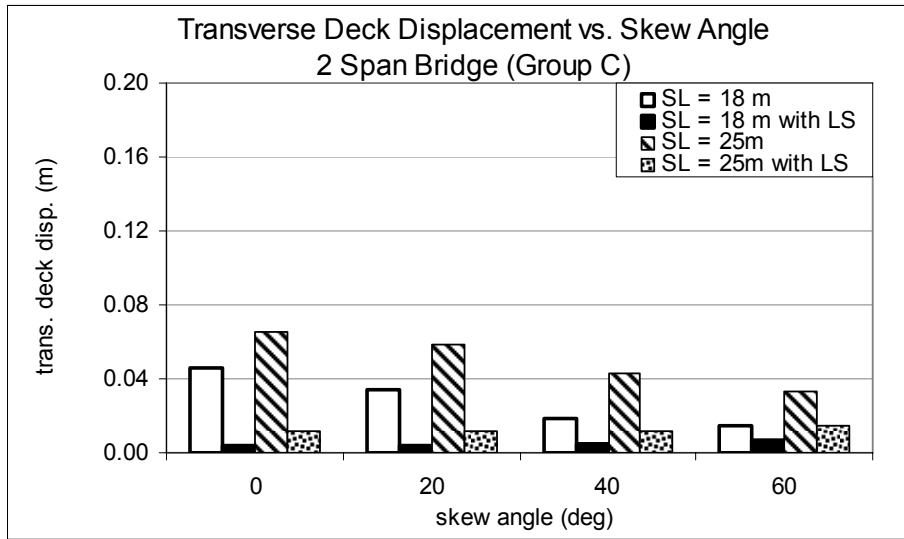


Figure 5.18: Change in transverse deck displacement with skew angle for 2 span bridges in Group C

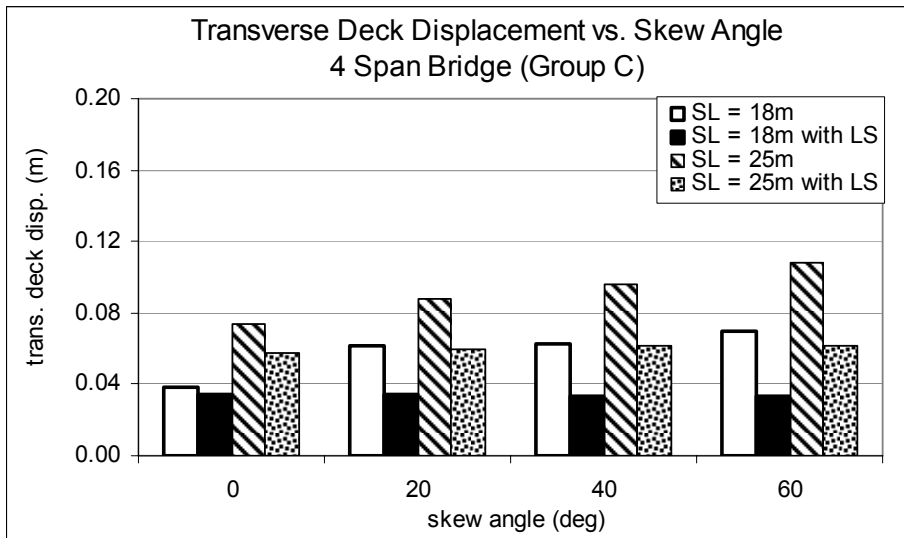


Figure 5.19: Change in transverse deck displacement with skew angle for 4 span bridges in Group C

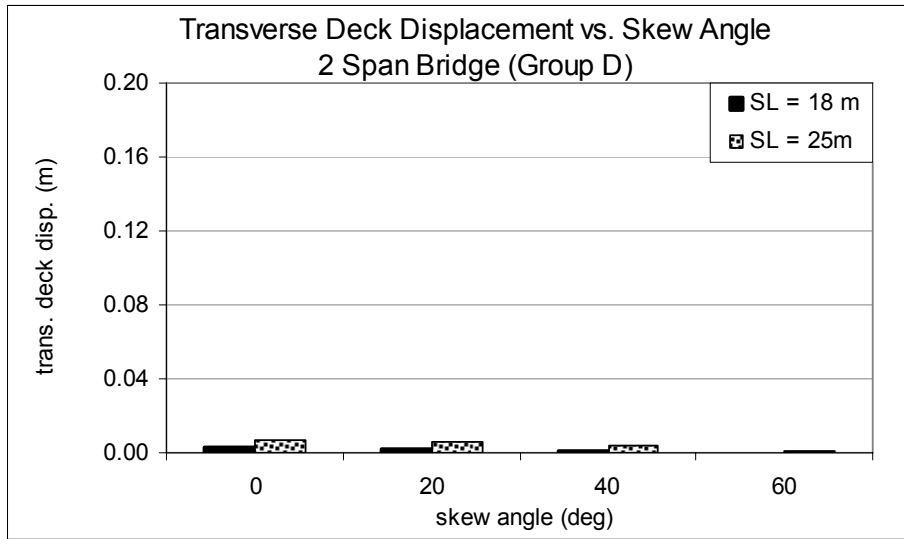


Figure 5.20: Change in transverse deck displacement with skew angle for 2 span bridges in Group D

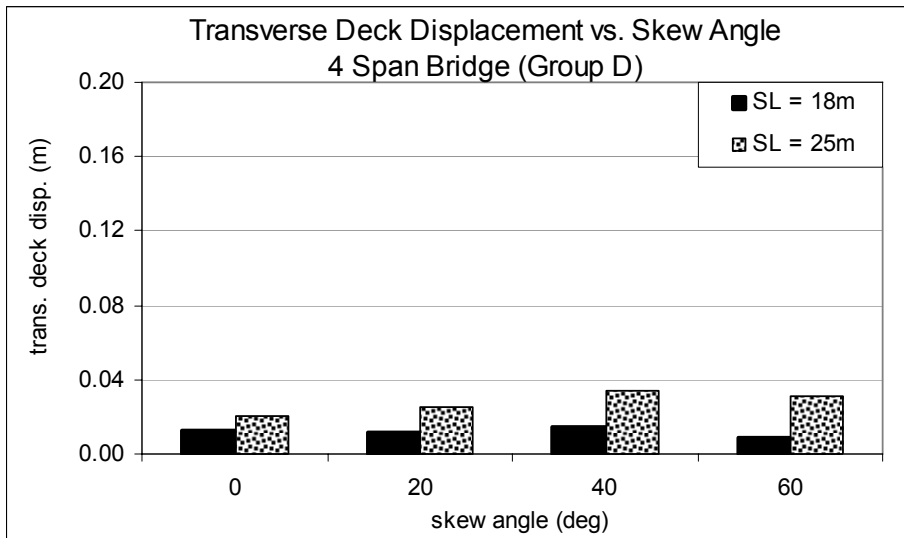


Figure 5.21: Change in transverse deck displacement with skew angle for 4 span bridges in Group D

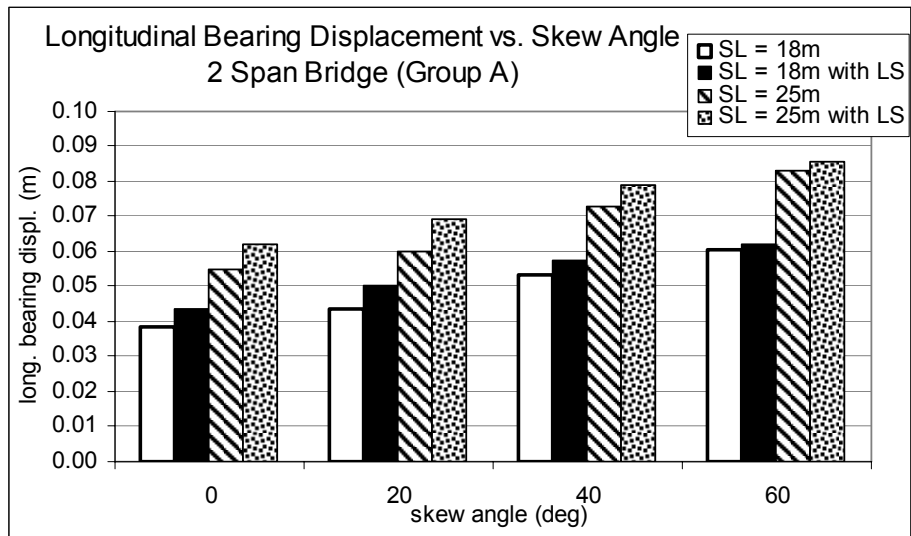


Figure 5.22: Change in longitudinal bearing displacement with skew angle for 2 span bridges in Group A

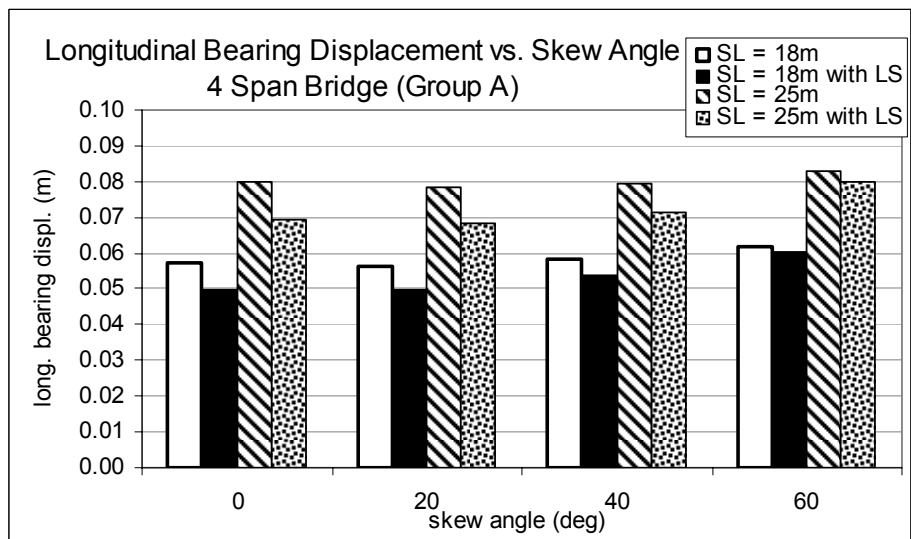


Figure 5.23: Change in longitudinal bearing displacement with skew angle for 4 span bridges in Group A

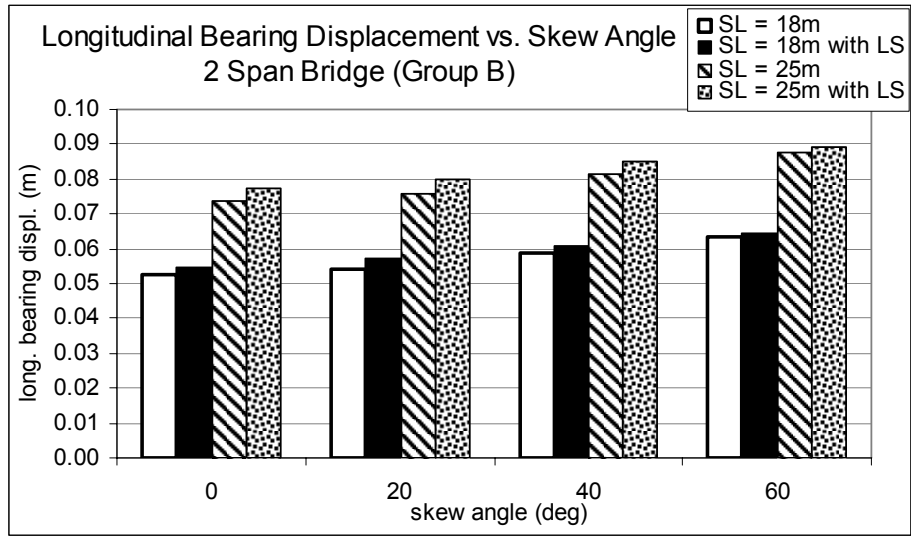


Figure 5.24: Change in longitudinal bearing displacement with skew angle for 2 span bridges in Group B

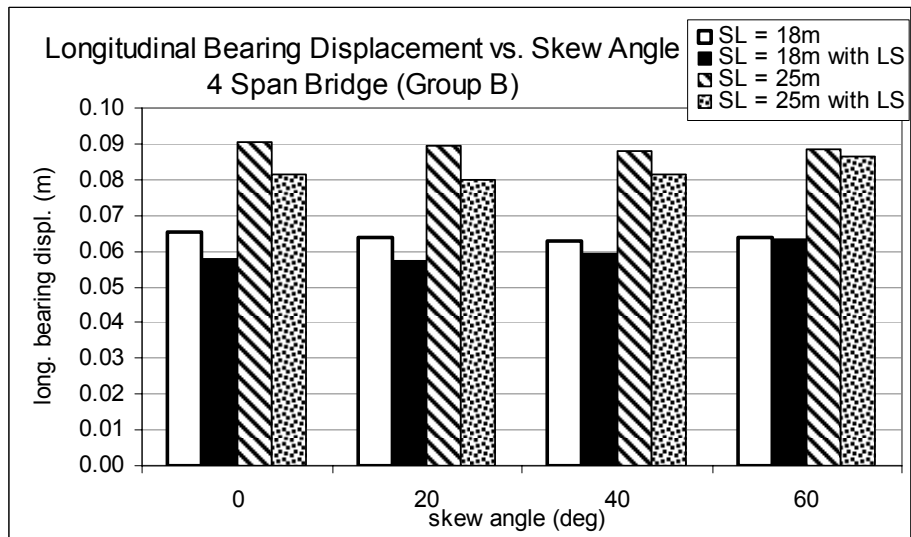


Figure 5.25: Change in longitudinal bearing displacement with skew angle for 4 span bridges in Group B

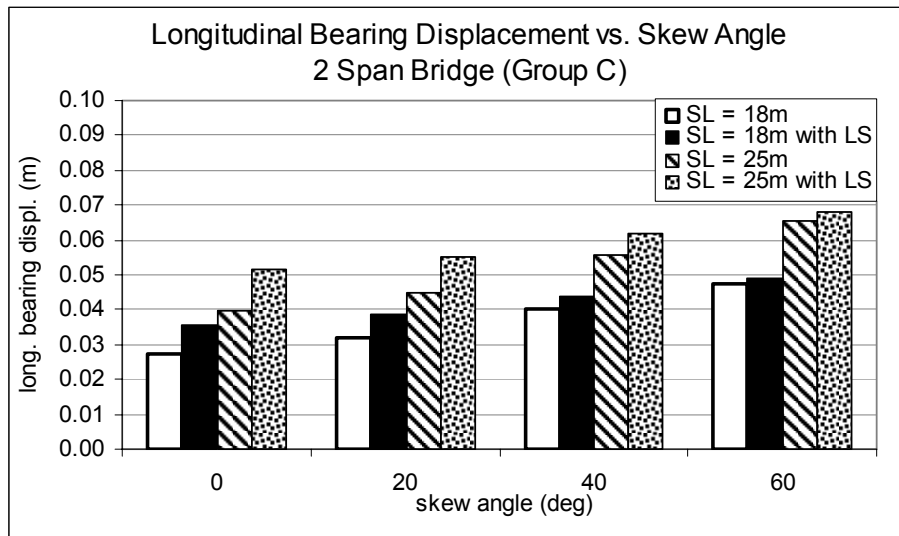


Figure 5.26: Change in longitudinal bearing displacement with skew angle for 2 span bridges in Group C

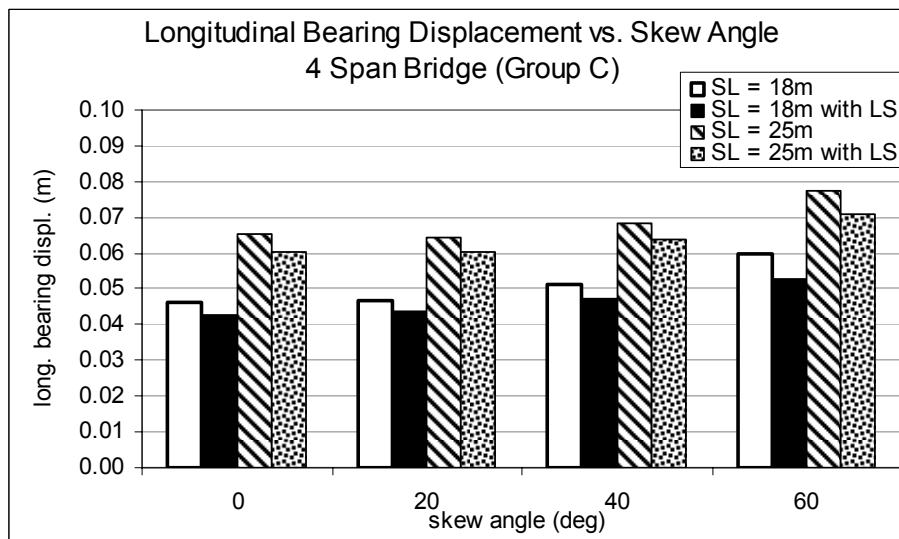


Figure 5.27: Change in longitudinal bearing displacement with skew angle for 4 span bridges in Group C

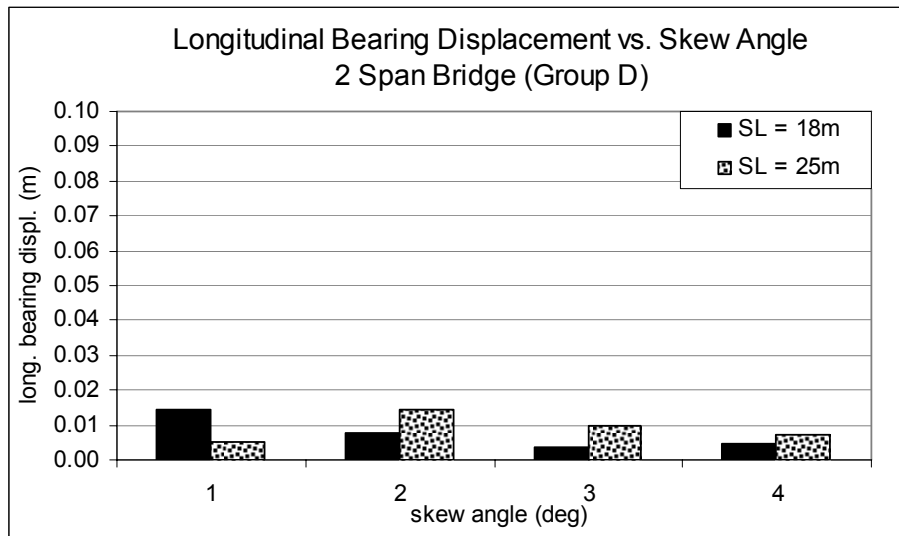


Figure 5.28: Change in longitudinal bearing displacement with skew angle for 2 span bridges in Group D

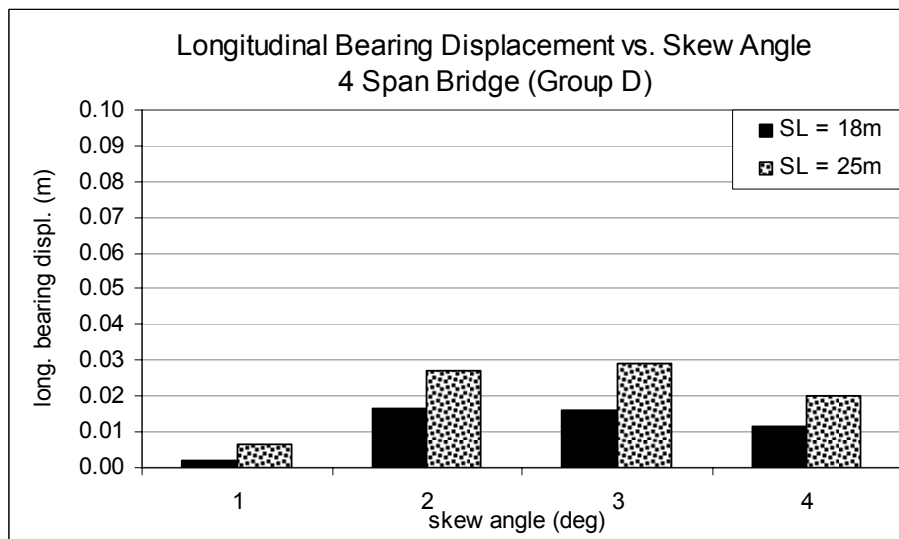


Figure 5.29: Change in longitudinal bearing displacement with skew angle for 4 span bridges in Group D

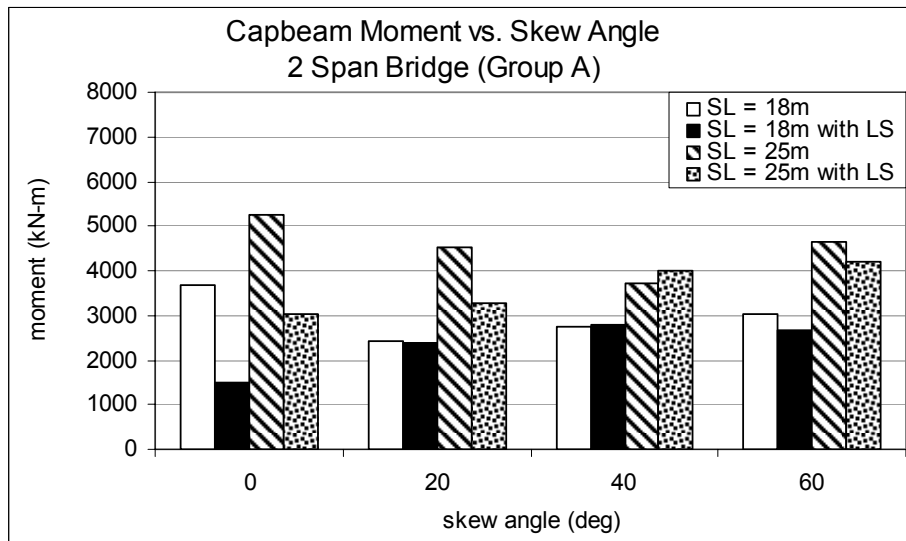


Figure 5.30: Change in local cap beam moment with skew angle for 2 span bridges in Group A

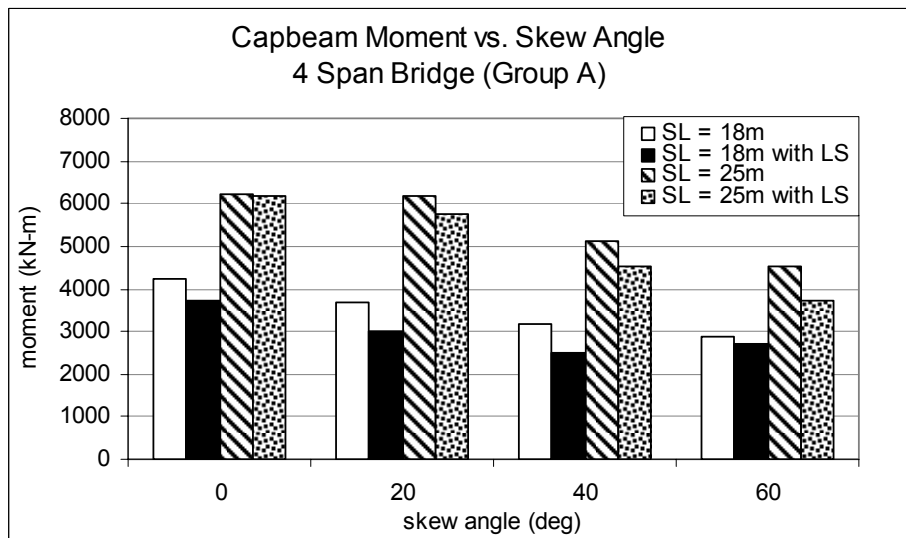


Figure 5.31: Change in local cap beam moment with skew angle for 4 span bridges in Group A

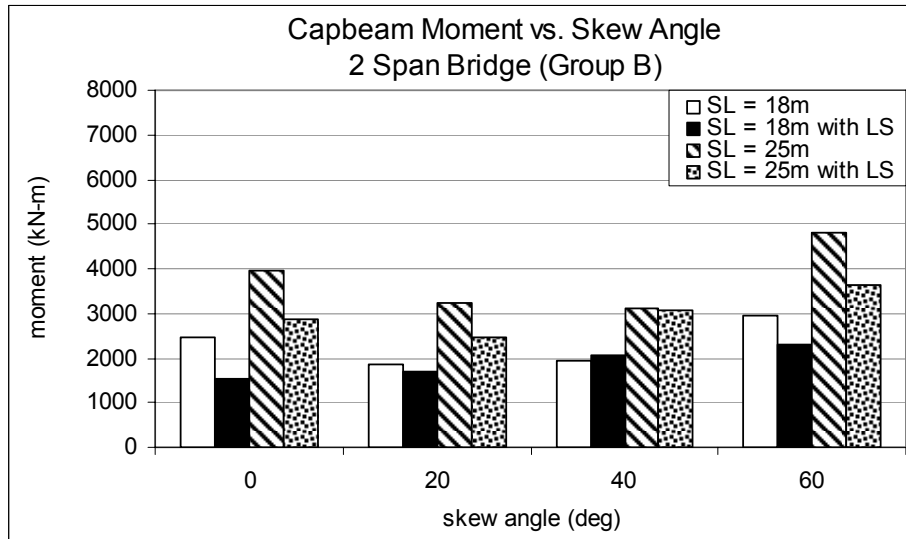


Figure 5.32: Change in local cap beam moment with skew angle for 2 span bridges in Group B

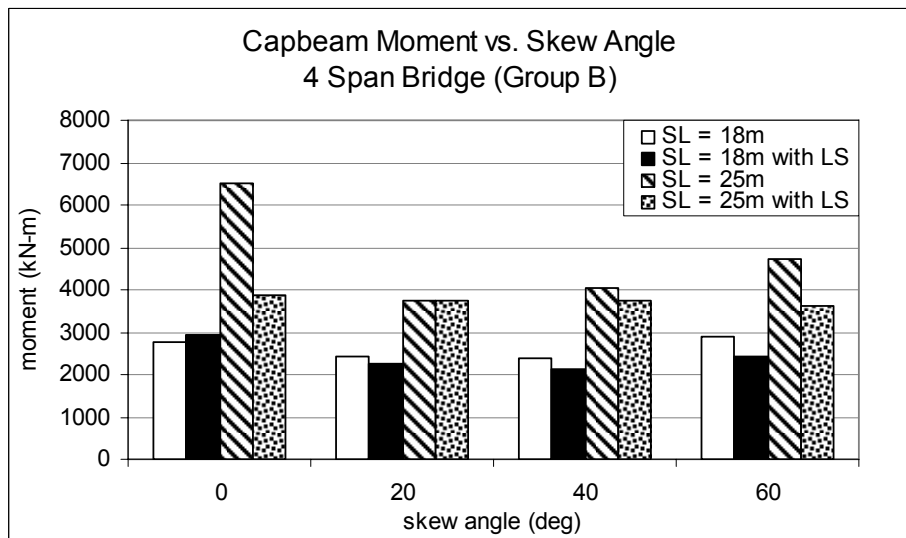


Figure 5.33: Change in local cap beam moment with skew angle for 4 span bridges in Group B

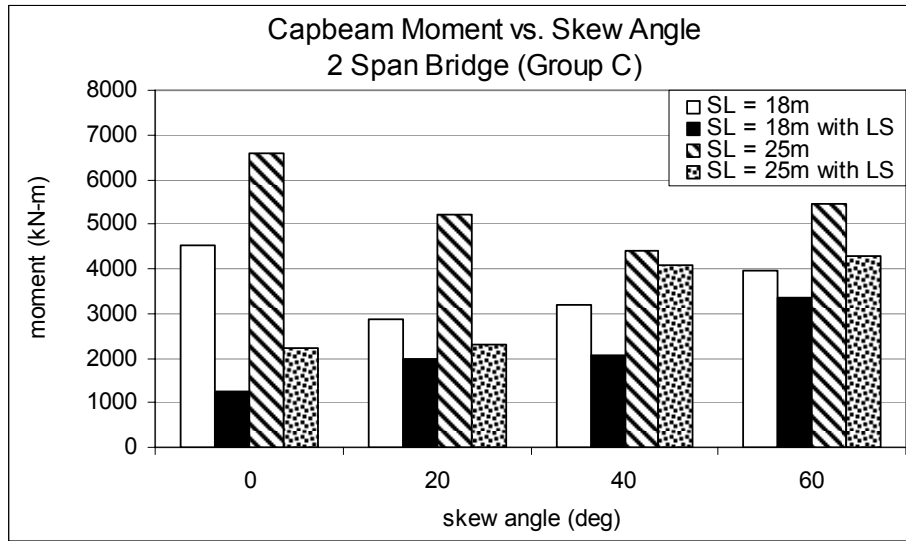


Figure 5.34: Change in local cap beam moment with skew angle for 2 span bridges in Group C

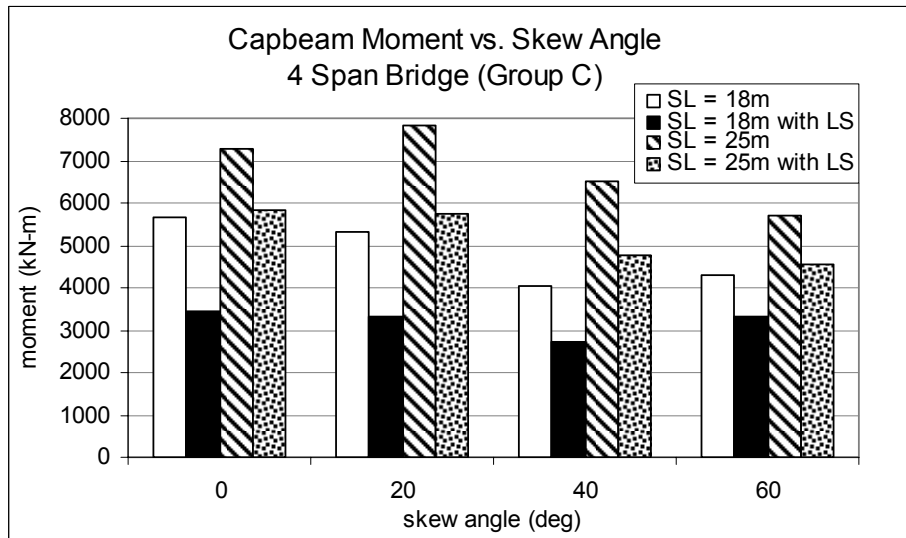


Figure 5.35: Change in local cap beam moment with skew angle for 4 span bridges in Group C

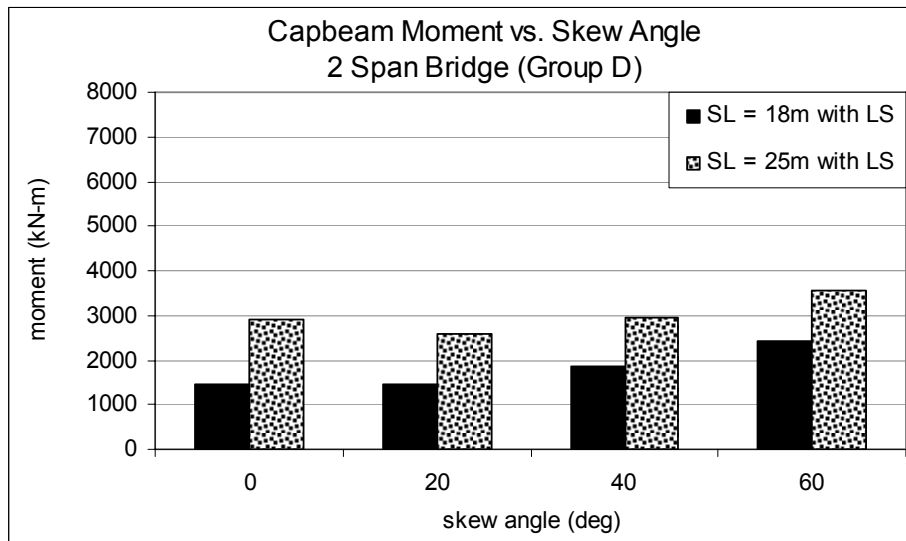


Figure 5.36: Change in local cap beam moment with skew angle for 2 span bridges in Group D

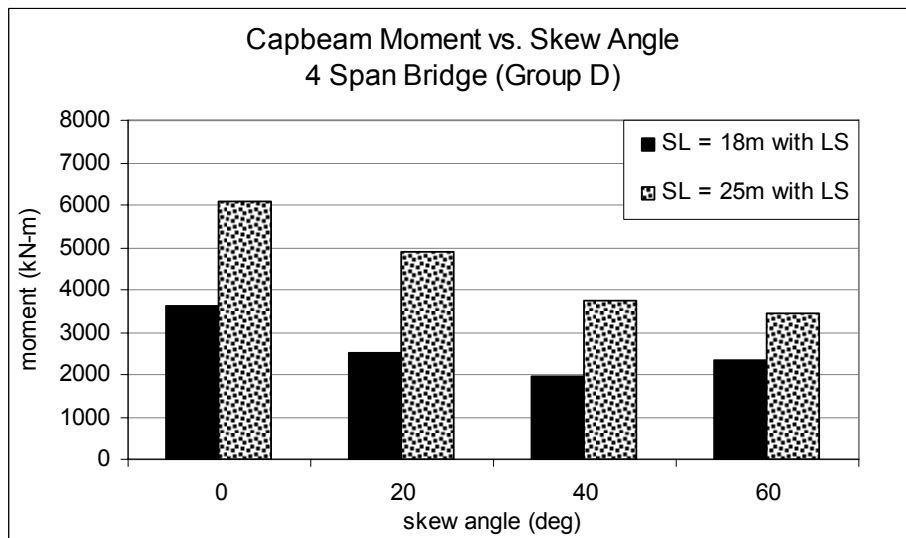


Figure 5.37: Change in local cap beam moment with skew angle for 4 span bridges in Group D

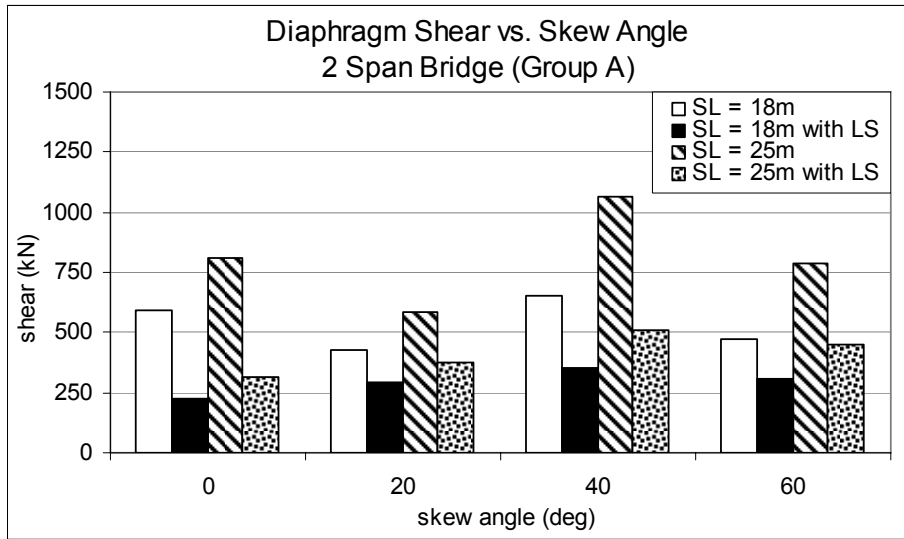


Figure 5.38: Change in local diaphragm shear with skew angle for 2 span bridges in Group A

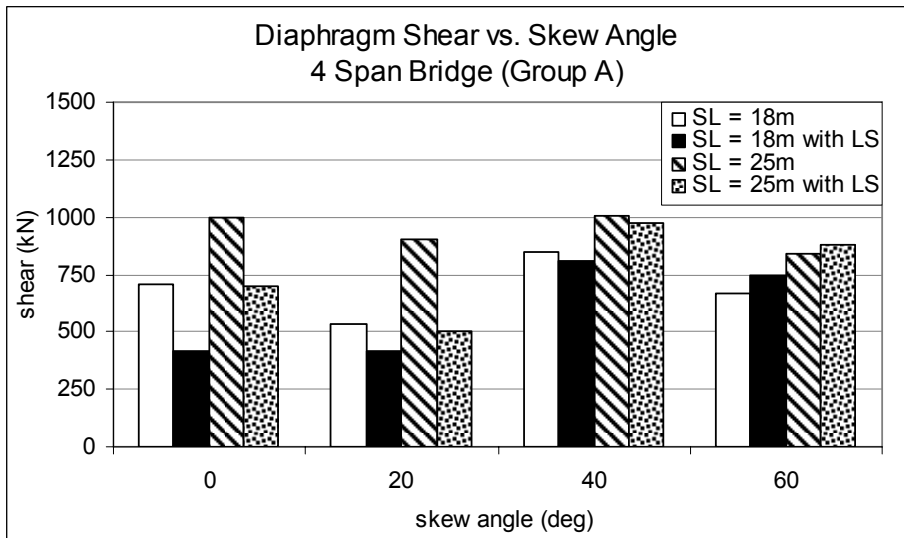


Figure 5.39: Change in local diaphragm shear with skew angle for 4 span bridges in Group A

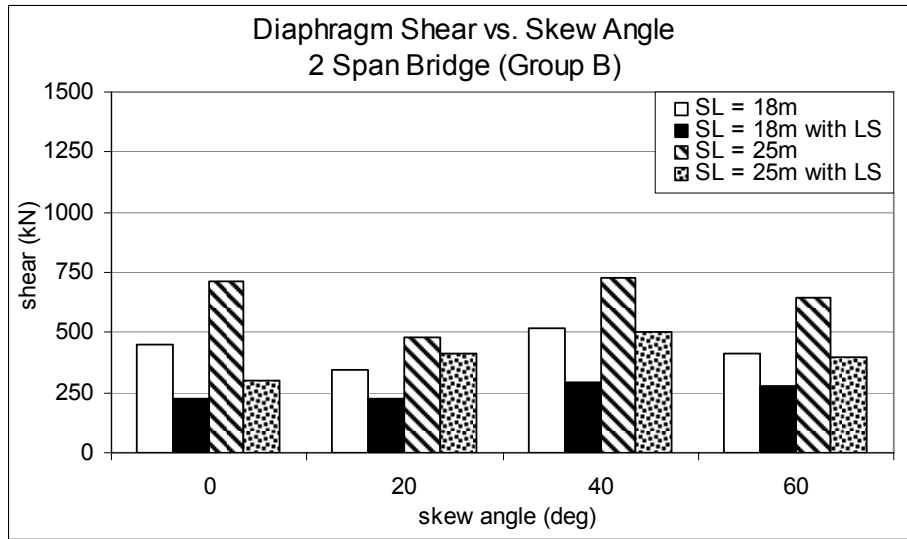


Figure 5.40: Change in local diaphragm shear with skew angle for 2 span bridges in Group B

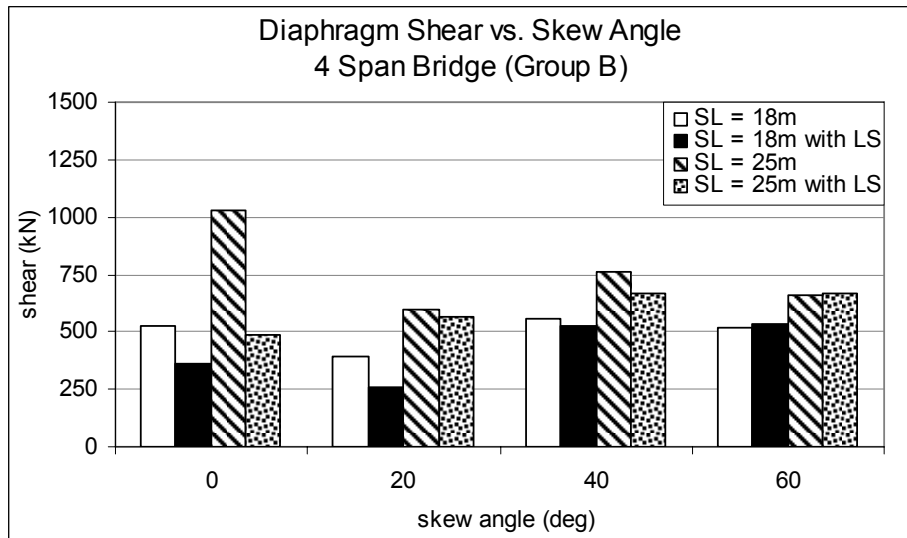


Figure 5.41: Change in local diaphragm shear with skew angle for 4 span bridges in Group B

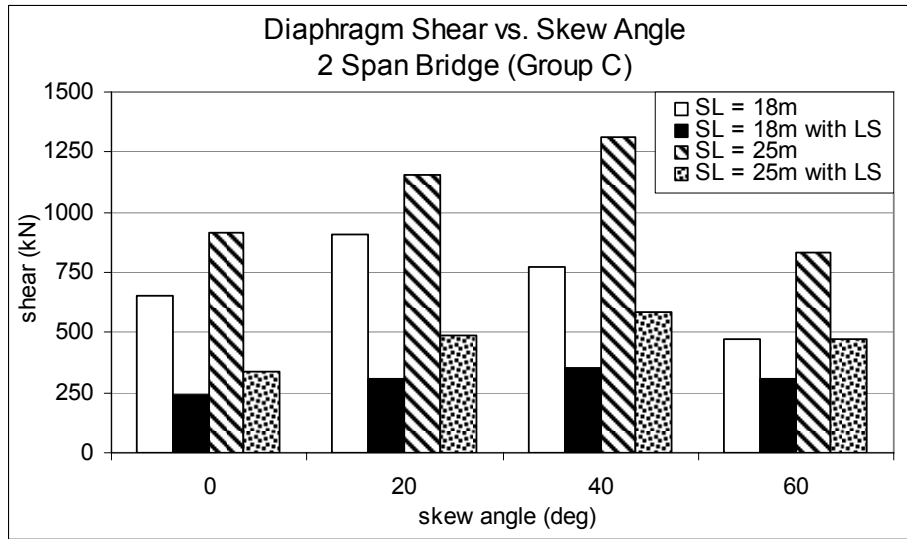


Figure 5.42: Change in local diaphragm shear with skew angle for 2 span bridges in Group C

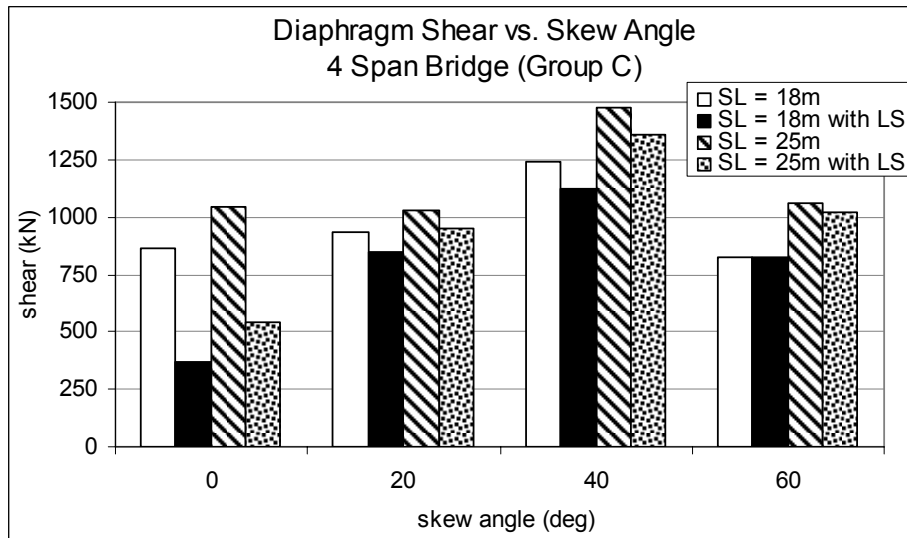


Figure 5.43: Change in local diaphragm shear with skew angle for 4 span bridges in Group C

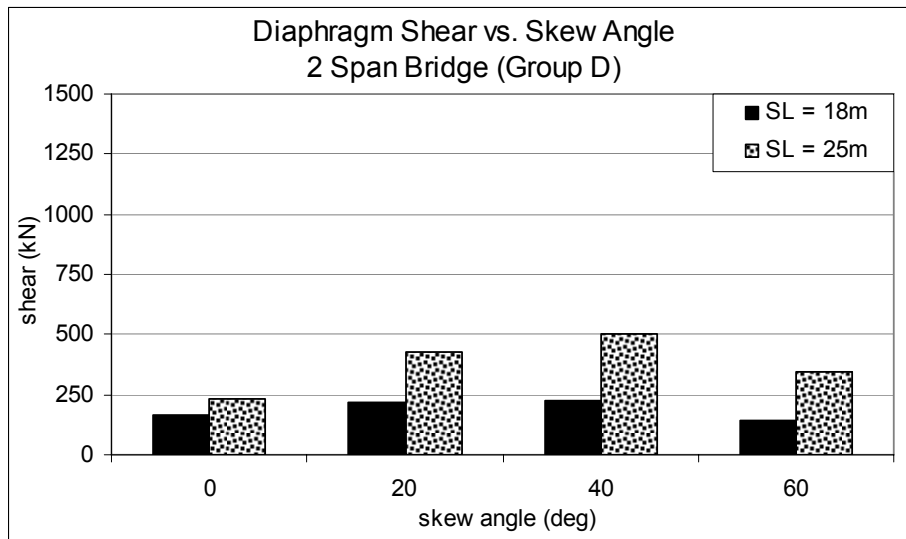


Figure 5.44: Change in local diaphragm shear with skew angle for 2 span bridges in Group D

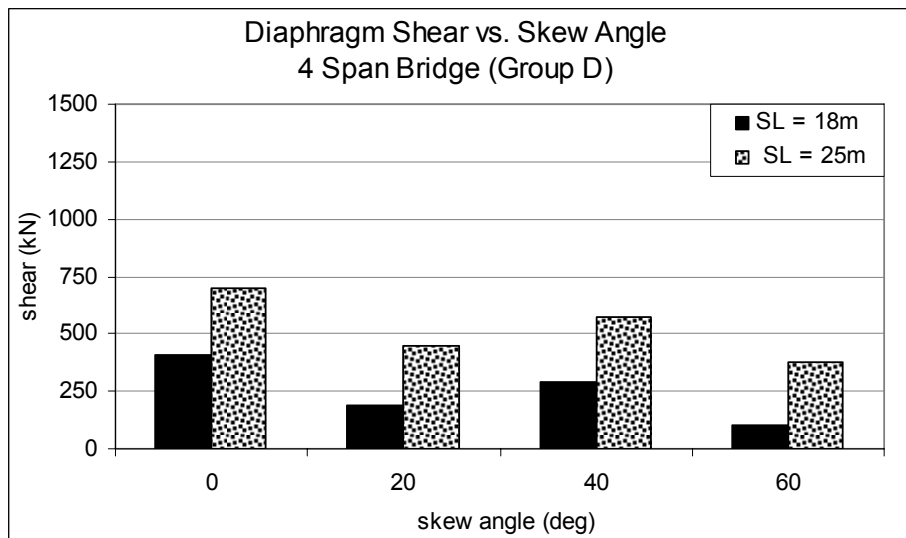


Figure 5.45: Change in local diaphragm shear with skew angle for 4 span bridges in Group D

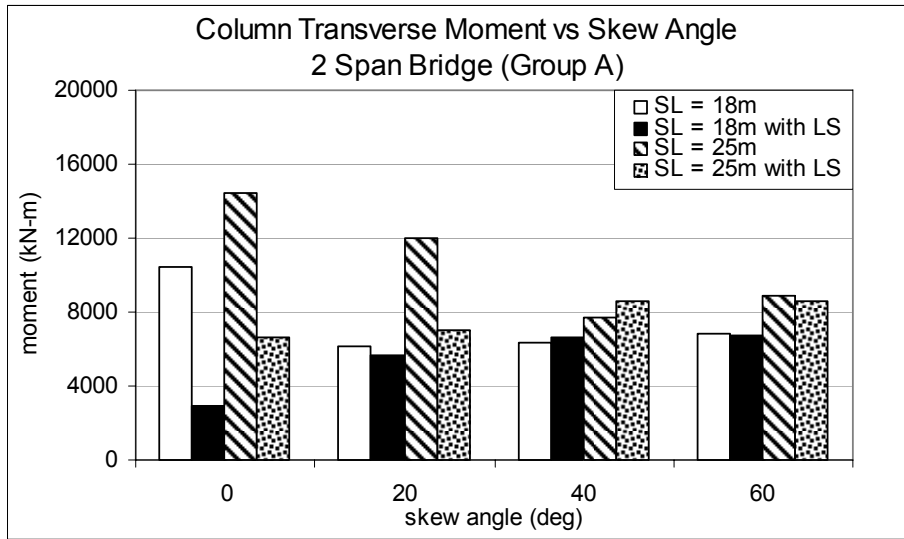


Figure 5.46: Change in local column transverse moment with skew angle for 2 span bridges in Group A

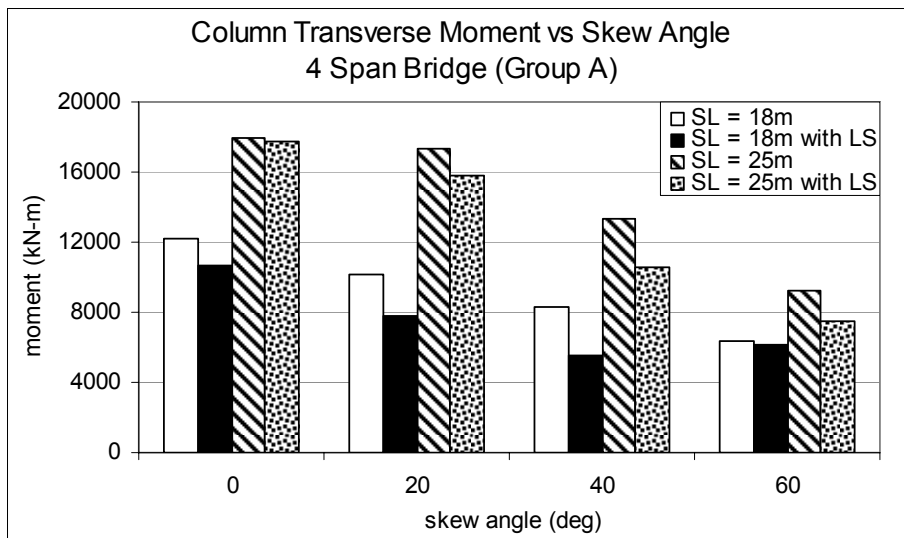


Figure 5.47: Change in local column transverse moment with skew angle for 4 span bridges in Group A

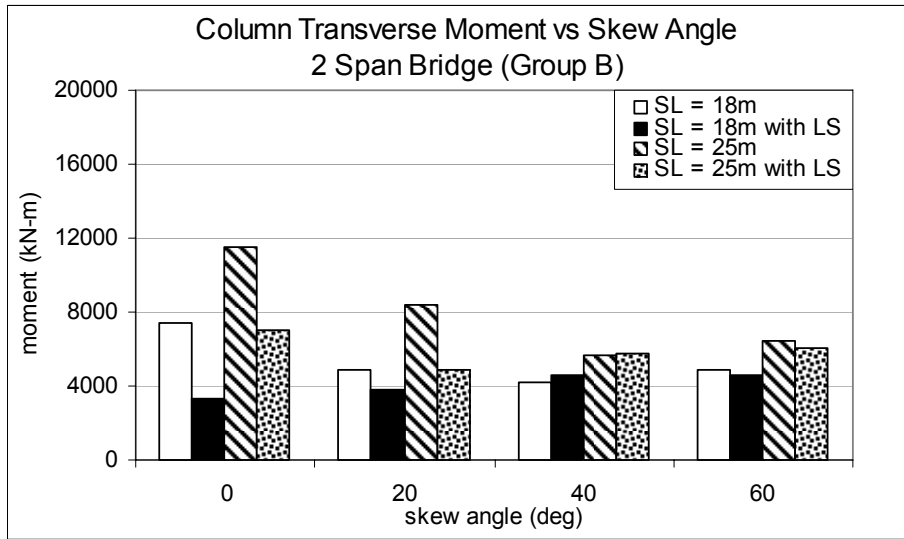


Figure 5.48: Change in local column transverse moment with skew angle for 2 span bridges in Group B

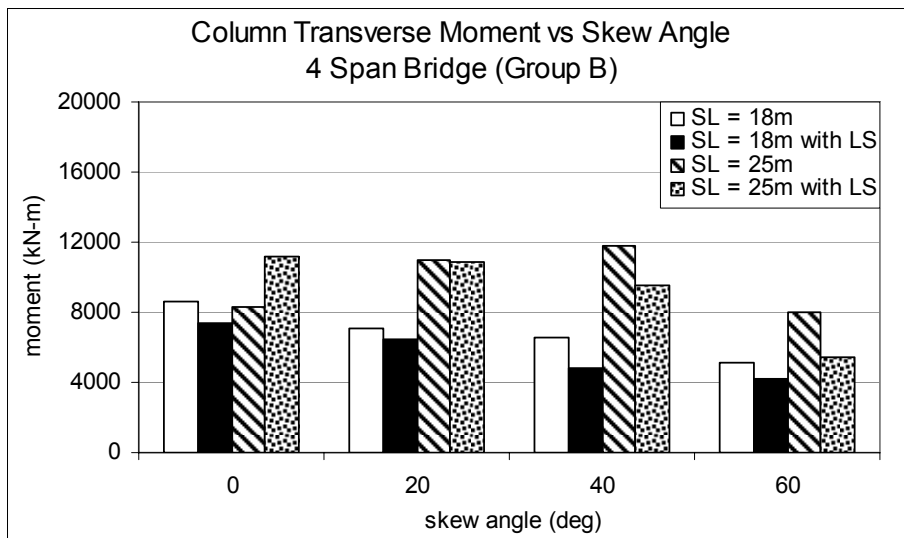


Figure 5.49: Change in local column transverse moment with skew angle for 4 span bridges in Group B

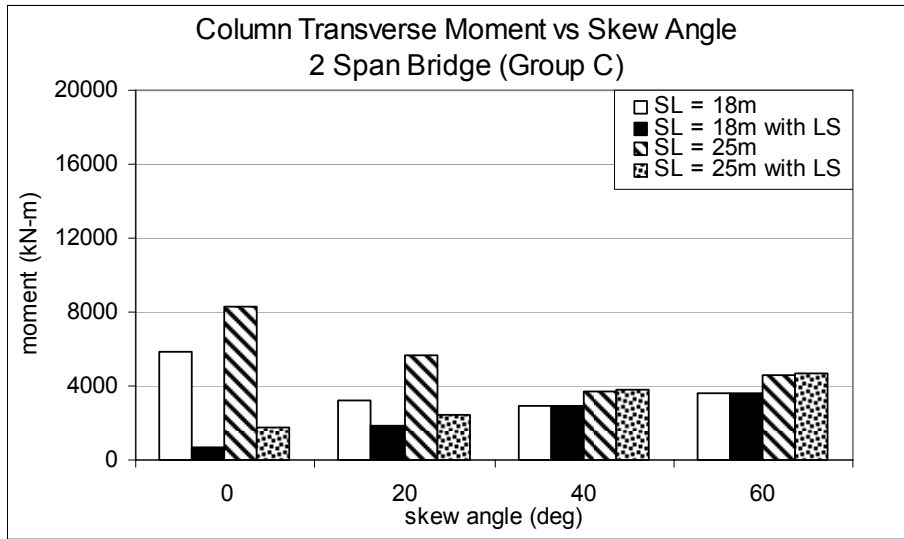


Figure 5.50: Change in local column transverse moment with skew angle for 2 span bridges in Group C

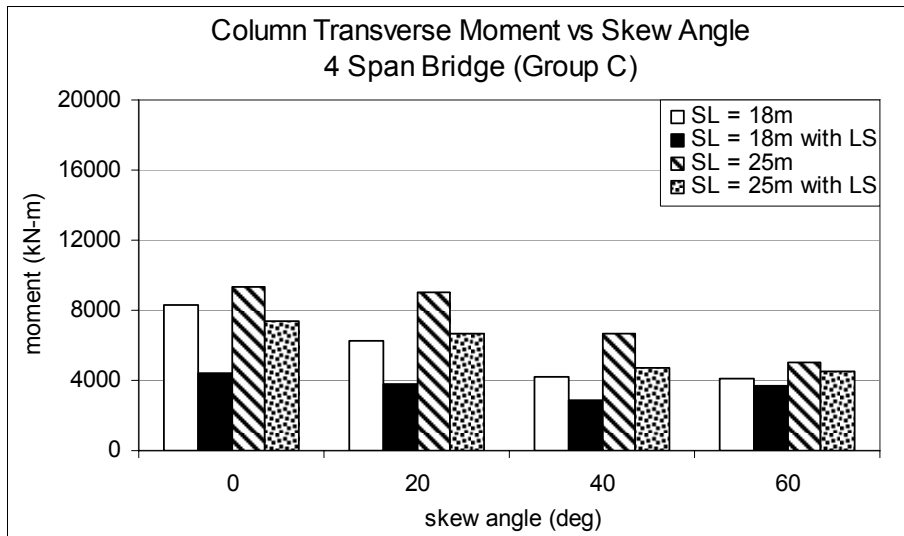


Figure 5.51: Change in local column transverse moment with skew angle for 4 span bridges in Group C

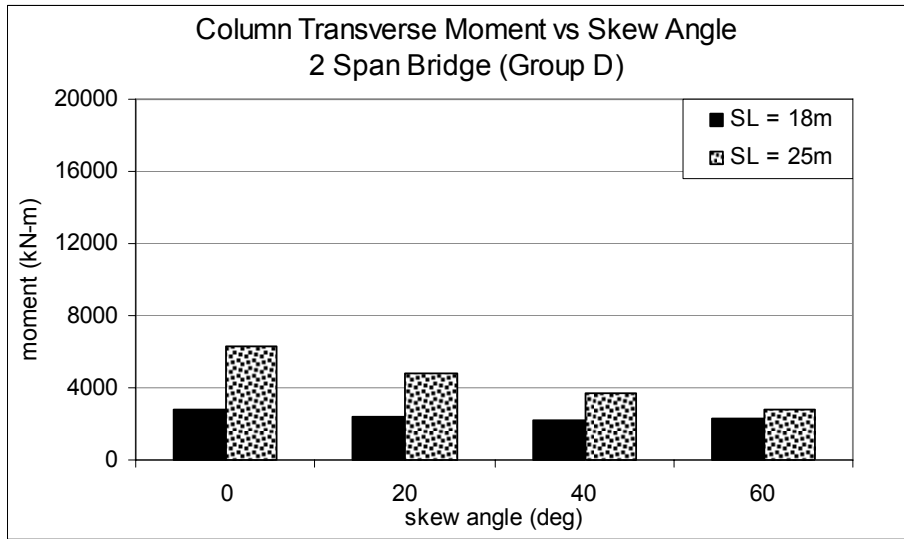


Figure 5.52: Change in local column transverse moment with skew angle for 2 span bridges in Group D

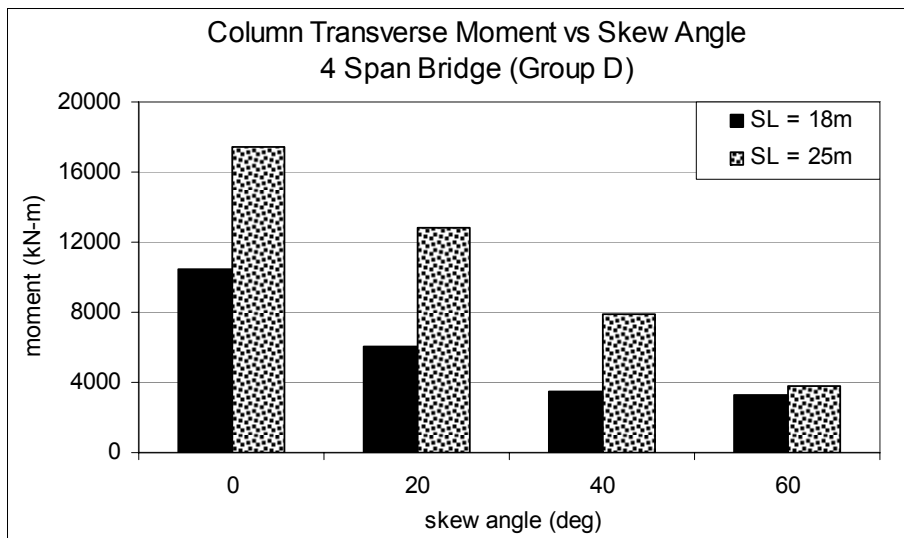


Figure 5.53: Change in local column transverse moment with skew angle for 4 span bridges in Group D

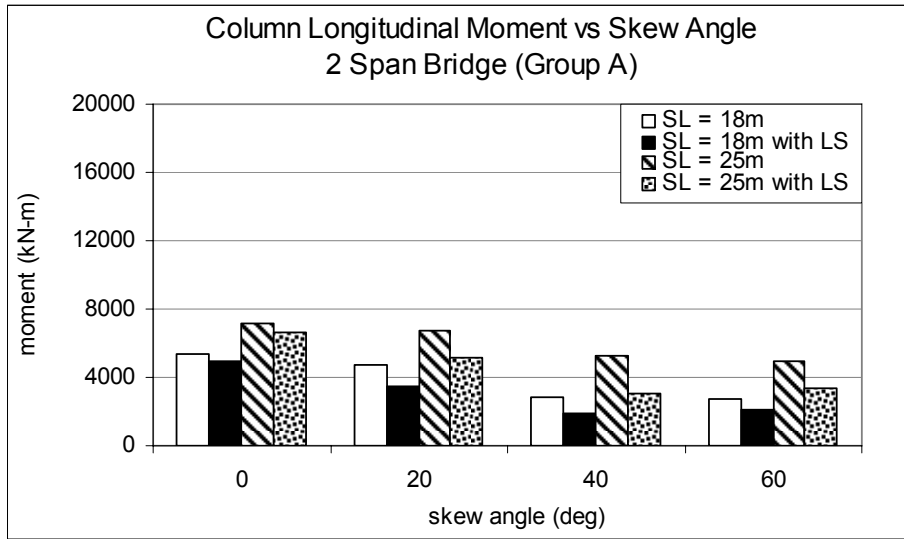


Figure 5.54: Change in local column longitudinal moment with skew angle for 2 span bridges in Group A

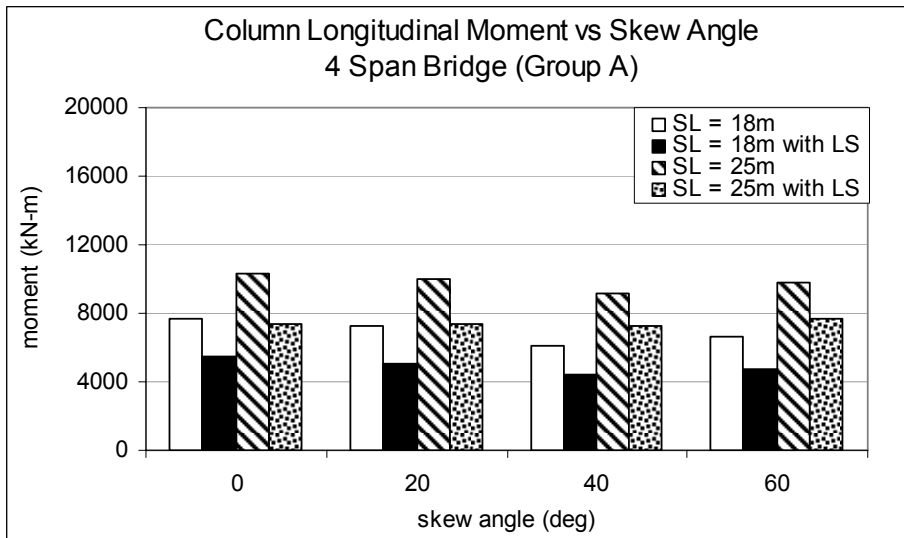


Figure 5.55: Change in local column longitudinal moment with skew angle for 4 span bridges in Group A

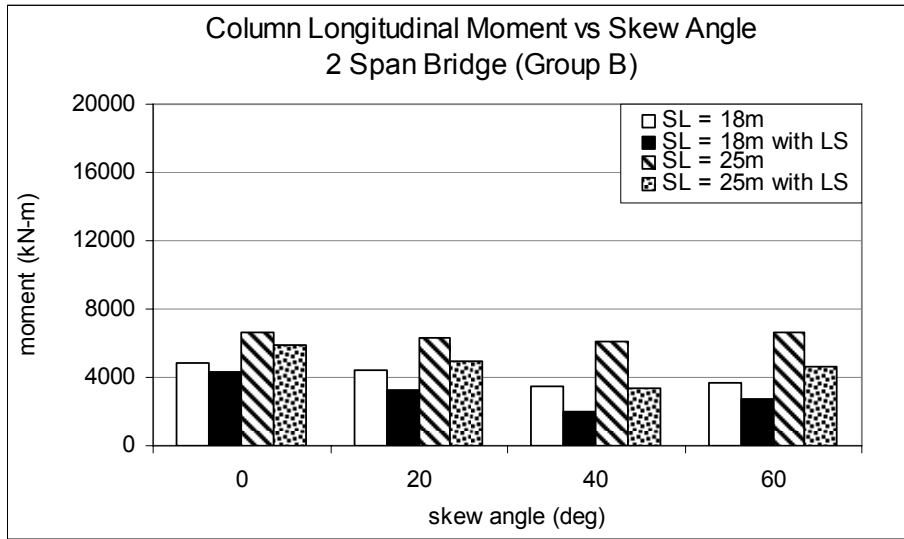


Figure 5.56: Change in local column longitudinal moment with skew angle for 2 span bridges in Group B

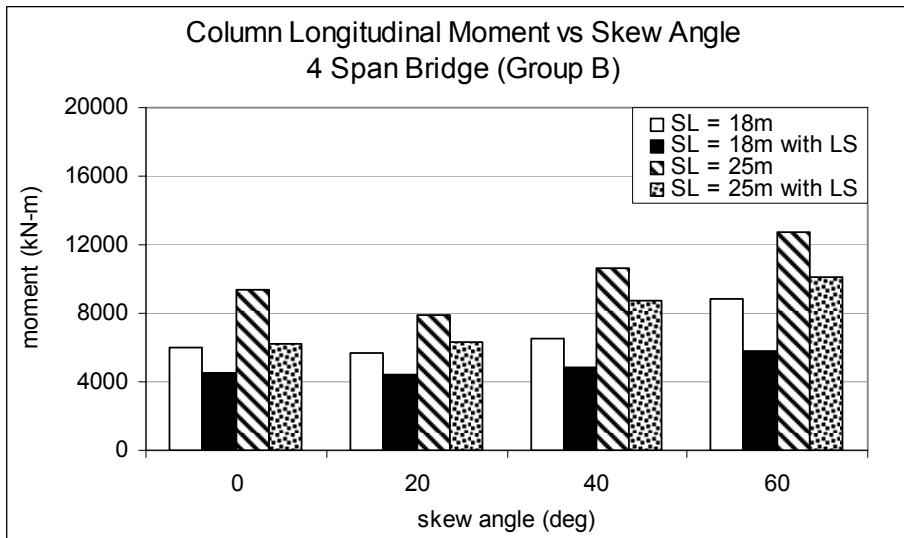


Figure 5.57: Change in local column longitudinal moment with skew angle for 4 span bridges in Group B

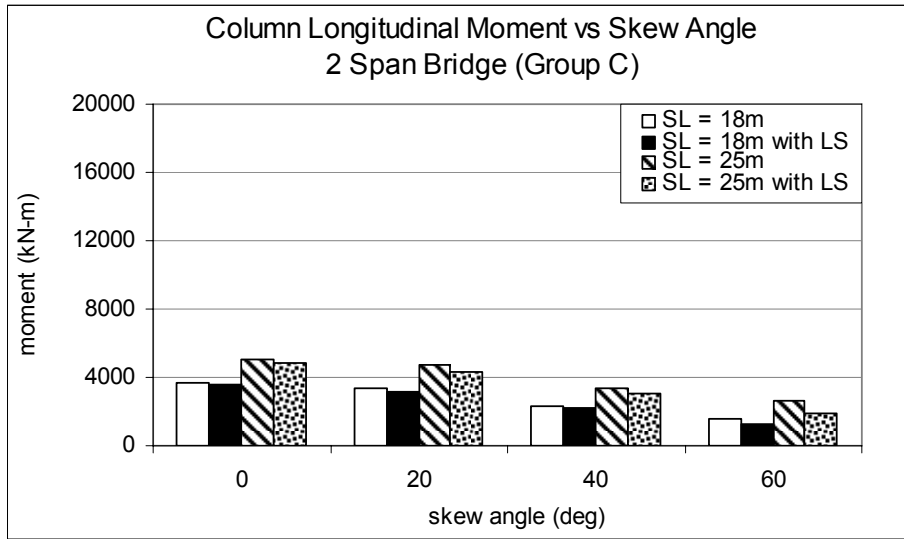


Figure 5.58: Change in local column longitudinal moment with skew angle for 2 span bridges in Group C

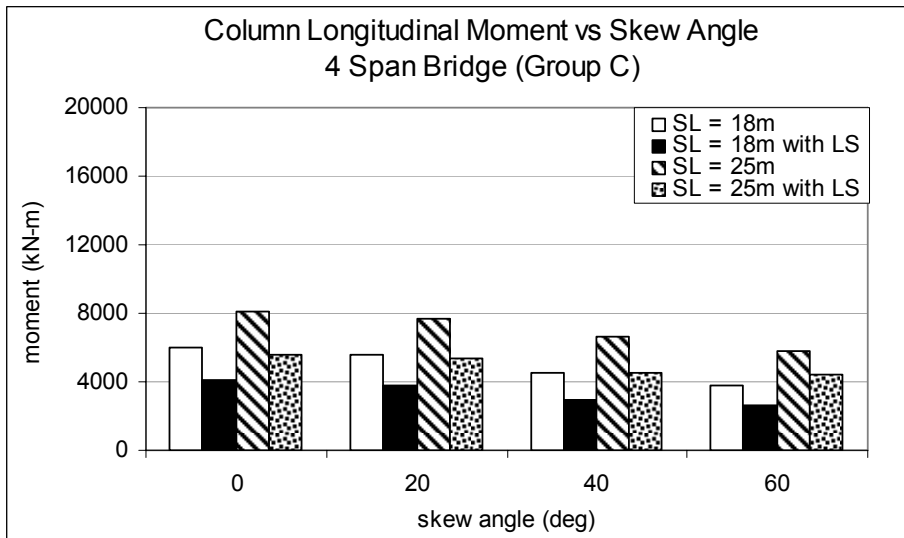


Figure 5.59: Change in local column longitudinal moment with skew angle for 4 span bridges in Group C

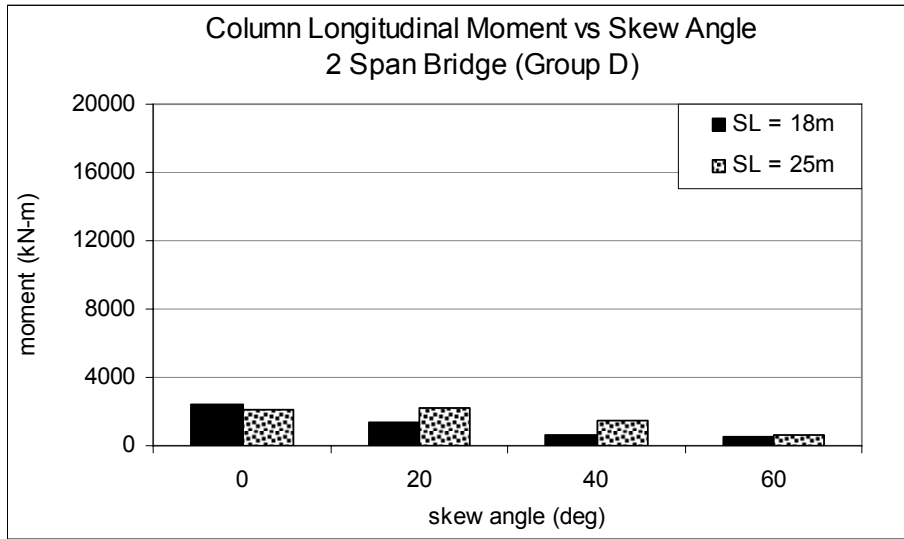


Figure 5.60: Change in local column longitudinal moment with skew angle for 2 span bridges in Group D

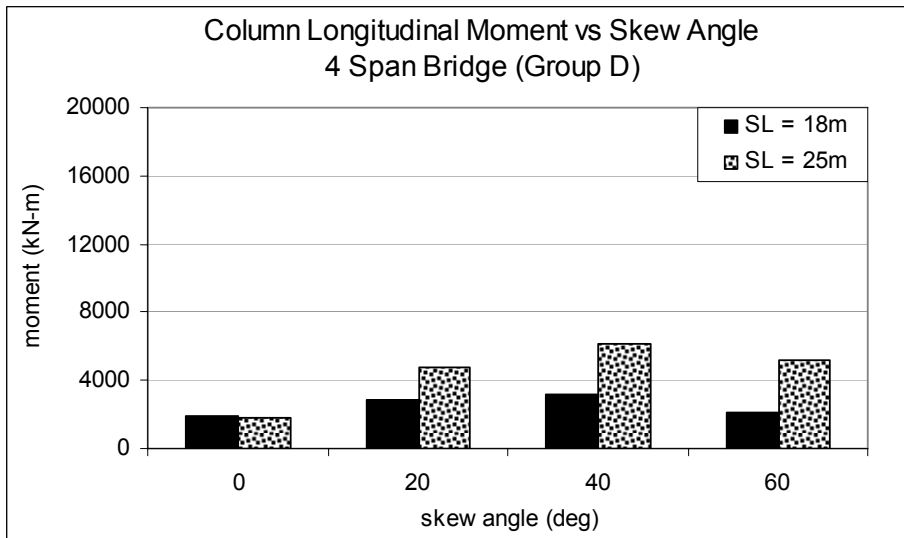


Figure 5.61: Change in local column longitudinal moment with skew angle for 4 span bridges in Group D

In the following Figures 5.62 to 5.77, link slab earthquake forces are sketched for all four groups. These graphs have two series, one for the models having spans lengths of 18m and the other for the ones having 25m of span lengths. The first series is shown by white blocks and the second one by gray blocks.

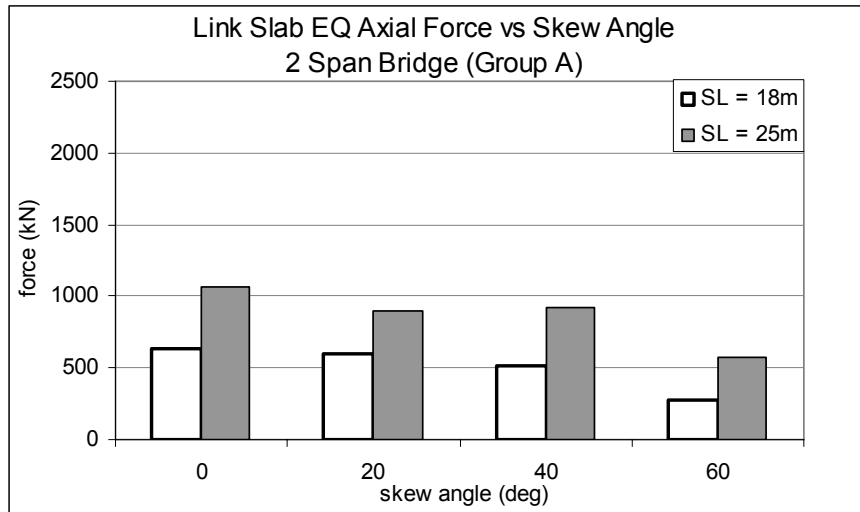


Figure 5.62: Change in link slab axial force with skew angle for 2 span bridges in Group A

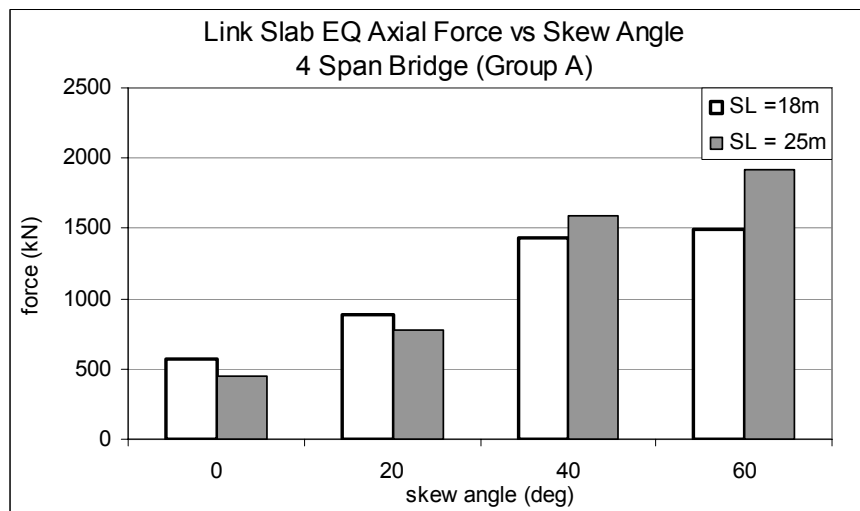


Figure 5.63: Change in link slab axial force with skew angle for 4 span bridges in Group A

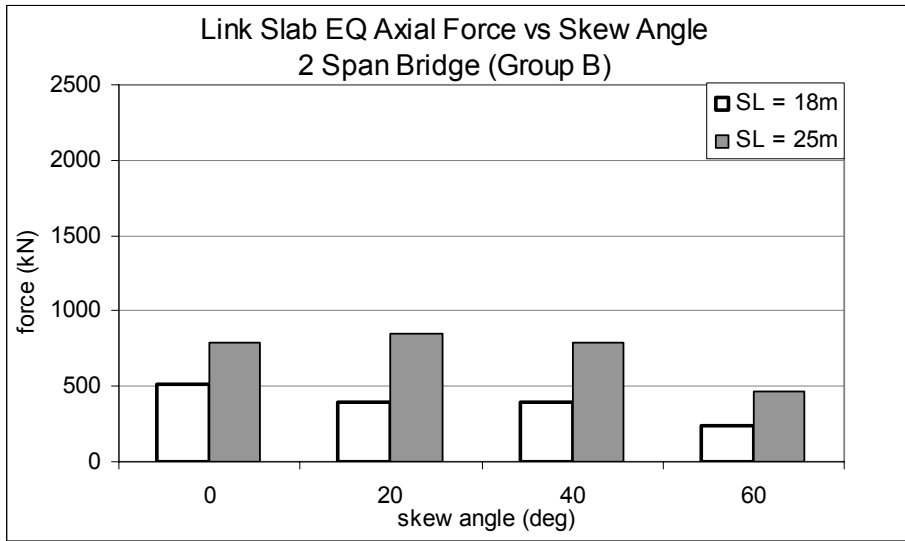


Figure 5.64: Change in link slab axial force with skew angle for 2 span bridges in Group B

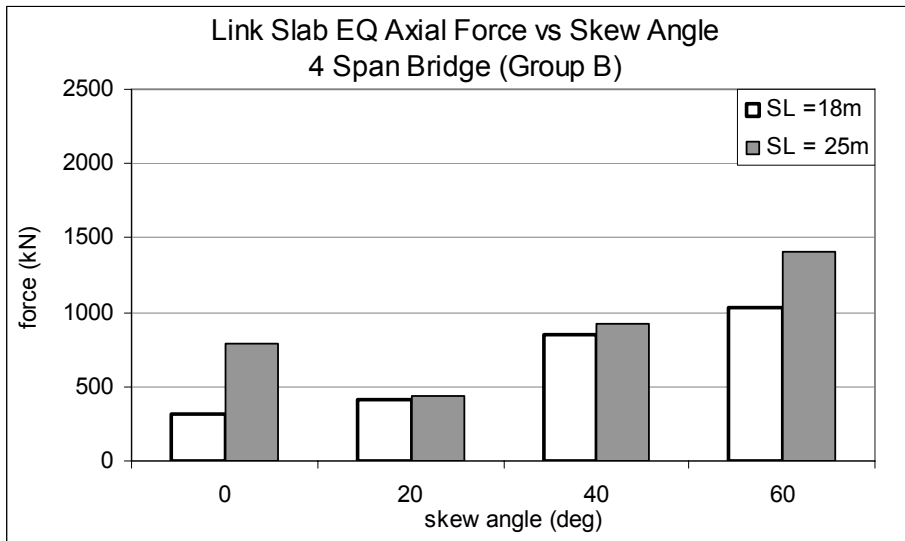


Figure 5.65: Change in link slab axial force with skew angle for 4 span bridges in Group B

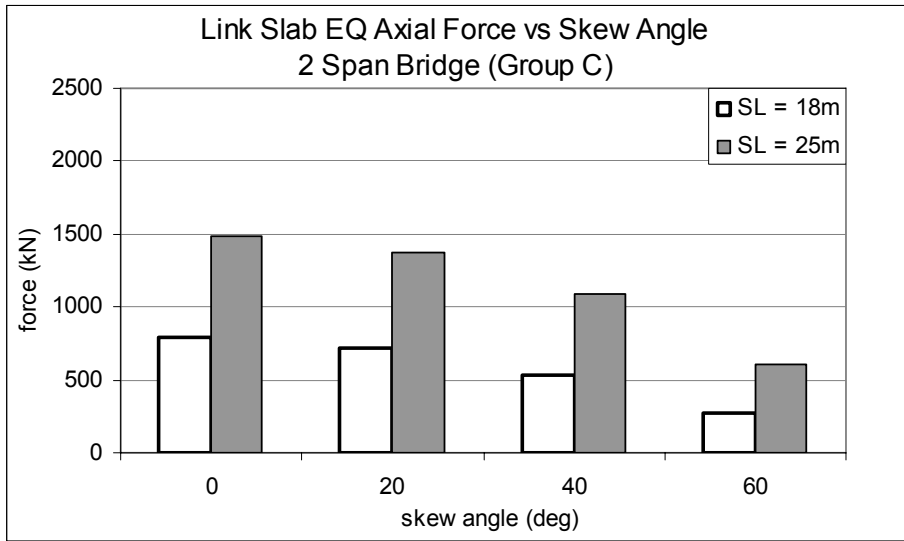


Figure 5.66: Change in link slab axial force with skew angle for 2 span bridges in Group C

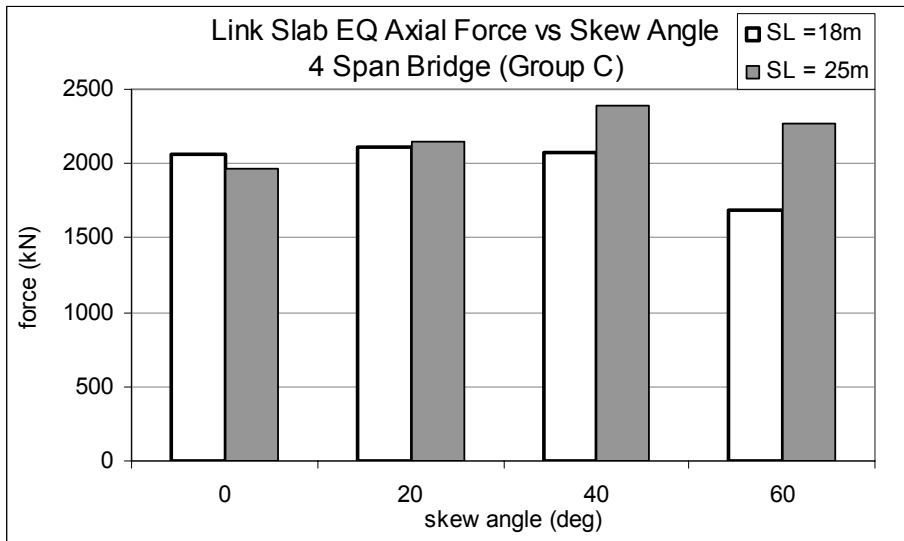


Figure 5.67: Change in link slab axial force with skew angle for 4 span bridges in Group C

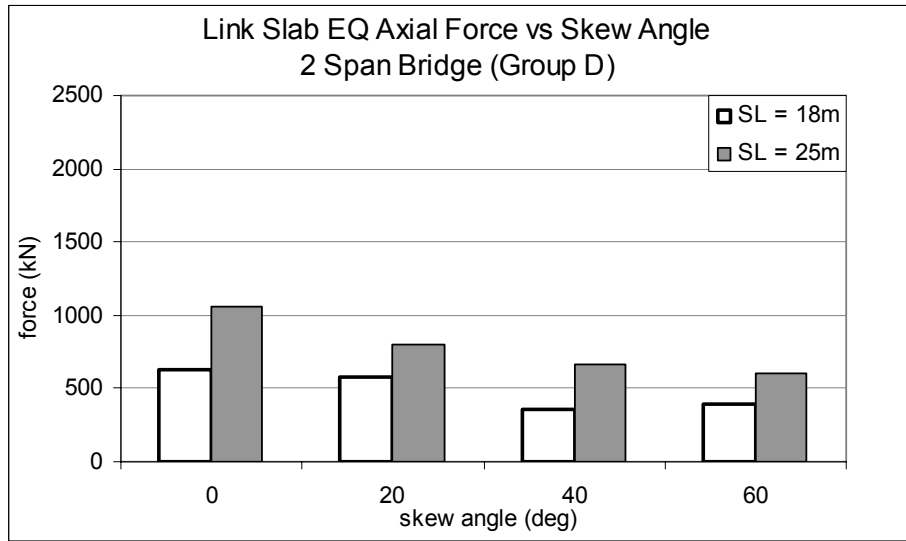


Figure 5.68: Change in link slab axial force with skew angle for 2 span bridges in Group D

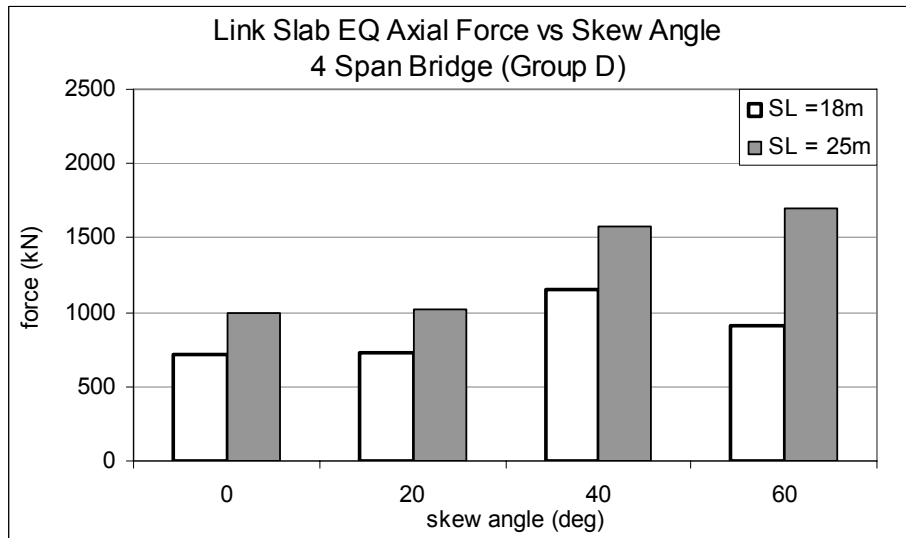


Figure 5.69: Change in link slab axial force with skew angle for 4 span bridges in Group D

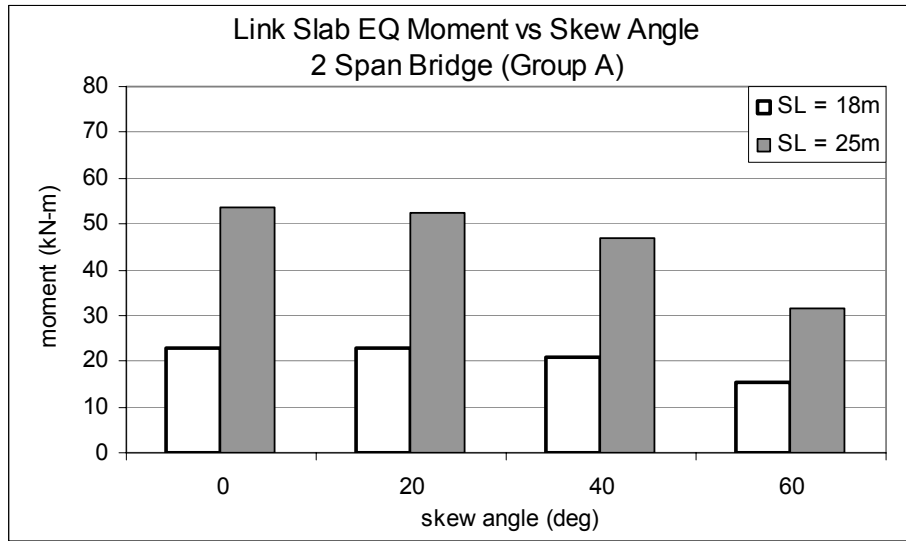


Figure 5.70: Change in link slab moment with skew angle for 2 span bridges in Group A

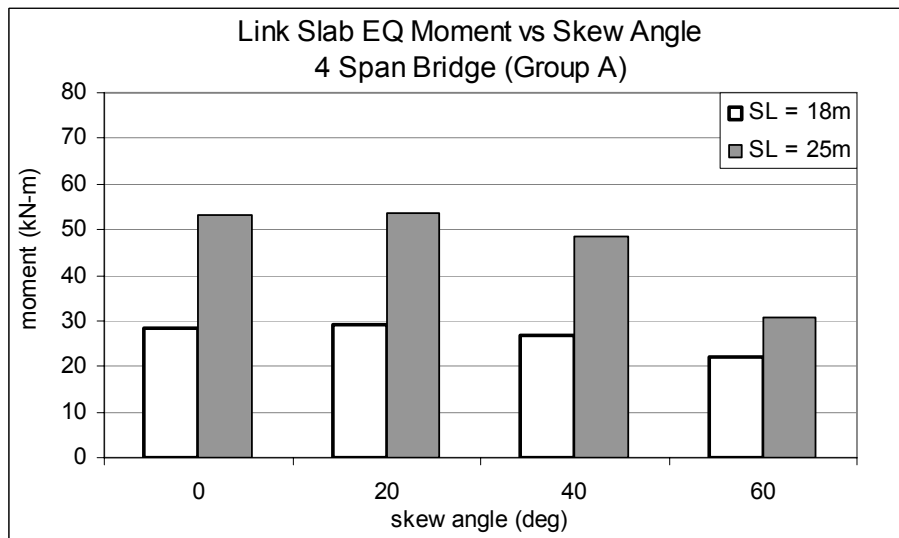


Figure 5.71: Change in link slab moment with skew angle for 4 span bridges in Group A

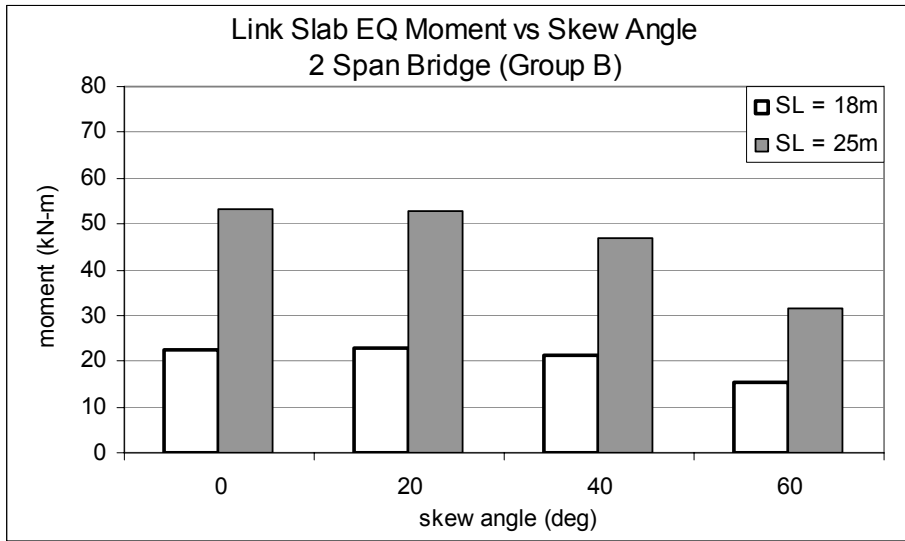


Figure 5.72: Change in link slab moment with skew angle for 2 span bridges in Group B

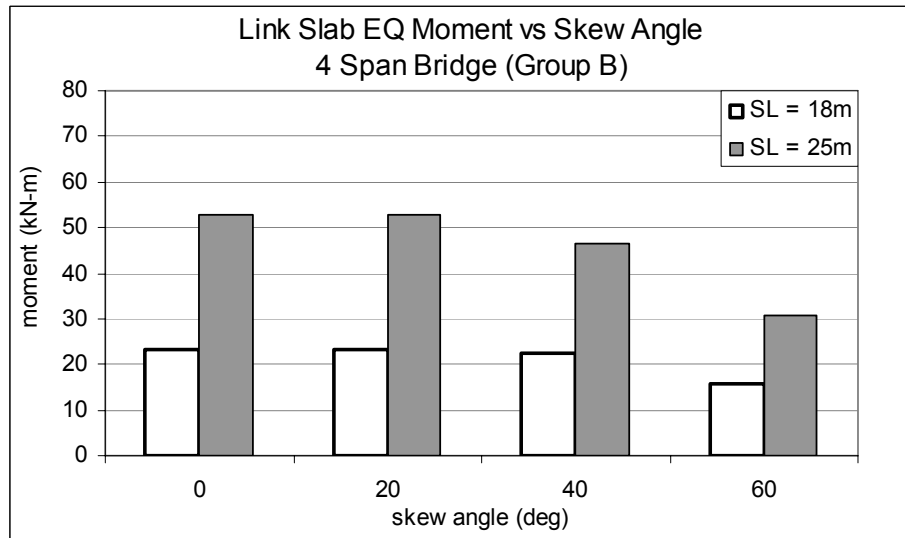


Figure 5.73: Change in link slab moment with skew angle for 4 span bridges in Group B

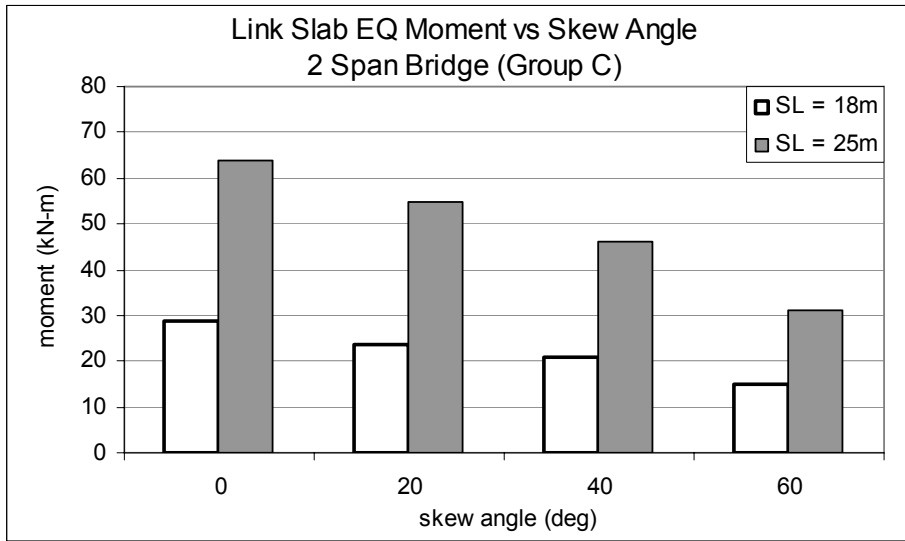


Figure 5.74: Change in link slab moment with skew angle for 2 span bridges in Group C

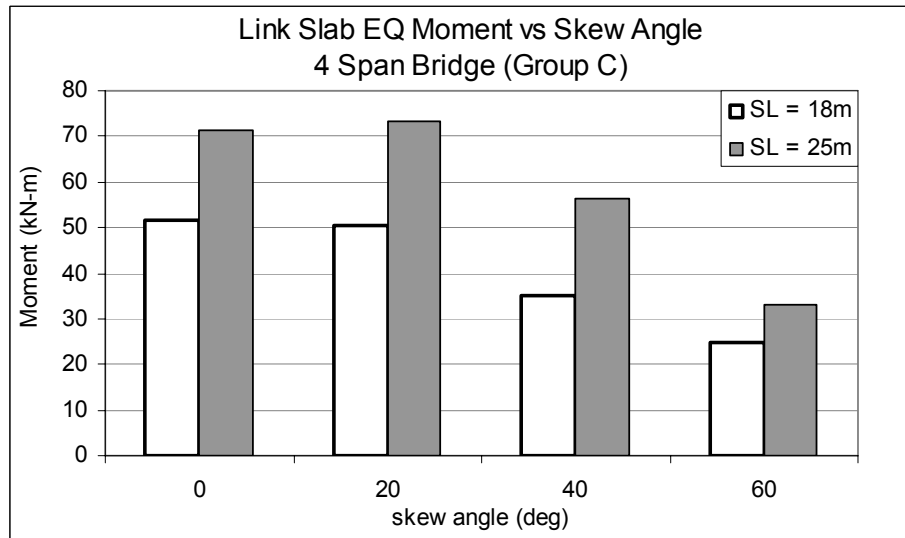


Figure 5.75: Change in link slab moment with skew angle for 4 span bridges in Group C

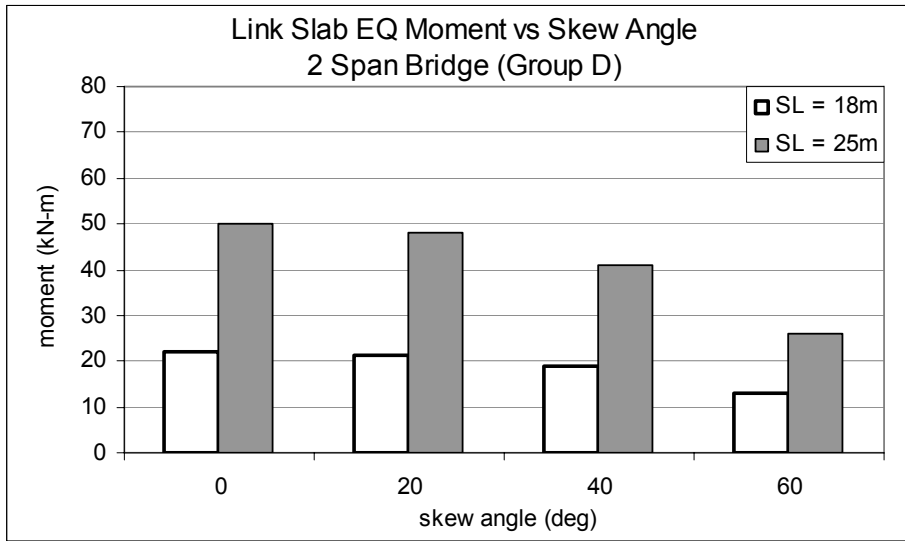


Figure 5.76: Change in link slab moment with skew angle for 2 span bridges in Group D

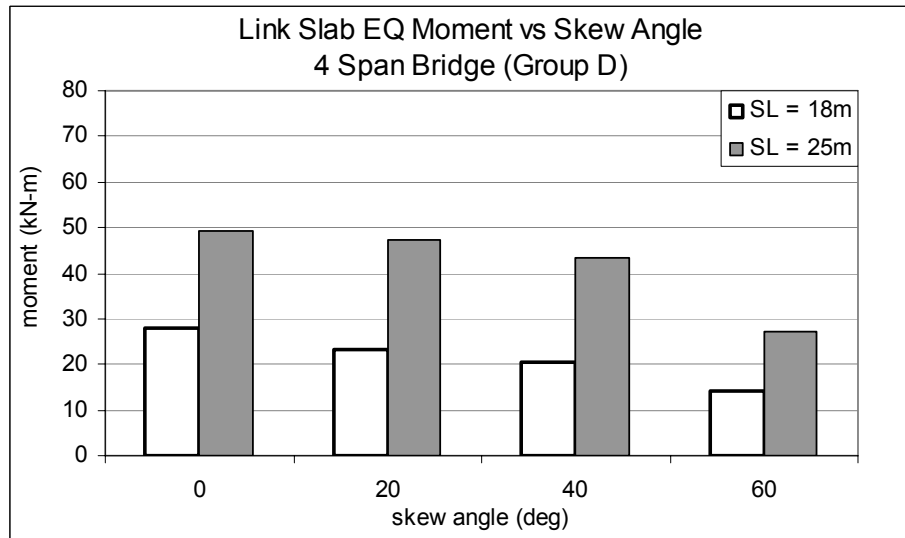


Figure 5.77: Change in link slab moment with skew angle for 4 span bridges in Group D

5.4 Service Load Analysis Results

In this section service load analysis results are represented in two subchapters. In the first one live load girder stresses were tabulated for each of the groups of models. In the second one, link slab cracking control criteria graphs are shown.

5.4.1 Live Load Girder Stresses

Table 5.5: Girder Live Load Stresses of Group A Bridges

Model #	# of spans	skew angle (deg)	SL (m)	LS	L/H	I_{cb}/I_c	Maximum Live load stresses on girder (kN/m ²)	
							Point 2 (envelope)	Point 3 (envelope)
A1	2	0	18	no	1	0.1	5598	7219
A2	2	0	18	yes	1	0.1	5540	7124
A3	2	0	25	no	1	0.1	5144	6293
A4	2	0	25	yes	1	0.1	5064	6184
A5	4	0	18	no	1	0.1	5596	7215
A6	4	0	18	yes	1	0.1	5428	6976
A7	4	0	25	no	1	0.1	5144	6290
A8	4	0	25	yes	1	0.1	4987	6031
A9	2	20	18	no	1	0.1	5106	6507
A10	2	20	18	yes	1	0.1	5048	6445
A11	2	20	25	no	1	0.1	4951	5947
A12	2	20	25	yes	1	0.1	4883	5876
A13	4	20	18	no	1	0.1	5136	6548
A14	4	20	18	yes	1	0.1	4934	6268
A15	4	20	25	no	1	0.1	4976	5981
A16	4	20	25	yes	1	0.1	4759	5699
A17	2	40	18	no	1	0.1	4659	5466
A18	2	40	18	yes	1	0.1	4475	5376
A19	2	40	25	no	1	0.1	4526	5082
A20	2	40	25	yes	1	0.1	4363	4952
A21	4	40	18	no	1	0.1	4658	5551
A22	4	40	18	yes	1	0.1	4238	5088

Table 5.5 Cont'd

Model #	# of spans	skew angle (deg)	SL (m)	LS	L/H	I_{cb}/I_c	Maximum Live load stresses on girder (kN/m ²)	
							Point 2 (envelope)	Point 3 (envelope)
A23	4	40	25	no	1	0.1	4574	5162
A24	4	40	25	yes	1	0.1	4120	4713
A25	2	60	18	no	1	0.1	4299	4289
A26	2	60	18	yes	1	0.1	3825	4053
A27	2	60	25	no	1	0.1	4083	4326
A28	2	60	25	yes	1	0.1	3727	3947
A29	4	60	18	no	1	0.1	4427	4723
A30	4	60	18	yes	1	0.1	3398	3707
A31	4	60	25	no	1	0.1	4249	4531
A32	4	60	25	yes	1	0.1	3268	3523

Table 5.6: Girder Live Load Stresses of Group B Bridges

Model #	# of spans	skew angle (deg)	SL (m)	LS	L/H	I _{cb} /I _c	Maximum Live load stresses on girder (kN/m ²)	
							Point 2 (envelope)	Point 3 (envelope)
B1	2	0	18	no	1.5	0.1	5601	7222
B2	2	0	18	yes	1.5	0.1	5535	7115
B3	2	0	25	no	1.5	0.1	5144	6293
B4	2	0	25	yes	1.5	0.1	5056	6168
B5	4	0	18	no	1.5	0.1	5597	7216
B6	4	0	18	yes	1.5	0.1	5425	6975
B7	4	0	25	no	1.5	0.1	5145	6290
B8	4	0	25	yes	1.5	0.1	4982	6017
B9	2	20	18	no	1.5	0.1	5100	6497
B10	2	20	18	yes	1.5	0.1	5040	6434
B11	2	20	25	no	1.5	0.1	4947	5941
B12	2	20	25	yes	1.5	0.1	4877	5866
B13	4	20	18	no	1.5	0.1	5125	6532
B14	4	20	18	yes	1.5	0.1	4918	6238
B15	4	20	25	no	1.5	0.1	4970	5974
B16	4	20	25	yes	1.5	0.1	4749	5677
B17	2	40	18	no	1.5	0.1	4642	5434
B18	2	40	18	yes	1.5	0.1	4449	5352
B19	2	40	25	no	1.5	0.1	4513	5064
B20	2	40	25	yes	1.5	0.1	4346	4939
B21	4	40	18	no	1.5	0.1	4615	5496
B22	4	40	18	yes	1.5	0.1	4217	5060
B23	4	40	25	no	1.5	0.1	4547	5127
B24	4	40	25	yes	1.5	0.1	4106	4695
B25	2	60	18	no	1.5	0.1	4264	4225
B26	2	60	18	yes	1.5	0.1	3770	3992
B27	2	60	25	no	1.5	0.1	4062	4287
B28	2	60	25	yes	1.5	0.1	3686	3903
B29	4	60	18	no	1.5	0.1	4369	4623
B30	4	60	18	yes	1.5	0.1	3358	3652
B31	4	60	25	no	1.5	0.1	4210	4474
B32	4	60	25	yes	1.5	0.1	3234	3479

Table 5.7: Girder Live Load Stresses of Group C Bridges

Model #	# of spans	skew angle (deg)	SL (m)	LS	L/H	I _{cb} /I _c	Maximum Live load stresses on girder (kN/m ²)	
							Point 2 (envelope)	Point 3 (envelope)
C1	2	0	18	no	1	1.5	5621	7246
C2	2	0	18	yes	1	1.5	5571	7169
C3	2	0	25	no	1	1.5	5144	6294
C4	2	0	25	yes	1	1.5	5081	6216
C5	4	0	18	no	1	1.5	5617	7237
C6	4	0	18	yes	1	1.5	5478	7045
C7	4	0	25	no	1	1.5	5145	6291
C8	4	0	25	yes	1	1.5	5007	6078
C9	2	20	18	no	1	1.5	5125	6522
C10	2	20	18	yes	1	1.5	5073	6470
C11	2	20	25	no	1	1.5	4950	5947
C12	2	20	25	yes	1	1.5	4890	5886
C13	4	20	18	no	1	1.5	5179	6598
C14	4	20	18	yes	1	1.5	4976	6330
C15	4	20	25	no	1	1.5	4989	6001
C16	4	20	25	yes	1	1.5	4778	5739
C17	2	40	18	no	1	1.5	4672	5485
C18	2	40	18	yes	1	1.5	4498	5405
C19	2	40	25	no	1	1.5	4529	5086
C20	2	40	25	yes	1	1.5	4375	4962
C21	4	40	18	no	1	1.5	4741	5661
C22	4	40	18	yes	1	1.5	4271	5128
C23	4	40	25	no	1	1.5	4613	5233
C24	4	40	25	yes	1	1.5	4135	4733
C25	2	60	18	no	1	1.5	4320	4302
C26	2	60	18	yes	1	1.5	3848	4089
C27	2	60	25	no	1	1.5	4097	4339
C28	2	60	25	yes	1	1.5	3744	3967
C29	4	60	18	no	1	1.5	4532	4823
C30	4	60	18	yes	1	1.5	3421	3739
C31	4	60	25	no	1	1.5	4311	4597
C32	4	60	25	yes	1	1.5	3283	3543

Table 5.8: Girder Live Load Stresses of Group D Bridges

Model #	# of spans	skew angle (deg)	SL (m)	LS	L/H	I _{cb} /I _c	Maximum Live load stresses on girder (kN/m ²)	
							Point 2 (envelope)	Point 3 (envelope)
D1	2	0	18	yes	1	0.1	5407	6983
D2	2	0	25	yes	1	0.1	4956	6044
D3	4	0	18	yes	1	0.1	5414	6959
D4	4	0	25	yes	1	0.1	4966	6009
D5	2	20	18	yes	1	0.1	4905	6240
D6	2	20	25	yes	1	0.1	4722	5687
D7	4	20	18	yes	1	0.1	4924	6256
D8	4	20	25	yes	1	0.1	4744	5683
D9	2	40	18	yes	1	0.1	4172	4998
D10	2	40	25	yes	1	0.1	4038	4609
D11	4	40	18	yes	1	0.1	4242	5094
D12	4	40	25	yes	1	0.1	4119	4714
D13	2	60	18	yes	1	0.1	4671	5235
D14	2	60	25	yes	1	0.1	2995	3194
D15	4	60	18	yes	1	0.1	3413	3708
D16	4	60	25	yes	1	0.1	3275	3527

5.4.2 Link Slab Cracking Control

Under service conditions, the crack width at the surface of the link slab should be checked against AASHTO (1996) Specifications. The crack control criterion of AASHTO (1996) gives the following formula to limit the width of the crack at the surface of the link slab to 0.33 mm [7].

$$Z \leq f_s (d_c A)^{1/3} \quad (5.2)$$

in which;

$$Z \leq 25000 \text{ kN/m,}$$

f_s = stress in the reinforcing steel (kPa), calculated by using the method proposed in Caner and Zia (1998) [1].

$$\begin{aligned}d_c &= \text{distance measured from extreme tension fiber to the closest} \\ &\text{longitudinal bar (m)} \\ A &= \text{effective tension area per bar (m}^2\text{)} \\ A &= 2d_c s \tag{5.3} \\ &\text{and } s \text{ is the longitudinal reinforcement spacing (m).}\end{aligned}$$

Models that have link slab in each group of bridges were analyzed for cracking control under live load conditions. Group D bridges, which have continuous decks through abutments, were also analyzed under thermal forces for cracking control. As it was indicated before, a temperature fall of 25°C were applied to the bridges. Since the aim is to check cracking phenomenon, bridges were exposed to only temperature fall that creates tension forces in the deck.

Φ16 longitudinal top and bottom reinforcement bars were placed for every 150 mm in the link slab. It was found out that for all of the cases, Φ16 longitudinal top and bottom reinforcement bars at 150 mm satisfy the crack control criterion of AASHTO, 1996 and consequently the crack width is kept smaller than 0.33 mm. Link slab crack control criteria are sketched for each of the group of bridges in the following Figures 5.78 to 5.81 for live loads, and in Figure 5.82 for temperature fall for Group D bridges.

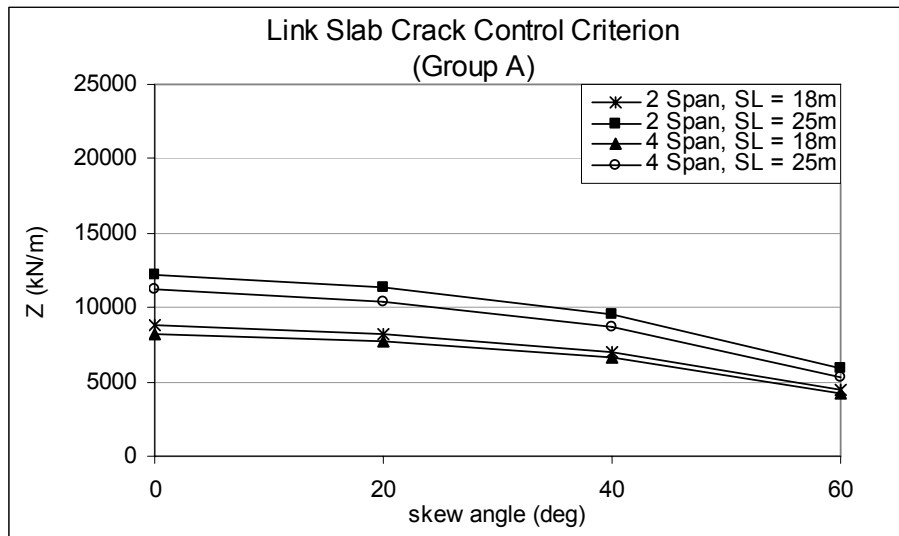


Figure 5.78: Link slab cracking control for Group A bridges under live loads

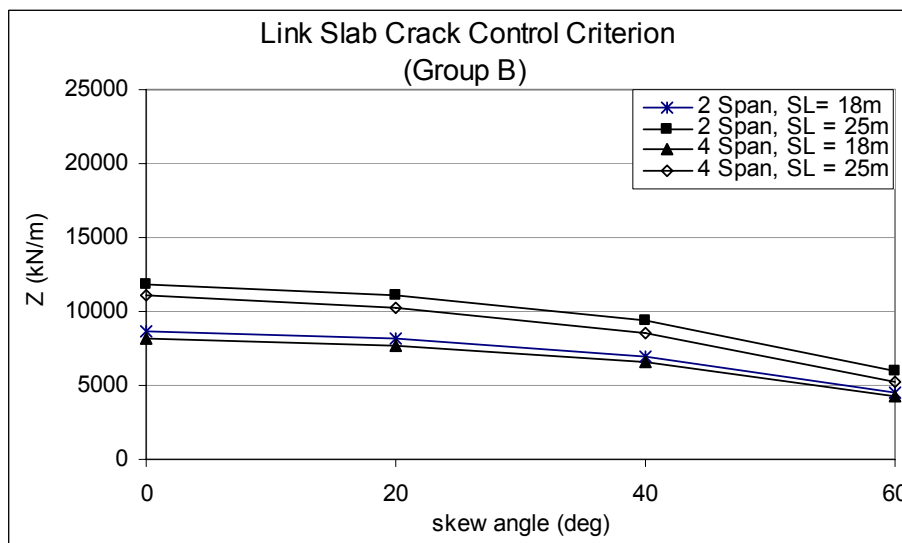


Figure 5.79: Link slab cracking control for Group B bridges under live loads

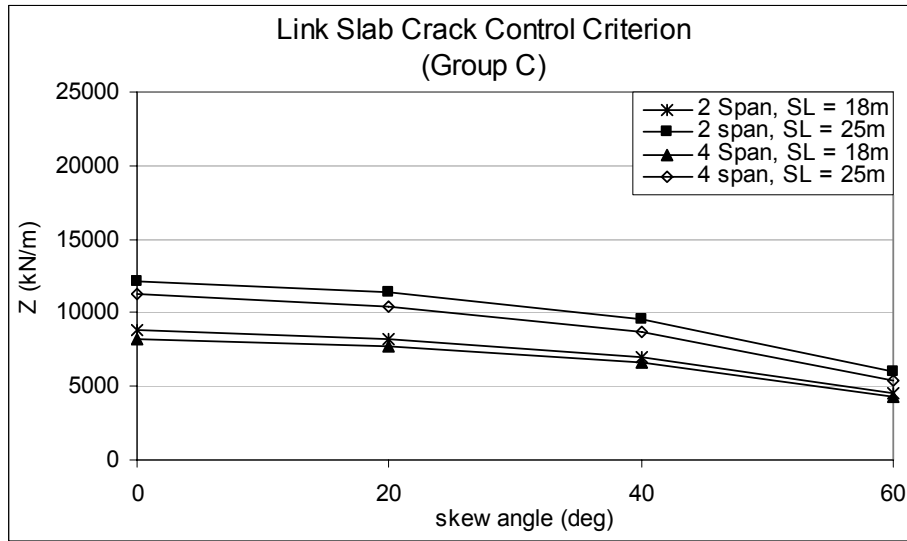


Figure 5.80: Link slab cracking control for Group C bridges under live loads

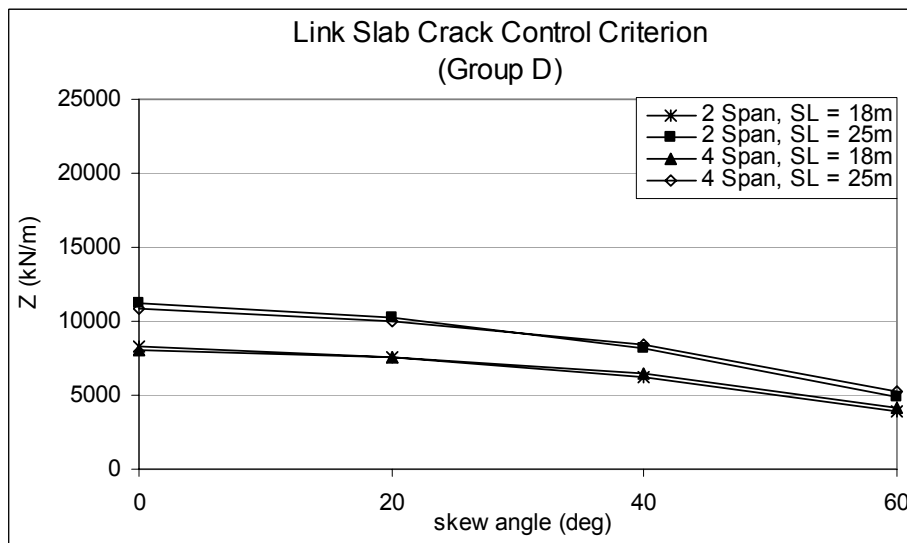


Figure 5.81: Link slab cracking control for Group D bridges under live loads

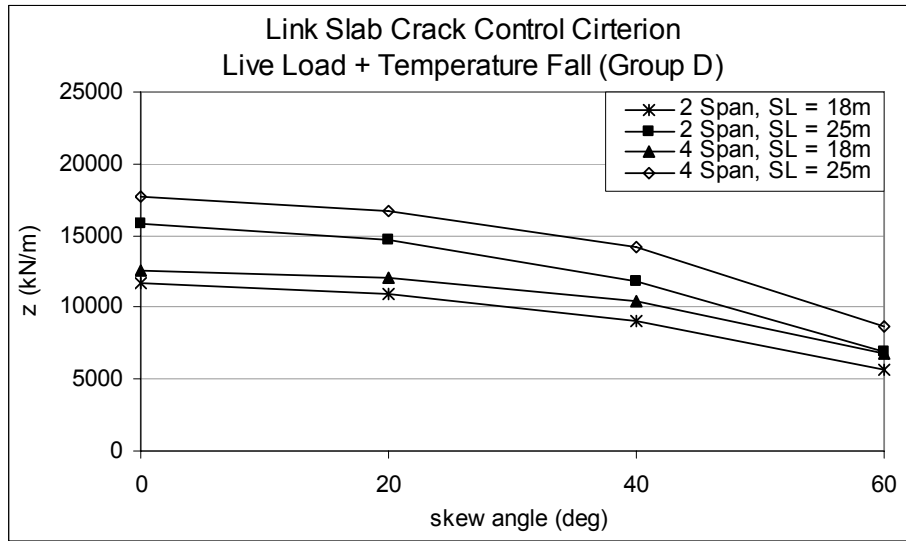


Figure 5.82: Link slab cracking control for Group D bridges under thermal and live loads

5.5 Linear Time History Analysis (LTHA) Results

As it was previously mentioned, LTHA was performed for four bridges namely, A7, A8, A31 and A32. For remembrance, the properties of these bridges are listed in Table 5.9.

Table 5.9: Properties of bridges used in LTHA

Model #	# of spans	skew angle (deg)	Span Length (m)	Link Slab	L/H	I_{cb}/I_c
A7	4	0	25	no	1	0.1
A8	4	0	25	yes	1	0.1
A31	4	60	25	no	1	0.1
A32	4	60	25	yes	1	0.1

The results of LTHA for selected records together with the averages of the results for three records taken on rock site (gebze, izmit, yarimca) and corresponding RSA results are tabulated in the following Tables 5.10 to 5.12.

Table 5.10: Displacements calculated from LTHA and RSA

Model # / record	Longitudinal Deck Displacement (m)	Transverse Deck Displacement (m)	Longitudinal Bearing Displacement (m)
A7 / gebze	0.054	0.007	0.029
A7 / izmit	0.094	0.028	0.048
A7 / yarimca	0.165	0.017	0.081
A7 / duzce	0.132	0.028	0.069
A7 / bolu	0.249	0.024	0.126
A7 average (rock)	0.104	0.017	0.053
A7 RSA	0.164	0.02	0.08
rsa/ltha (avr.)	1.57	1.15	1.52
A8 / gebze	0.071	0.007	0.042
A8 / izmit	0.091	0.028	0.054
A8 / yarimca	0.11	0.02	0.066
A8 / duzce	0.118	0.031	0.07
A8 / bolu	0.217	0.023	0.125
A8 average (rock)	0.091	0.018	0.054
A8 RSA	0.122	0.021	0.07
rsa/ltha (avr.)	1.35	1.15	1.30
A31 / gebze	0.085	0.055	0.063
A31 / izmit	0.114	0.096	0.114
A31 / yarimca	0.124	0.108	0.111
A31 / duzce	0.12	0.144	0.12
A31 / bolu	0.302	0.272	0.305
A31 average (rock)	0.108	0.086	0.096
A31 RSA	0.109	0.08	0.083
rsa/ltha (avr.)	1.01	0.93	0.86
A32 / gebze	0.074	0.044	0.069
A32 / izmit	0.072	0.034	0.065
A32 / yarimca	0.108	0.059	0.104
A32 / duzce	0.091	0.073	0.082
A32 / bolu	0.213	0.118	0.208
A32 average (rock)	0.085	0.046	0.079
A32 RSA	0.096	0.052	0.08
rsa/ltha (avr.)	1.13	1.14	1.01

Table 5.11: Member forces and moments calculated from LTHA and RSA

Model # / record	Cap beam Moment (kNm)	Diaphragm Shear (kN)	Column Local Transverse Moment (kNm)	Column Local Longitudinal Moment (kNm)
A7 / gebze	1999	354	6508	3767
A7 / izmit	7358	1403	25668	6008
A7 / yarimca	4873	863	15845	10341
A7 / duzce	7204	1365	25278	8102
A7 / bolu	6577	1186	22002	15191
A7average(rock)	4743	873	16007	6705
A7 RSA	6241	999	17976	10337
rsa/ltha (avr.)	1.32	1.14	1.12	1.54
A8 / gebze	1978	252	6371	4389
A8 / izmit	6955	962	24431	5675
A8 / yarimca	5264	695	17543	6846
A8 / duzce	7790	1056	26678	7143
A8 / bolu	5944	793	19832	12821
A8average(rock)	4732	636	16115	5637
A8 RSA	6159	702	17765	7370
rsa/ltha (avr.)	1.30	1.10	1.10	1.31
A31 / gebze	1875	234	7281	6835
A31 / izmit	2995	455	12849	12308
A31 / yarimca	3348	437	14712	13135
A31 / duzce	3459	620	13502	17268
A31 / bolu	8522	1082	34872	34018
A31average(rock)	2739	375	11614	10759
A31 RSA	4547	844	9252	9778
rsa/ltha (avr.)	1.66	2.25	0.80	0.91
A32 / gebze	2322	229	7455	7125
A32 / izmit	1714	173	6023	4866
A32 / yarimca	3552	422	10640	8853
A32 / duzce	2473	326	9521	10857
A32 / bolu	5880	648	24135	16865
A32average(rock)	2529	275	8039	6948
A32 RSA	3716	877	7463	7681
rsa/ltha (avr.)	1.47	3.19	0.93	1.11

Table 5.12: Link Slab Forces calculated from LTHA and RSA

Model # / record	Link Slab EQ Axial Force (kN/m)	Link Slab EQ Moment (kN-m/m)
A8 / gebze	300	31
A8 / izmit	363	63
A8 / yarimca	238	69
A8 / duzce	355	72
A8 / bolu	468	71
A8 average (rock)	300	54
A8 RSA	447	53
rsa/ltha (avr.)	1.49	0.98
A32 / gebze	1810	27
A32 / izmit	1223	20
A32 / yarimca	2263	60
A32 / duzce	2683	39
A32 / bolu	4216	69
A32 average (rock)	1765	36
A32 RSA	1913	31
rsa/ltha (avr.)	1.08	0.87

5.6 Non-Linear Time History Analysis (NLTHA) Results

As it was previously stated, NLTHA was performed for two bridges (A31 and A32). The properties of these bridges can be found in Table 5.9. For these analysis cases, again deck displacements and column end moments were studied to make a comparison with RSA and NLTHA results. In addition, pounding forces and link slab axial forces were also checked. The results of the NLTHA are sketched in the following Figures 5.83 to 5.90.

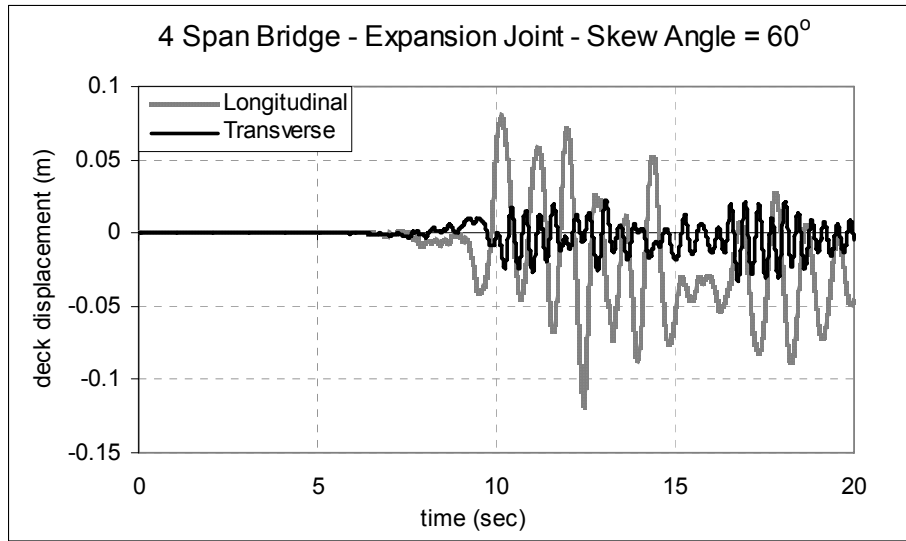


Figure 5.83: Longitudinal and transverse deck displacements of the bridge without link slab

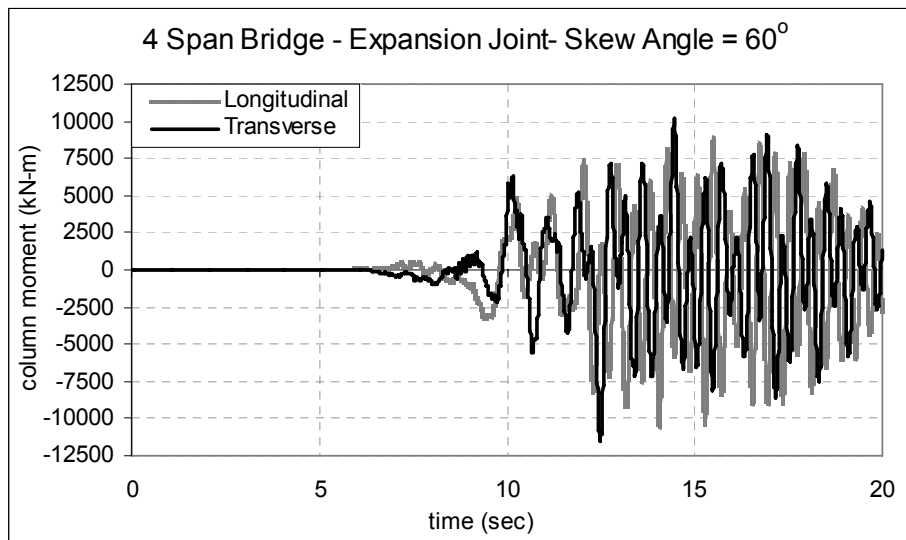


Figure 5.84: Local longitudinal and transverse column moments of the bridge without link slab



Figure 5.85: Pounding force at the center pier of the bridge without link slab

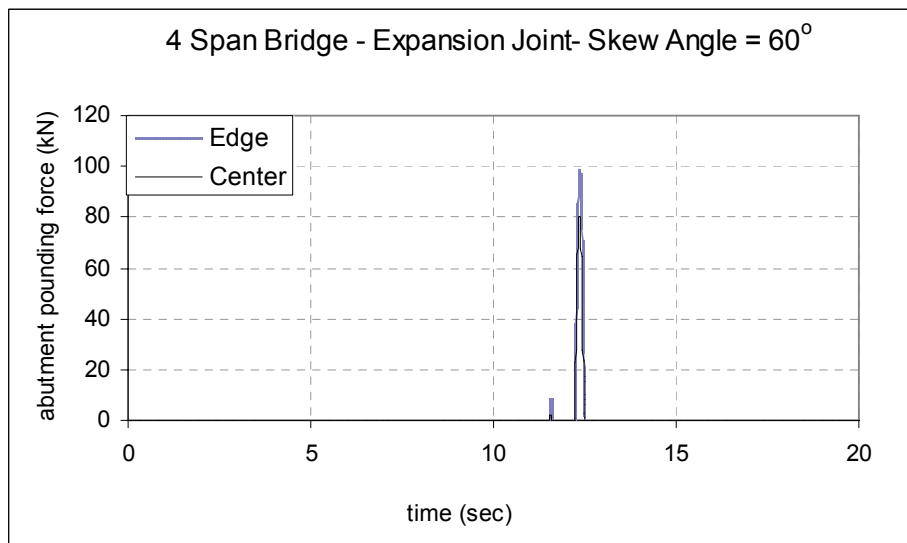


Figure 5.86: Abutment pounding force of the bridge without link slab

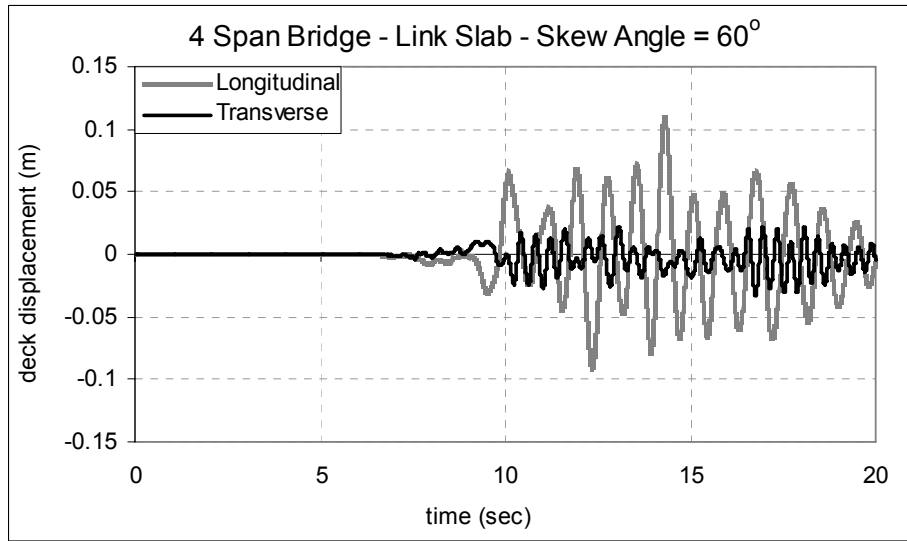


Figure 5.87: Longitudinal and transverse deck displacements of the bridge with link slab

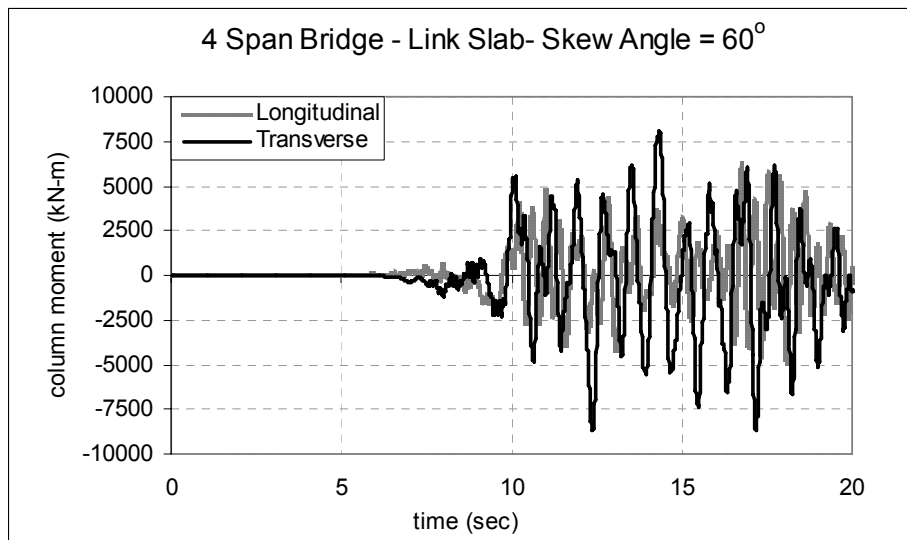


Figure 5.88: Local longitudinal and transverse column moments of the bridge with link slab

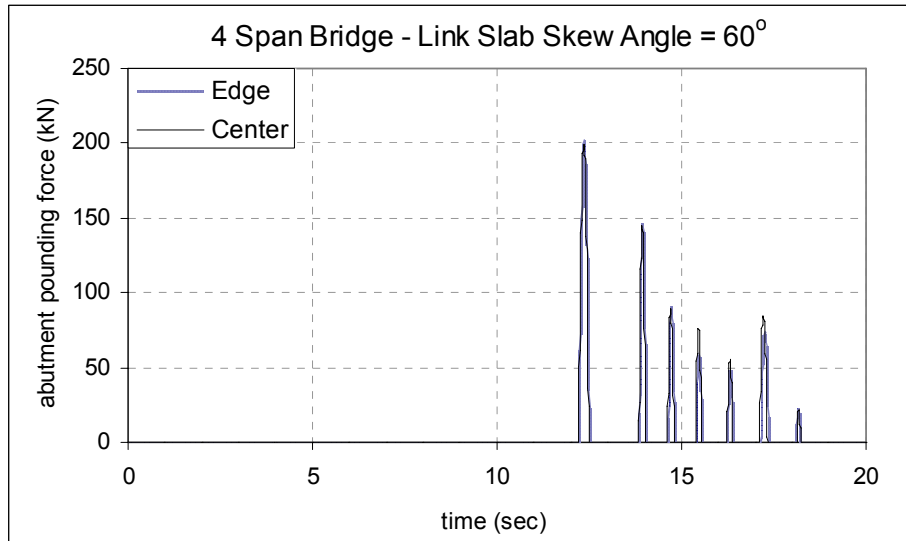


Figure 5.89: Abutment pounding force of the bridge with link slab

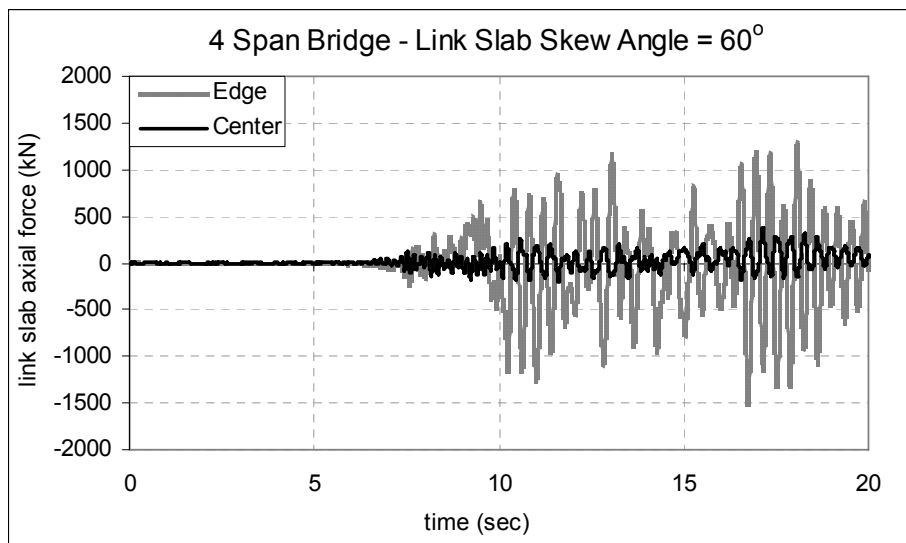


Figure 5.90: Link slab axial force at edge and center

In Table 5.13, NLTHA and LTHA results for Yarımca record are listed for models A31 and A32.

Table 5.13: NLTHA and LTHA Results

	Longitudinal deck displacement (m)	Transverse deck displacement (m)	Longitudinal column moment (kNm)	Transverse column moment (kNm)
A31 ltha	0.124	0.108	13135	14712
A31 nltha	0.119	0.054	10570	11544
A32 ltha	0.108	0.059	8853	10640
A32 nltha	0.109	0.033	6226	8658

CHAPTER 6

DISCUSSION OF RESULTS

6.1 Discussions on Eigenvalue Analysis Results

From eigenvalue analysis results it is understood that, addition of link slab to the deck decreases the fundamental periods of the bridges in longitudinal and transverse directions. The decrease in the periods for four spanned bridges caused by the addition of link slab appears to be greater than for two spanned ones. All bridge models are more flexible in longitudinal direction compared to transverse direction. As the skew angle increases, the longitudinal periods decrease and the transverse periods increase.

Group B bridges have smaller longitudinal and transverse periods compared to the Group A bridges. Group B bridges have smaller pier heights; correspondingly less flexibility in longitudinal and transverse directions of the bridges. The columns of Group C bridges have smaller cross-sections than the ones in Group A and have more flexibility in longitudinal and transverse directions. Consequently, the fundamental periods of the bridges in Group C appears to be greater than the ones in Group A. group D bridges are the most rigid ones among the bridges in all groups and they have the lowest fundamental periods in horizontal directions.

It is also observed from the analysis results that, the height of the columns, the column cross-section or continuity of the deck do not affect the fundamental period in vertical direction. The vertical periods do not vary between groups.

6.2 Discussions on Response Spectra Analysis (RSA) Results

With increasing skew angle, longitudinal deck displacements of the bridges decrease. The placement of link slab decreases the deck displacements. For longitudinal deck displacement the reduction can be up to around 30% for mild skew angles. The decrease in displacements due to addition of link slab decreases with increasing skew angle. Generally, the decrease in longitudinal displacements with the addition of link slab for four spanned models is greater than the decrease in two spanned ones.

Transverse deck displacements increase with increasing skew angles. The addition of link slab decreases the deck displacements also in the transverse direction but the reduction is more apparent (up to 90%) than in the longitudinal direction of the bridge.

When link slabs are used the deck becomes a continuous huge mass and consequently its stiffness both in longitudinal and transverse directions restrain excessive movements. Therefore, the corresponding displacements decrease with the addition of link slab. The transverse deck displacements are comparatively lower than the longitudinal displacements. This situation is caused by the shear blocks placed between the girders to control the transverse displacement of the superstructure. For four spanned bridges the deck displacements in both longitudinal and transverse directions are greater than the ones for two spanned bridges. The span length of the bridges directly

affects the deck displacements of the investigated bridges. For longer span lengths, deck displacements appear to be greater.

Stiffness of the substructure has an influence on the displacements observed in the superstructure. Longitudinal and transverse deck displacements of Group B bridges are smaller than the displacements of Group A since the substructures of the models in Group B have stiffer substructures (smaller column heights). Similarly, the substructures of the models in Group C are more flexible than the ones in Group A because of their reduced column cross-sections. As a result, the deck displacements of Group C bridges appear to be higher than the deck displacements of Group A bridges.

Group D bridges have stiffer decks compared to the Group A bridges, since they have continuous decks that are connected directly to their abutments. Accordingly, the deck displacements occurred in Group D bridges are much smaller than the ones in other groups.

In Figure 6.1 and 6.2 mode shapes of a multisimple-span bridge with expansion joints are shown. For the mode shape shown in Figure 6.1, span separation and for the mode shape shown in Figure 6.2 pounding of the spans may take place. In Figure 6.3, the mode shape of the same bridge after retrofitting with link slab is shown. As it can be observed from these figures, addition of link slab decreases the tendency for span separation. Also pounding of the spans does not happen since the spans are connected to each other from the deck level with the addition of link slab. But, it should be underlined that, pounding still may occur at the abutments.

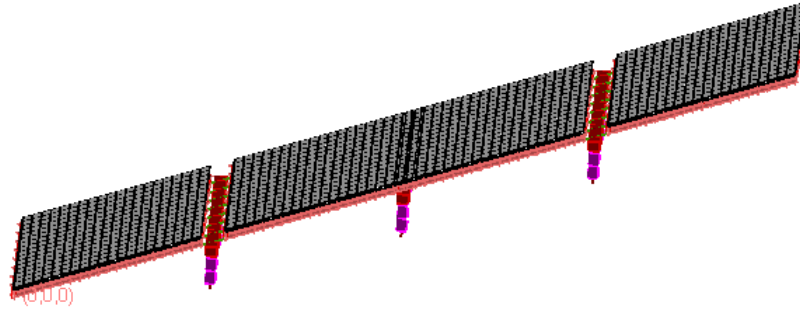


Figure 6.1: Span separation problem of the multisimple-span bridge with expansion joints.

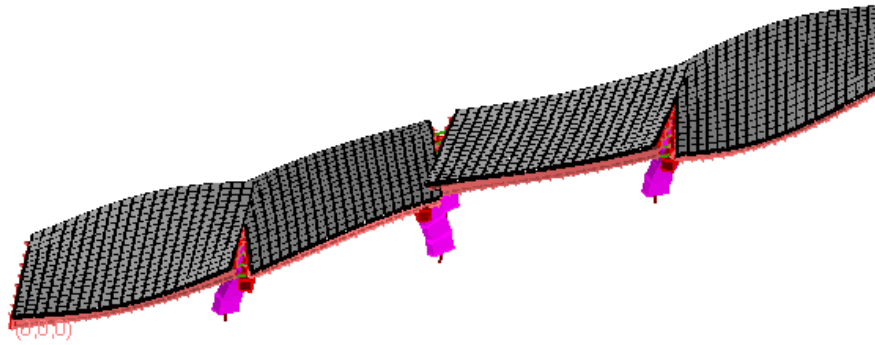


Figure 6.2: Pounding of the spans in the multisimple-span bridge with expansion joints.

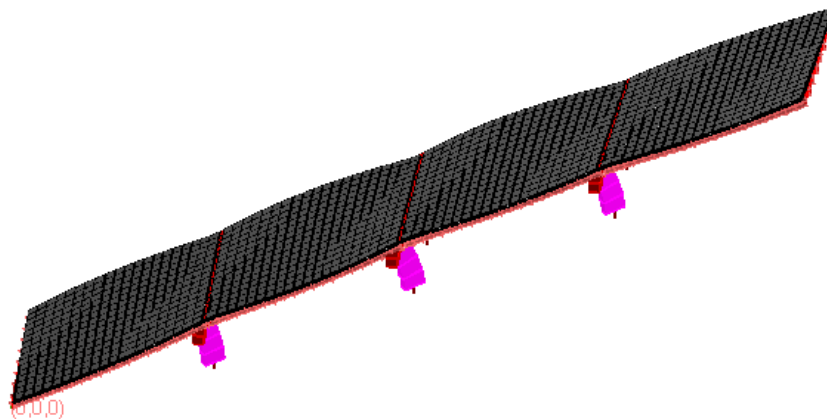


Figure 6.3: The deformed shape of the multisimple-span bridge retrofitted with link slabs.

It is observed from the analysis results that, the addition of link slab typically decreases the cap beam moments. The reduction can reach up to around 70%. The effect of link slab on the cap beam moments is higher for smaller skew angles. Cap beam moments are also directly proportional to the span length. As the span length increases, cap beam moments increase. It is also observed that cap beam moments are generally higher for four spanned bridges.

Moments occur in the cap beams are related to the transverse displacement of the column bent. As the displacement of the bent increases, the cap beam moments are expected to increase. Since the addition of link slab decreases the deck displacements, it also decreases the moments in cap beams. The cap beam moments for Group A bridges are greater than the cap beam moments for Group B bridges. The stiffness of the bents in Group B is higher leading to smaller superstructure displacements and cap beam moments. Group C bridges have pier bents which are more flexible compared to the ones in Group A bridges. As a result, cap beam moments of Group C bridges are greater than the moments in Group A. Since Group D bridges have stiffer superstructure, the cap beam moments for Group D bridges are smaller than the ones for other groups of bridges.

By addition of link slabs, the shear forces in the diaphragms (cross beams) are reduced up to around 60%. Typically, the diaphragm shear forces are larger for four spanned bridges. As the span length increases, the diaphragm forces also increase. The same relationship for diaphragm shear is also observed between different groups. Group C bridges have the most flexible bents and subsequently the higher diaphragm shears. Group B bridges have smaller diaphragm shears compared to Group A bridges and Group D bridges have the smallest diaphragm shear values among all groups.

Column local transverse moments are reduced by the addition of link slabs up to around 80%, for mild skew angles. The effect of link slab decreases as the skew angle increases. The addition of link slab decreases the column local longitudinal moments up to approximately 40%. Typically, as the skew angle increases, column local transverse and longitudinal moments decrease. Column moments are greater for bridges having longer spans, and for four spanned bridges. The local transverse moments appear to be greater than the local longitudinal moments, since the transverse direction of the columns is stronger.

The local column moments of the bridges in Group A are greater than the ones in Group B for small skew angles although the stiffness of the columns of bridges in Group B is higher. But, the bent displacements in Group A are greater leading to higher column moments. On the contrary, for the skew angles of 40 and 60, the longitudinal column moments of the bridges in Group A become smaller than the ones in Group B. Group C bridges have more slender columns compared to the bridges of Group A. Correspondingly, the column moments of the bridges in Group A are greater than the moments of the Group C bridges. The bridges of Group D have smaller column moments compared to Group A bridges since they have stiffer deck and their superstructure displacements are more restricted than the bridges of Group A.

For the link slab forces governing earthquake load combination is $DL+0.3EQ_I+EQ_T+0.3EQ_V$. Therefore it can be said that, the link slab forces are influenced by the transverse displacement of the deck like the other member forces discussed previously. In a general trend, link slab moment decreases slightly with increasing skew angle. Link slab moment is higher for greater span length. The link slab moments in two spanned and four spanned bridges do not differ significantly from each other.

The axial forces and moments at link slabs of bridges in Group A are higher than the ones in Group B. Group C bridges have smaller moments and axial forces at their link slabs compared to Group A bridges. The moments and axial forces of Group A are greater than the ones of Group D.

For two spanned and four spanned bridges, the effects of increasing skew angle on link slab axial force is different. Link slab axial force decreases with increasing skew angle for two spanned bridges. On the contrary, for four spanned bridges increasing skew angle increases the link slab axial force. For two spanned bridges, transverse movement is influenced by the stiffness of mid-pier only. As the skew angle increases, the effect of EQ_t is reduced due to changing geometry and accordingly link slab axial force decreases. For four spanned bridges, transverse movement of the bridge is influenced by stiffness of three piers. The difference between transverse deck displacements of the two and four spanned bridges increases with increasing skew angle. This means that, four spanned bridges can deflect easier than two spanned ones at greater skew angles. Accordingly, although the effect of EQ_t is also reduced due to skew angle, link slab axial forces of four spanned bridges increase with increasing skew angle.

Not only in Turkish engineering design practice, but also in other countries typically a constant reinforcement ratio for the link slab is used along the width of the bridge. An example for link slab details practiced in Turkish practice is given in Figure 6.4.

On the other hand, as it can be observed from the following Figure 6.5, it was found out that link slab axial force is not evenly distributed along the width. At the edges of the link slab, axial force is found to be higher than the one at the middle. Consequently, rather than a constant reinforcement ratio along the

width, a higher one can be used at the edges compared to the middle of the width of the bridge.

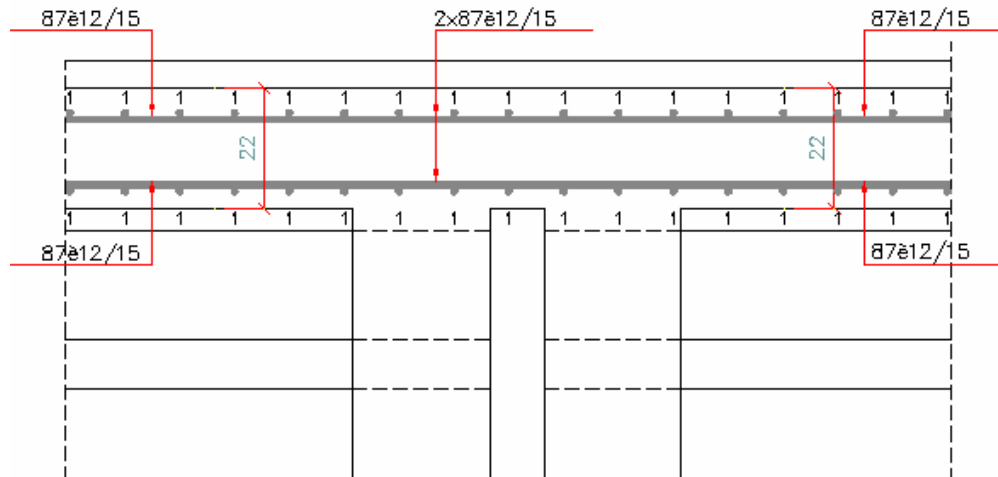


Figure 6.4: A sample link slab details practiced in Turkey

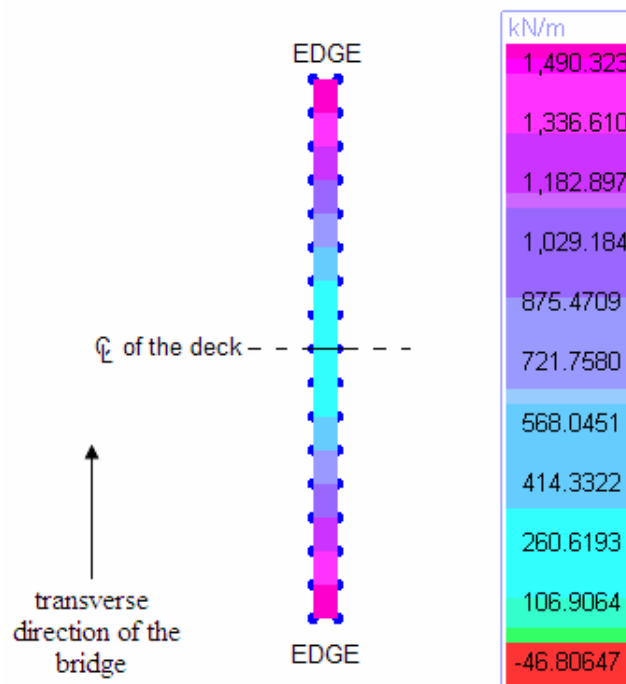


Figure 6.5: A sample link slab axial force distribution due to earthquake loading along the bridge width

For most of the member forces and displacements, the governing earthquake load combination appears to be $DL+0.3EQ_I+EQ_T+0.3EQ_V$. For a small part of the member forces and displacements the governing equation becomes $DL+1.0EQ_I+0.3EQ_T+0.3EQ_V$ for higher skew angles. One of the points considered while choosing the earthquake records for THA was the presence of vertical component of the record. As it was previously pointed out that, the vertical components of earthquake records are important for structural design of bridges. It was observed from RSA results that, earthquake load combination of $DL+0.3EQ_L+0.3EQ_T+EQ_V$ governs the design of cap beam, cross beam and link slab in some models. Out of 32 bridge models in a group, for three models in Group A, eleven models in Group B, three models in Group C and six models in Group D, load combination of $DL+0.3EQ_L+0.3EQ_T+EQ_V$ governs the design of cap beam. It is observed that for Group B models, whose piers having smaller length, i.e. the models having a stiffer substructure, vertical component of earthquake is more important than the other groups. For diaphragm shear, $DL+0.3EQ_L+0.3EQ_T+EQ_V$ load combination governs the design only in seven models of Group D. Therefore, it could be concluded that, vertical earthquake component should be considered in design of bridges.

6.3 Discussion on Service Load Analysis Results

In all group of bridges, addition of link slab decreases the girder tensile stresses at the bottom of the cross-section up to 25%. The decrease in tensile stress is more pronounced for four spanned bridges with a skew angle of 60° . Live load girder stresses of the bridges do not change significantly between Groups A, B and C. Hence, it can be said that substructure stiffness does not have any effect on the girder stresses. The live load stresses occurred in the Group D bridges are smaller than the ones in Group A meaning that, addition of exterior link

slabs, i.e. making the deck continuous through the abutments, is a more preferable option when live load stresses are concerned.

It is also observed from the analysis results that skew angle has a significant influence on the maximum live load girder stresses. With increasing skew angle, live load tension stresses at the bottom of the girders decrease remarkably. For 20°, 40° and 60° skewed bridges, the reduction can be up to approximately 10%, 25% and 45%, respectively. The main reason for such reduction in service response is the distribution of live load not only in longitudinal direction but also more in transverse direction due to closeness to supports at a skew bridge as shown in Figure 6.6. Therefore, for an economical girder design, benefit of skew angle should be considered.

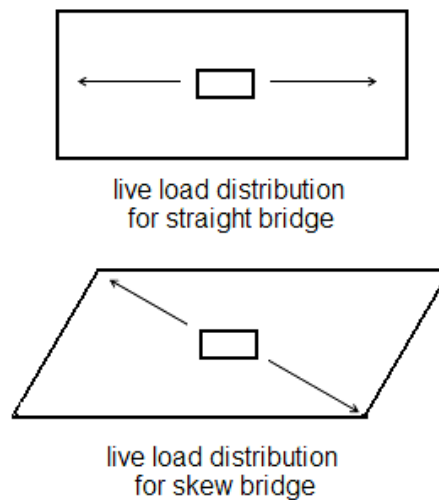


Figure 6.6: Live load distribution for straight and skew bridges

6.4 Discussion on Linear Time History Analysis (LTHA) Results

It is observed from the LTHA results that, for the investigated straight bridges (A7 and A8), AASHTO RSA gives conservative results compared to the

LTHA results of the selected earthquake excitations recorded on rock. But when the skew angles of the bridges are increased to 60° (for models A31 and A32), AASHTO RSA becomes nonconservative in some of the results for the selected records having 250 years of return periods. Although some of the RSA results are nonconservative for 60° skewed bridges, the differences are not very significant considering the high return periods of the records. The situation can be also clearly seen from Figures 4.12, 4.14 and 4.16 that, the pseudo acceleration response spectra of Yarimca, İzmit and Gebze records are below the AASHTO response spectra as a general trend except some peak points. In the light of these findings, it can be recommended that, more attention should be taken while designing the skewed bridges that are in the close vicinity of an active fault.

From Figures 4.18 and 4.20 it can be said that, local site conditions have a great influence on the shapes and amplitudes of the response spectra. Local site conditions can change the frequency content of the response spectra, such that deep and soft soil deposits produce greater amplifications of low-frequency (long-period) motion. Therefore, for structures having long-periods of vibration such as bridges, soft soil conditions significantly influence the seismic behavior [27]. The amplitudes of the pseudo acceleration response spectra of the excitations taken from soil sites (Düzce and Bolu) exceed the amplitudes of AASHTO response spectra especially between the periods of 0.5 to 1.5 seconds which is the range of the fundamental periods of the generated models (Figures 4.18 and 4.20). Accordingly, the LTHA results of these records appear to be greater compared to the RSA results of the records on rock sites.

6.5 Discussion on Non-Linear Time History Analysis (NLTHA)

Results

The results of NLTHA results of the model without link slab (A31) show that no pounding between adjacent spans is observed under the Yarımca record. On the contrary, pounding takes place between the abutments and the spans of the bridge. For the model with link slab (A32) pounding also occurs at the abutment locations. The pounding force for the model having link slab (A32) is greater than the model without link slab (A31). This can be due to the increased mass and stiffness of the deck caused by the continuity.

The pounding force at the middle of the width of the bridge is 20% lower than the one at the edge for the model without link slab. On the other hand, for the model with link slab, the pounding forces at the edge and at the middle are approximately the same. Therefore, it can be said that the addition of link slab increases the torsional stiffness of the superstructure. Consequently, the large displacements of skewed bridges at their supports due to the rotation of their superstructure, which can cause unseating of the deck, can be reduced with the addition of link slab.

Deck displacements and column end forces calculated by NLTHA are smaller than the ones calculated by LTHA, as it can be observed from Table 5.13 due to pounding. Pounding restrained excessive deck displacement and accordingly reduced column moments.

CHAPTER 7

SUMMARY AND CONCLUSIONS

In this study, a total of 112 bridge models were investigated in order to figure out the effect of skew angle on bridge behavior. Addition of link slab as a retrofit procedure was also studied. The conclusions of this study can be summarized as follows:

- Earthquake induced deck displacements in transverse direction are high for skewed bridges compared to straight ones. Addition of link slab between adjacent spans decreases both transverse and longitudinal displacements at deck level.
- Addition of link slab decreases the tendency for span separation. When link slabs are used, pounding does not take place between adjacent spans since they are connected to each other.
- Addition of link slab can reduce the substructure forces caused by the earthquake such as cap beam moments and column end moments.
- Earthquake induced diaphragm shear forces can be reduced by link slabs.
- Link slab axial forces at the edges of the link slab were found to be higher than the one at the middle. Therefore, a higher reinforcement

ratio at the edges of the link slab can be utilized compared to the center parts of the link slab.

- Vertical components of the earthquake records governed the design of some components. Therefore, vertical earthquake component should be considered in design of bridges.
- Addition of link slab decreases girder live load stresses.
- As the skew angle increases, girder live load stresses decrease.
- Among all groups of bridges, Group D bridges were found to have the smallest demands against earthquake loading. Therefore it can be said that, to have a fully continuous deck through abutments leads to an economical design.

Using link slabs is generally considered as a cost effective approach taking into account especially high maintenance expenses due to frequent changes of repairs of the classical joints. But, it would be also underlined that the working care and discipline to be applied in construction of link slabs is not widely established in some of the developing countries. The full acceptance of the link slab system conceptually and practically could necessitate some time. Finally, it is hopefully expected that the construction of link slabs would be more frequently practiced soon in Turkey.

REFERENCES

- [1] Caner, A., and Zia, P., 1998, “Behavior and Design of Link Slabs for Jointless Bridge Decks”, *PCI Journal*, 43(3), 68 – 80.
- [2] Caner, A. and Sevgili, G., 2006, “Seismic Performance of Multisimple-Span Skew Bridges Retrofitted with Link Slabs”, *International Bridge Conference*, Pittsburgh, PA.
- [3] Fobo, W., “Noisy Neighbours”, *Bridge Design and Engineering* web site: <http://www.bridgeweb.com/>, June 2006.
- [4] Caner, A., 1996, “Analysis and Design of Jointless Bridge Decks Supported by Simple-Span Girders”, Ph.D. Dissertation, North Carolina State University, Raleigh.
- [5] Caner, A., Dogan, E., and Zia, P., 2002, “Seismic Performance of Multisimple-span Bridges Retrofitted with Link Slabs”, *Journal of Bridge Engineering*, 7(2), 85 – 93.
- [6] El-Safty, A., K., 1994, “Analysis of Jointless Bridge Decks with Partially Debonded Simple Span Beams”, Ph.D. Dissertation, North Carolina State University, Raleigh.
- [7] AASHTO (American Association of State Highway and Transportation Officials), 1996, “Standard Specifications for Highway Bridges”, Washington D.C.

- [8] Arema (American Railway Engineering and Maintenance of Way Association), 2006, "Manual for Railway Engineering", Lanham, MD.
- [9] Wasserman, 1987, E., P., "Jointless Bridge Decks", Engineering Journal, AISC, V.24, No.3.
- [10] Loveall, C., L., 1985, "Jointless Bridge Decks", Civil Engineering, ASCE.
- [11] Burke, M., P., Jr., 1992, "Integral Bridges: Attributes and Limitations", paper presented at the ACI National Concrete Engineering Conference, Chicago, IL.
- [12] Osterle, R., G., Glikin, J., D., Larson, S.C., 1989, "Design of Precast, Prestressed Bridge Girder Made Continuous", NCHRP Report 322, Transportation Research Board, National Research Council, Washington D.C.
- [13] Freyermuth, L., C., 1969, "Design of Continuous Highway Bridges with Precast, Prestressed Concrete Girders", PCI Journal, 15-39.
- [14] Zuk, W., 1981, "Jointless Bridges", Research Report No. FHWA/VA-81/48, Virginia Highway and Transportation Research Council.
- [15] Gastal F., and Zia, P., 1989, "Analysis of Bridge Beams with Jointless Decks", Proceedings of IASBE Symposium, Lisbon.

- [16] Richardson, D., R., 1989, "Simplified Design Procedures for the Removal of Expansion Joints from Bridges Using Partial Debonded Continuous Decks", Master's Thesis, North Carolina State University, Raleigh.
- [17] Wing, K., M., and Kowalsky, M., J., 2005, "Behavior, Analysis, and Design of an Instrumented Link Slab Bridge", *Journal of Bridge Engineering*, Vol. 10, No.3. 331-344.
- [18] Ebedio, T., Kennedy, J., B., 1996, "Girder Moments in Continuous Skew Composite Bridges", *Journal of Bridge Engineering*, Vol. 1, No.1. 37-45.
- [19] AASHTO (American Association of State Highway and Transportation Officials), 1998, "LRFD Bridge Design Specifications", Washington D.C.
- [20] Barr, P., J., Eberhard, M., O., Stanton, F., 2001, "Live Load Distribution Factors in Prestressed Concrete Girder Bridges", *Journal of Bridge Engineering*, Vol. 6, No.5. 298-306.
- [21] Meng, J., -Y., Lui, E., M., 2002, "Refined Stick Model for Dynamic Analysis of Skew Highway Bridges", *Journal of Bridge Engineering*, Vol. 7, No.3. 184-194.
- [22] Caner, A., Yanmaz, M., Yakut, A., Avsar, O., and Yilmaz, T., 2006, "Service Life Assessment of Existing Highway Bridges with No Planned Regular Inspections", unpublished paper.

- [23] ATC (Applied Technology Council)-32-1, 1996, "Improved Seismic Design Criteria for California Bridges: Resource Document", Redwood City, California.
- [24] LARSA Inc., "LARSA 2000 Reference for LARSA 2000 Finite Element Analysis and Design Software", 2004, Melville, New York.
- [25] Priestley M. J., Seible F., Calvi M., 1996, "Seismic Design and Retrofit of Bridges", John Wiley and Sons, New York.
- [26] Caner, A., 2006, "CE767 Highway and Railroad Infrastructures Lecture Notes", METU, Ankara
- [27] Kramer, S., 1996, "Geotechnical Earthquake Engineering", Prentice Hall, New Jersey.
- [28] Chopra, A., 2000, "Dynamics of Structures", Prentice Hall, New Jersey.
- [29] Ministry of Public Works and Settlement, Government of Republic of Turkey, 1998, "Specification for Structures to be Built in Disaster Areas", Ankara
- [30] Akkar, S., 2001, "Near-Field Earthquakes and Their Implications on Seismic Design Codes", Ph.D. Dissertation, Middle East Technical University (METU), Ankara.
- [31] METU Earthquake Engineering Research Center web site, <http://eerc.ce.metu.edu.tr/> , July 2006.

- [32] Uniform Building Code, 1997, “Structural Engineering Design Provisions”, International Conference of Building Officials, California
- [33] Caltrans, 2001, “Seismic Design Criteria Version 1.2”, California
- [34] Erkay, C., Karaesmen E., 1997, “Düzlemsel Spektrum Kavramı Üzerine Bir İrdeleme”, 4. Ulusal Deprem Mühendisliği Konferansı Bildiriler Kitabı, Ankara
- [35] Erkay, C., Karaesmen En., Karaesmen Er., 2002, “Significance of Spatial Variation of Seismic Motion and Consequences Affecting Design Procedures”, Proceedings of the 12th European Conference on Earthquake Engineering, London.
- [36] Karaesmen E., Erkay, C., 1994, “An Approach for the Evaluation of Seismic Action”, Proceedings of the 10th European Conference on Earthquake Engineering, Vienna.

APPENDIX A

BRIDGE SURVEY RESULTS

Table A.1: Properties of the surveyed bridges

					Column Properties		Cap Beam Properties		
ID	Location	# of Spans	Max SL (m)	Skew Angle (deg)	L (m)	H (m)	L _{cb} (m)	W _{cb} (m)	H _{cb} (m)
1	Bartın	4	19,35	15	5	8	9,32	1,2	1,1
2	Turhal	4	17,9	41,5	5,34	12	15,7	1,4	1,1
3	Boyabat	3	17,5	50	6,6	6,39	12,7	1,4	1,1
4	Boyabat	2	17,3	10	8,2	5,27	12,7	1,2	1,1
5	Saimbeyli	3	17,6	10	6,9	5,28	13	1,2	1,1
6	Saimbeyli	2	20,3	27	6,9	5,68	12,7	1,25	1,1
7	Saimbeyli	3	17,75	38	5,39	9,19	12,7	1,3	1,1
8	Saimbeyli	3	17,7	25	4,69	7,89	12,7	1,25	1,1
9	Denizli	6	36	0	7,25	13	13,7	3	1,5
10	Denizli	7	38,4	28,4	8,8	5	19,8	3	1,5
11	Antep	3	26,8	30,1	7,5	8,5	17,2	3,6	1,1
12	Boyabat	3	17,6	20	8,4	2,5	13,4	1,2	1,1
13	Boyabat	2	20,3	0	4,7	4,43	13,4	1,2	1,1
14	Boyabat	4	17,6	0	8,4	5,4	12,4	1,2	1,1
15	Golmarmara	3	26,7	58	7,75	7	15,7	1,7	1,1
16	Golmarmara	5	25,95	40	7,25	4,75	20,5	1,5	1,1

Table A.1 Cont'd

					Column Properties		Cap Beam Properties		
ID	Location	# of Spans	Max SL (m)	Skew Angle (deg)	L (m)	H (m)	L _{cb} (m)	W _{cb} (m)	H _{cb} (m)
17	Golmarmara	2	29,3	54,8	7,1	5,59	16,0	1,5	1,1
18	Duzce	2	20,55	8,6	5,14	6,55	10,3	2,1	0,75
19	Duzce	2	22,55	1,5	5,35	6,8	10,3	2,1	0,75
20	Duzce	4	28,6	0	8	9,12	16	2,1	0,75
21	Duzce	2	20,55	9,7	5,43	6,75	10,3	2,1	0,75
22	Duzce	2	20,55	24,3	6,86	5,95	12,5	2,1	0,75
23	Duzce	2	20,55	7,4	6,25	5,95	12,5	2,1	0,75
24	Duzce	2	20,55	30,7	7,27	5,8	12,5	2,1	0,75
25	Duzce	2	20,55	6,1	6,28	6,44	12,5	2,1	0,75
26	Duzce	2	20,55	16,5	6,52	7,17	12,5	2,1	0,75
27	Duzce	2	20,55	18	6,52	5,9	12,5	2,1	0,75
28	Duzce	2	20,55	25,5	6,93	6	12,5	2,1	0,75
29	Duzce	2	17,55	1	8	6,49	13,2	2,1	0,75
30	Duzce	2	22,55	3,7	7,52	6,02	15	2,1	0,75
31	Duzce	4	26,1	13,8	8,13	8,23	15,8	2,1	0,75
32	Duzce	2	20,55	0	6,25	5,8	12,5	2,1	0,75
33	Duzce	2	25,55	0	5,25	5,42	10,5	2,1	0,75
34	Sivas	3	18	46,3	6,3	7,07	18,9	1,5	1,1
35	Sincan	2	22,8	0	7	2,3	20	1,2	1,1
36	Ankara	5	36,15	20,3	6,13	5,79	13,4	2	0,75
37	Sungurlu	2	17,45	40	9,16	4,34	12,7	1,4	1,2

Table A.1 Cont'd

					Column Properties		Cap Beam Properties		
ID	Location	# of Spans	Max SL (m)	Skew Angle (deg)	L (m)	H (m)	L _{cb} (m)	W _{cb} (m)	H _{cb} (m)
38	Akhisar	4	16,3	20	3,2	8,74	13,5	1,2	1,1
39	Tokat	2	14,24	0	8,45	3,17	14,4	1,2	1,1
40	Tokat	2	13,3	0	8,5	3,12	13,7	1,2	1,1
41	Ankara	2	30	53,9	10	5,25	22,2	2	0,75
42	Ankara	5	36,15	20,3	6,24	5,79	13,4	2	0,75
43	Bitlis	3	24,4	37	7	7,1	17,3	2,1	0,75
44	Bitlis	4	30	32,8	14	15,14	28	3,5	1,4
45	Bitlis	2	30,9	53,5	7,5	4	38,5	2,25	0,75
46	Bitlis	2	23,5	1,8	5	6,27	10,3	2	0,75
47	Bitlis	2	28,5	30	6	10,16	11,9	2,1	0,75
48	Bitlis	2	28,65	43	8,25	7,79	32,4	2,1	0,75
49	Bitlis	6	32,2	7,2	0	36,93	13	3,5	1,4
50	Bitlis	4	24,8	49,8	6	10,64	20,5	2,25	0,75
51	Bitlis	3	24,4	38	7,5	10,19	29,4	2,2	0,75
52	Bitlis	3	29,8	53,2	6	12,01	19,4	2,3	0,75
53	Bitlis	4	31,1	21,2	0	30,93	14	3,5	1,4
54	Bitlis	4	32,2	7,6	0	27,52	13,0	3,5	1,4
55	Bitlis	4	31,1	4,6	0	30,67	13,2	3,5	1,4
56	Bursa	9	22	0	-	-	-	-	-
57	Bursa	7	21,4	0	-	-	-	-	-
58	Bursa	9	22	20	-	-	-	-	-

Table A.1 Cont'd

					Column Properties		Cap Beam Properties		
ID	Location	# of Spans	Max SL (m)	Skew Angle (deg)	L (m)	H (m)	L _{cb} (m)	W _{cb} (m)	H _{cb} (m)
59	Bursa	9	22	0	-	-	-	-	-
60	Bursa	2	13	25	-	-	-	-	-
61	Bursa	5	19	0	-	-	-	-	-
62	Bursa	2	12,5	0	-	-	-	-	-
63	Bandırma	3	11	0	-	-	-	-	-
64	Balıkesir	7	15,7	20	-	-	-	-	-
65	Çanakkale	1	13,4	15	-	-	-	-	-
66	Çanakkale	4	12	25	-	-	-	-	-
67	Çanakkale	8	12	0	-	-	-	-	-
68	Çanakkale	3	15	20	-	-	-	-	-
69	Çanakkale	3	9,5	20	-	-	-	-	-
70	Çanakkale	1	16,3	15	-	-	-	-	-
71	Çanakkale	3	11	0	-	-	-	-	-
72	Çanakkale	3	10	0	-	-	-	-	-
73	Çanakkale	3	10,5	20	-	-	-	-	-
74	Çanakkale	3	15,7	20	-	-	-	-	-
75	Çanakkale	3	17,5	45	-	-	-	-	-
76	Çanakkale	3	14,6	40	-	-	-	-	-

APPENDIX B

BRIDGE MODELS

Table B.1: Group A Bridges: L/H = 1.0 and I_{capbeam}/I_{column} = 0.1

ID	Skew Angle				# of Spans		Span Length		Link Slab	
	0°	20°	40°	60°	2	4	18m	25m	yes	no
A1	X				X		X			X
A2	X				X		X		X	
A3	X				X			X		X
A4	X				X			X	X	
A5	X					X	X			X
A6	X					X	X		X	
A7	X					X		X		X
A8	X					X		X	X	
A9		X			X		X			X
A10		X			X		X		X	
A11		X			X			X		X
A12		X			X			X	X	
A13		X				X	X			X
A14		X				X	X		X	
A15		X				X		X		X
A16		X				X		X	X	
A17			X		X		X			X
A18			X		X		X		X	
A19			X		X			X		X
A20			X		X			X	X	
A21			X			X	X			X
A22			X			X	X		X	
A23			X			X		X		X
A24			X			X		X	X	
A25				X	X		X			X
A26				X	X		X		X	
A27				X	X			X		X
A28				X	X			X	X	
A29				X		X	X			X
A30				X		X	X		X	
A31				X		X		X		X
A32				X		X		X	X	

Table B.2: Group B Bridges: L/H = 1.5 and Icapbeam/Icolumn = 0.1

ID	Skew Angle				# of Spans		Span Length		Link Slab	
	0°	20°	40°	60°	2	4	18m	25m	yes	no
B1	X				X		X			X
B2	X				X		X		X	
B3	X				X			X		X
B4	X				X			X	X	
B5	X					X	X			X
B6	X					X	X		X	
B7	X					X		X		X
B8	X					X		X	X	
B9		X			X		X			X
B10		X			X		X		X	
B11		X			X			X		X
B12		X			X			X	X	
B13		X				X	X			X
B14		X				X	X		X	
B15		X				X		X		X
B16		X				X		X	X	
B17			X		X		X			X
B18			X		X		X		X	
B19			X		X			X		X
B20			X		X			X	X	
B21			X			X	X			X
B22			X			X	X		X	
B23			X			X		X		X
B24			X			X		X	X	
B25				X	X		X			X
B26				X	X		X		X	
B27				X	X			X		X
B28				X	X			X	X	
B29				X		X	X			X
B30				X		X	X		X	
B31				X		X		X		X
B32				X		X		X	X	

Table B.3: Group C Bridges: L/H = 1.0 and Icapbeam/Icolumn = 1.5

ID	Skew Angle				# of Spans		Span Length		Link Slab	
	0°	20°	40°	60°	2	4	18m	25m	yes	no
C1	X				X		X			X
C2	X				X		X		X	
C3	X				X			X		X
C4	X				X			X	X	
C5	X					X	X			X
C6	X					X	X		X	
C7	X					X		X		X
C8	X					X		X	X	
C9		X			X		X			X
C10		X			X		X		X	
C11		X			X			X		X
C12		X			X			X	X	
C13		X				X	X			X
C14		X				X	X		X	
C15		X				X		X		X
C16		X				X		X	X	
C17			X		X		X			X
C18			X		X		X		X	
C19			X		X			X		X
C20			X		X			X	X	
C21			X			X	X			X
C22			X			X	X		X	
C23			X			X		X		X
C24			X			X		X	X	
C25				X	X		X			X
C26				X	X		X		X	
C27				X	X			X		X
C28				X	X			X	X	
C29				X		X	X			X
C30				X		X	X		X	
C31				X		X		X		X
C32				X		X		X	X	

Table B.4: Group D Bridges: $L/H = 1.0$ and $I_{cb}/I_{col} = 0.1$ with fully continuous deck

ID	Skew Angle				# of Spans		Span Length	
	0°	20°	40°	60°	2	4	18m	25m
D1	X				X		X	
D2	X				X			X
D3	X					X	X	
D4	X					X		X
D5		X			X		X	
D6		X			X			X
D7		X				X	X	
D8		X				X		X
D9			X		X		X	
D10			X		X			X
D11			X			X	X	
D12			X			X		X
D13				X	X		X	
D14				X	X			X
D15				X		X	X	
D16				X		X		X

APPENDIX C

MACRO CODE FOR BRIDGE MODEL GENERATION

```
Sub newc()
'For real numbers
'x for coor, xinc for longitudinal direction, xs for span, ri for rigid link
Dim x, xinc, xs As Double
Dim y As Double
Dim z, ri, th, bh As Double
'ej expansion joint, sd support distance gls girder longitudinal spacing
Dim ej, sd, gls As Double
Dim gsp, rcont, le, xskew As Double
'for integer numbers
Dim n, ngirder, nginc, nr, nspan, ns As Long
Dim nsinc As Long
Dim tp, ng, nxi, nf As Long
'for plate elements, tx
Dim tx, jumpno As Long
'input data for bearings bh= bearing height
Sheets("Bearings").Select
bh = Cells(14, 5)
Sheets("Spans").Select
' deck thicness to be used in plate elements th
th = Cells(4, 5)
'girder coordinate computation
```

```

x = 0#
y = 0#
z = 0#
nginc = 0
nsinc = 0
xs = 0
nr = 0
xskew = 0
xinc = Cells(5, 5) / 20#
ngirder = Cells(7, 5)
nspan = Cells(3, 5)
ej = Cells(11, 5)
sd = Cells(9, 5)
gls = ej + sd * 2
For ns = 1 To nspan
For m = 1 To ngirder
For n = 1 To 21
    Cells(36 + n + nr, 1) = n + 1100 + nginc + nsinc
    Cells(36 + n + nr, 2) = (n - 1) * xinc + xs + xskew
    Cells(36 + n + nr, 3) = y
    Cells(36 + n + nr, 4) = z
Next n
y = y + Cells(13, 5)
nginc = nginc + 100
nr = nr + 21
xskew = xskew + Cells(13, 5) * Cells(9, 8)
Next m
nsinc = nsinc + 1000
nginc = 0

```

```

xs = xs + Cells(5, 5) + gls
y = 0
xskew = 0
Next ns
' joints for deck
' ri is the z coordinate
ri = Cells(4, 5) / 2 + Cells(32, 2) + 0.05
ng = ngirder * nspan * 21
y = -Cells(13, 5) / 2
nr = 0
nxi = 0
nsinc = 0
xs = 0
xskew = y * Cells(9, 8)
For ns = 1 To nspan
For m = 1 To 2 * ngirder + 1
    For n = 1 To 21
        Cells(36 + ng + n + nr, 1) = 10100 + n + nxi + nsinc
        Cells(36 + ng + n + nr, 2) = (n - 1) * xinc + xs + xskew
        Cells(36 + ng + n + nr, 3) = y
        Cells(36 + ng + n + nr, 4) = ri
    Next n
    nr = nr + 21
    nxi = nxi + 100
    y = y + Cells(13, 5) / 2
    xskew = y * Cells(9, 8)
Next m
nsinc = nsinc + 10000
xs = xs + Cells(5, 5) + gls

```

```

y = -Cells(13, 5) / 2
xskew = y * Cells(9, 8)
nxi = 0
Next ns
' joints for end zones of girders
ng = nspan * ngirder * 21 * 3 + nspan * 21
y = 0
x = 0
z = Cells(32, 4)
xi = 0
nginc = 0
tp = 0
nr = 0
xskew = 0
For ns = 1 To nspan
  For n = 1 To 2
    For m = 1 To ngirder
      Cells(ng + m + 36 + tp, 1) = 1122 + nginc + xi + nr
      Cells(ng + m + 36 + tp, 2) = x + xskew
      Cells(ng + m + 36 + tp, 3) = y
      Cells(ng + m + 36 + tp, 4) = z
      y = y + Cells(13, 5)
      xskew = y * Cells(9, 8)
      nginc = nginc + 100
    Next m
    xi = 1
    x = x + Cells(5, 5)
    nginc = 0
    y = 0
  
```

```

xskew = 0
tp = tp + ngirder
Next n
nginc = 0
y = 0
xskew = 0
xi = 0
x = ns * Cells(5, 5) + ns * (2 * Cells(9, 5) + Cells(11, 5))
nr = nr + 1000
Next ns
'joints for bottom of bearings
ng = nspan * ngirder * 21 * 3 + nspan * 21 + ngirder * 2 * nspan
x = 0
y = 0
xskew = 0
z = Cells(32, 4) - bh
xi = 0
nginc = 0
tp = 0
nr = 0
For ns = 1 To nspan
  For n = 1 To 2
    For m = 1 To ngirder
      Cells(ng + m + 36 + tp, 1) = 1124 + nginc + xi + nr
      Cells(ng + m + 36 + tp, 2) = x + xskew
      Cells(ng + m + 36 + tp, 3) = y
      Cells(ng + m + 36 + tp, 4) = z
      y = y + Cells(13, 5)
      xskew = y * Cells(9, 8)
    
```

```

        nginc = nginc + 100
    Next m
xi = 1
    x = x + Cells(5, 5)
    nginc = 0
    y = 0
    xskew = 0
    tp = tp + ngirder
    Next n
nginc = 0
y = 0
xskew = 0
xi = 0
x = ns * Cells(5, 5) + ns * (2 * Cells(9, 5) + Cells(11, 5))
nr = nr + 1000
Next ns
'joints for capbeam
gsp = Cells(13, 5)
rcont = (Cells(6, 5) - Cells(5, 8)) / 2
le = Cells(5, 8)
xi = 0
tp = 0
xskew = 0
For ns = 1 To nspan - 1
    nginc = 0
    Sheets("Spans").Select
    x = (Cells(5, 5) + Cells(9, 5) + Cells(11, 5) / 2) * ns + (Cells(9, 5) + Cells(11,
    5) / 2) * (ns - 1)
    y = -Cells(13, 5) / 2

```

$z = \text{Cells}(32, 4) - bh - \text{Cells}(3, 8) / 2$

'for this portion xskew became tan angle for above section $xskew=y*\tan \text{ angle}$

$xskew = \text{Cells}(9, 8)$

Sheets("Subj").Select

For n = 1 To ngirder + 4

If n = 1 Then

$\text{Cells}(n + 1 + tp, 1) = 1127 + xi$

$\text{Cells}(n + 1 + tp, 2) = x + xskew * y$

$\text{Cells}(n + 1 + tp, 3) = y$

$\text{Cells}(n + 1 + tp, 4) = z$

End If

If n = 2 Then

$\text{Cells}(n + 1 + tp, 1) = 1126 + xi$

$\text{Cells}(n + 1 + tp, 2) = x + xskew * (y + gsp / 2)$

$\text{Cells}(n + 1 + tp, 3) = y + gsp / 2$

$\text{Cells}(n + 1 + tp, 4) = z$

End If

If n > 2 Then

$y = y + gsp$

$\text{Cells}(n + 1 + tp, 1) = 1126 + nginc - 100 + xi$

$\text{Cells}(n + 1 + tp, 2) = x + xskew * (y + gsp / 2)$

$\text{Cells}(n + 1 + tp, 3) = y + gsp / 2$

$\text{Cells}(n + 1 + tp, 4) = z$

If n = ngirder + 2 Then

$y = y + gsp$

$\text{Cells}(n + 1 + tp, 1) = 1227 + xi$

$\text{Cells}(n + 1 + tp, 2) = x + xskew * (rcont - gsp / 2)$

$\text{Cells}(n + 1 + tp, 3) = rcont - gsp / 2$

$\text{Cells}(n + 1 + tp, 4) = z$

```

End If
End If
If n = ngirder + 3 Then
y = y + gsp
Cells(n + 1 + tp, 1) = 1527 + xi
Cells(n + 1 + tp, 2) = x + xskew * (le + rcont - gsp / 2)
Cells(n + 1 + tp, 3) = le + rcont - gsp / 2
Cells(n + 1 + tp, 4) = z
End If
If n = ngirder + 4 Then
y = y + gsp
Cells(n + 1 + tp, 1) = 1528 + xi
Cells(n + 1 + tp, 2) = x + xskew * (le + 2 * rcont - gsp / 2)
Cells(n + 1 + tp, 3) = le + 2 * rcont - gsp / 2
Cells(n + 1 + tp, 4) = z
End If
nginc = nginc + 100
Next n
xi = xi + 1000
tp = tp + ngirder + 4
Next ns
'member incidance for girders
Sheets("Members").Select
xi = 0
tp = 0
nginc = 0
For ns = 1 To nspan
For m = 1 To ngirder
    For n = 1 To 20

```

```

Cells(1 + n + tp, 1) = n + 1100 + xi + nginc
Cells(1 + n + tp, 2) = n + 1100 + xi + nginc
Cells(1 + n + tp, 3) = n + 1100 + xi + 1 + nginc
Cells(1 + n + tp, 5) = "Beam"
Cells(1 + n + tp, 6) = "PrecastGirder"
Cells(1 + n + tp, 7) = "PrecastGirder"
Cells(1 + n + tp, 8) = "PGirder"
Cells(1 + n + tp, 9) = 0#
Cells(1 + n + tp, 11) = 0#
Cells(1 + n + tp, 12) = 0#
Cells(1 + n + tp, 13) = 90#
Cells(1 + n + tp, 14) = 0#
Cells(1 + n + tp, 15) = "Girder"
Next n
tp = tp + 20
nginc = nginc + 100
Next m
xi = xi + 1000
nginc = 0
Next ns
' member incidence for rigid link between girder and deck
tp = nspan * 20 * ngirder
xi = 0
nginc = 0
nf = 0
nsz = 0
For ns = 1 To nspan
For m = 1 To ngirder
For n = 1 To 21

```

```

Cells(1 + n + tp + nf, 1) = n + 1120 + xi + nginc
Cells(1 + n + tp + nf, 2) = n + 1100 + xi + nginc
Cells(1 + n + tp + nf, 3) = n + 1100 + xi * 10 + 9100 + nginc * 2
Cells(1 + n + tp + nf, 5) = "Beam"
Cells(1 + n + tp + nf, 6) = "Rigid"
Cells(1 + n + tp + nf, 7) = "Rigid"
Cells(1 + n + tp + nf, 8) = "Rigid"
Cells(1 + n + tp + nf, 9) = 0#
Cells(1 + n + tp + nf, 11) = 0#
Cells(1 + n + tp + nf, 12) = 0#
Cells(1 + n + tp + nf, 13) = 90#
Cells(1 + n + tp + nf, 14) = 0#
Cells(1 + n + tp + nf, 15) = "Rigid"
Next n
nf = nf + 21
nginc = nginc + 100
Next m
xi = xi + 1000
nginc = 0
Next ns
'Member incidence for girder end andtop of bearing - rigid link
jumpno = nspan * ngirder * 21 + nspan * ngirder * 20
nginc = 0
xi = 0
nsz = 0
nr = 0
tp = 0
nf = 0
For ns = 1 To nspan

```

```

For n = 1 To 2
  For m = 1 To ngirder
    Cells(jumpno + 1 + m + tp, 1) = 1149 + m + xi + nf
    Cells(jumpno + 1 + m + tp, 2) = 1122 + nginc + nsz + nf
    Cells(jumpno + 1 + m + tp, 3) = 1101 + nginc + nr + nf
    Cells(jumpno + 1 + m + tp, 5) = "Beam"
    Cells(jumpno + 1 + m + tp, 6) = "Rigid"
    Cells(jumpno + 1 + m + tp, 7) = "Rigid"
    Cells(jumpno + 1 + m + tp, 8) = "Rigid"
    Cells(jumpno + 1 + m + tp, 9) = 0#
    Cells(jumpno + 1 + m + tp, 11) = 0#
    Cells(jumpno + 1 + m + tp, 12) = 0#
    Cells(jumpno + 1 + m + tp, 13) = 90#
    Cells(jumpno + 1 + m + tp, 14) = 0#
    Cells(jumpno + 1 + m + tp, 15) = "Rigid"
    nginc = nginc + 100
  Next m
  nginc = 0
  nsz = 1
  nr = 20
  xi = xi + ngirder
  tp = tp + ngirder
Next n
xi = 0
nsz = 0
nr = 0
nf = nf + 1000
Next ns
'capbeam elements

```

```

Sheets("Subm").Select
jumpno = 0
tp = 0
m = 1
' For m = 1 To ngirder + 3
'   If m = 1 Then
Cells(jumpno + 1 + m + tp, 1) = 11000 + m
Cells(jumpno + 1 + m + tp, 2) = 1127
Cells(jumpno + 1 + m + tp, 3) = 1126
Cells(jumpno + 1 + m + tp, 5) = "Beam"
Cells(jumpno + 1 + m + tp, 6) = "CapBeamEff"
Cells(jumpno + 1 + m + tp, 7) = "CapBeamEff"
Cells(jumpno + 1 + m + tp, 8) = "CapBeam"
Cells(jumpno + 1 + m + tp, 9) = 0#
Cells(jumpno + 1 + m + tp, 11) = 0#
Cells(jumpno + 1 + m + tp, 12) = 0#
Cells(jumpno + 1 + m + tp, 13) = 90#
Cells(jumpno + 1 + m + tp, 14) = 0#
Cells(jumpno + 1 + m + tp, 15) = "CapBeam"
'   End If
' Next m
'deck plate elements
Sheets("Plates").Select
nli = 2 * 20 * ngirder
nx = 2 * ngirder
tx = 0
nginc = 0
nf = 0
xi = 0

```

```

tp = 0
For ns = 1 To nspan
  For m = 1 To 2 * ngirder
    For n = 1 To 20
      Cells(4 + n + tp, 1) = 1000 + n + tx + nf
      Cells(4 + n + tp, 2) = "Shell"
      Cells(4 + n + tp, 3) = 10100 + n + nginc + xi
      Cells(4 + n + tp, 4) = 10100 + n + 1 + nginc + xi
      Cells(4 + n + tp, 5) = Cells(4 + n + tp, 4) + 100
      Cells(4 + n + tp, 6) = Cells(4 + n + tp, 3) + 100
      Cells(4 + n + tp, 7) = "Deck"
      Cells(4 + n + tp, 8) = th
      Cells(4 + n + tp, 9) = "(NONE)"
      Cells(4 + n + tp, 10) = 0
      Cells(4 + n + tp, 11) = "Deck"
    Next n
  tp = tp + 20
  tx = tx + 20
  nginc = nginc + 100
  Next m
  nf = nf + 1000
  tx = 0
  nginc = 0
  xi = xi + 10000
  Next ns
  'linear elastic springs for bridge bearings
  Sheets("Bearings").Select
  nginc = 0
  nf = 0

```

```

tx = 0
xi = 0
For ns = 1 To nspan
For nr = 1 To 2
For m = 1 To ngirder
  For n = 1 To 5
    Cells(34 + n + tx, 1) = n + nf
    Cells(34 + n + tx, 2) = 1124 + nginc + nr - 1 + xi
    Cells(34 + n + tx, 3) = 1122 + nginc + nr - 1 + xi
    Cells(34 + n + tx, 4) = "Linear"
    If n = 1 Then
      Cells(34 + n + tx, 5) = "Trans. X"
      Cells(34 + n + tx, 6) = Cells(26, 5)
      Cells(34 + n + tx, 7) = Cells(26, 5)
    End If
    If n = 2 Then
      Cells(34 + n + tx, 5) = "Trans. Y"
      Cells(34 + n + tx, 6) = Cells(27, 5)
      Cells(34 + n + tx, 7) = Cells(27, 5)
    End If
    If n = 3 Then
      Cells(34 + n + tx, 5) = "Trans. Z"
      Cells(34 + n + tx, 6) = Cells(28, 5)
      Cells(34 + n + tx, 7) = Cells(28, 5)
    End If
    If n = 4 Then
      Cells(34 + n + tx, 5) = "Rot. X"
      Cells(34 + n + tx, 6) = Cells(29, 5)
      Cells(34 + n + tx, 7) = Cells(29, 5)
    End If
  End For
End For
End For
End For

```

```
End If
If n = 5 Then
Cells(34 + n + tx, 5) = "Rot. Y"
Cells(34 + n + tx, 6) = Cells(30, 5)
Cells(34 + n + tx, 7) = Cells(30, 5)
End If
Cells(34 + n + tx, 12) = "(none)"
Cells(34 + n + tx, 13) = "Bearing"
Next n
nginc = nginc + 100
nf = nf + 5
tx = tx + 5
Next m
nginc = 0
Next nr
xi = xi + 1000
Next ns
End Sub
```